

2010

A study of storm-induced variations in the littoral sediment transport patterns of central Monterey Bay

Jeremiah J. Brower
California State University, Monterey Bay

Follow this and additional works at: https://digitalcommons.csumb.edu/caps_thes

Recommended Citation

Brower, Jeremiah J., "A study of storm-induced variations in the littoral sediment transport patterns of central Monterey Bay" (2010). *Capstone Projects and Master's Theses*. 66.
https://digitalcommons.csumb.edu/caps_thes/66

This Master's Thesis is brought to you for free and open access by Digital Commons @ CSUMB. It has been accepted for inclusion in Capstone Projects and Master's Theses by an authorized administrator of Digital Commons @ CSUMB. Unless otherwise indicated, this project was conducted as practicum not subject to IRB review but conducted in keeping with applicable regulatory guidance for training purposes. For more information, please contact digitalcommons@csumb.edu.

**A STUDY OF STORM-INDUCED VARIATIONS IN THE
LITTORAL SEDIMENT TRANSPORT PATTERNS OF
CENTRAL MONTEREY BAY.**

A Thesis
Presented to the
Faculty of the
Division of Science and Environmental Policy
California State University Monterey Bay

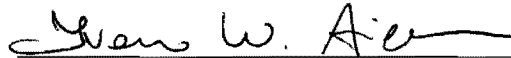
In Partial Fulfillment
of the Requirements for the Degree
Master of Science
in
Marine Science

by
Jeremiah J. Brower
Term Completed: Fall 2010

CALIFORNIA STATE UNIVERSITY MONTEREY BAY

The Undersigned Faculty Committee Approves the
Thesis of Jeremiah J. Brower

A STUDY OF STORM-INDUCED VARIATIONS IN THE LITTORAL
SEDIMENT TRANSPORT PATTERNS OF CENTRAL MONTEREY
BAY.



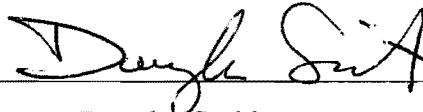
Ivano Aiello

Moss Landing Marine Laboratories



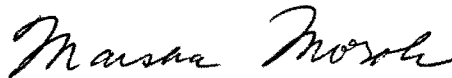
Erika McPhee-Shaw

Moss Landing Marine Laboratories



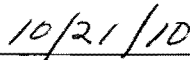
Douglas Smith

California State University Monterey Bay



Marsha Moroh, Dean

College of Science, Media Arts, and Technology



Approval Date

Copyright © 2010

by

Jeremiah J. Brower

All Rights Reserved

DEDICATION

I would like to dedicate this project to the scientists, mentors, tutors and all around great people who have guided me towards this degree: Dr. Ivano Aiello, Dr. Erika McPhee-Shaw, Dr. Douglas Smith, Dr. Jeffry Borgeld, Dr. Hal Genger. I would also like to dedicate this to my family who have given me unwavering support and love during this arduous and rewarding journey.

ABSTRACT

A study of storm-induced variations in the littoral sediment transport patterns of central Monterey Bay.

by

Jeremiah J. Brower

Masters of Science in Marine Science

California State University Monterey Bay, Year

Recent trends in sea level rise threaten both beaches and coastal communities, making it critical to understand sediment resupply patterns along tectonically active, wave-dominated coastlines. The Monterey Bay coastline is a high-energy environment characterized by well-defined sediment sources and sinks, but poorly defined littoral transport patterns. This 2009 study focuses on identifying sources for littoral sediment, littoral transport trends, and how both vary from summer to winter conditions. Petrographic analysis of heavy minerals from the Salinas River, Pajaro River and coastal Aromas sandstone dune fields were used to determine the provenance of littoral sediment within central Monterey Bay. Littoral transport in central Monterey Bay were determined using grain size, heavy mineral petrography, and alongshore transport estimates generated by changes in swell direction.

The lithic and heavy mineral composition of both the Pajaro and Salinas transects describes unique sources of sediment for each river: erosion of detrital basalt-bearing sandstone units likely part of the Franciscan complex exposed in the Pajaro watershed provides large amounts of pyroxene into the Pajaro river, and erosion of granodiorite and granite outcrops along the Santa Lucia range provides garnet to the Salinas watershed. The amount of heavy minerals along the coast varies seasonally, and the winter erosion of Aromas sandstone paleo-dunes as well as the summer progradation of offshore bar sediments are possible contributors to coastal mineral assemblages. Heavy mineral deposition within the study area supports the conclusion that there are two dominant littoral cells in Monterey Bay isolated by the Monterey Submarine Canyon: a year-round “Pajaro” cell that transports sediment southward along the coast from the Pajaro River Mouth, and a seasonal “Salinas” cell that transports sediment northward from the Salinas River Mouth during summer W-SW swell conditions. Similarities in beach composition across the canyon is thought to be generated by a combination of seasonal mixing of fluvial material from the Pajaro and Salinas watersheds, and the erosion of the Aromas Sandstones.

TABLE OF CONTENTS

	PAGE
ABSTRACT.....	v
LIST OF TABLES.....	viii
LIST OF FIGURES.....	ix
ACKNOWLEDGEMENTS.....	x
i. INTRODUCTION	1
1.1 Beach dynamics along wave-exposed coastlines.....	1
1.2 Littoral transport.....	3
1.3 Sediment transport trends	5
1.4 Beach composition	7
1.5 Provenance studies	8
1.6 Description of study area	10
1.7 Purpose of study	13
ii. METHODS	15
2.1 Sampling strategy	15
2.2 Grain size analysis	17
2.3 Thin section petrography	17
2.4 Upper watershed pebble analysis	19
2.5 Grain size trends	20
iii. RESULTS	22
3.1 Grain size data	22
3.2 Vector trends	23
3.3 Petrographic data	24
3.4 Upper salinas and pajaro data	26
3.5 Aromas sandstone and san lorenzo river	27
iv. DISCUSSION.....	29

4.1 Seasonal changes in grain-size	31
4.2 Littoral transport trends	33
4.3 Upper watershed analysis	35
4.4 Seasonal changes in composition and beach morphology	36
4.5 Littoral contributions Aromas Sandstones and San Lorenzo River.....	38
4.6 Conclusions & future study	40
v. Literature Cited	43
vi. Appendix	56

LIST OF TABLES

	PAGE
Table 1: Heavy mineral Specific Gravities.....	56
Table 2: Transect location and dates.....	56
Table 3: Location of Swash zone samples.....	57
Table 4: Optical properties.....	58
Table 5: Grain size data.....	59
Table 6: Grain size trend & variance data.....	62
Table 7: Framework mineral counts.....	63
Table 8: Lithic counts.....	65
Table 9: Mineral counts.....	66
Table 10: San Lorenzo, Aromas and upper channel mineral counts.....	69
Table 11: Pebble counts.....	70

LIST OF FIGURES

	PAGE
Figure 1: Beach terminology.....	71
Figure 2: General littoral cell pattern	72
Figure 3: Generalized sediment-type provinces.....	72
Figure 4: Diagrammatic summary of grain size distributions.....	73
Figure 5: Map of fault blocks surrounding the Monterey Bay area.....	74
Figure 6: Aerial map of the Pajaro and Salinas Watersheds.....	74
Figure 7: Aerial map of central Monterey Bay	75
Figure 8: Diagram of arbitrary sample transects.....	76
Figure 9: Random point-count procedure for thin section analysis.....	77
Figure 10: Grain size plotted against Transect location.....	77
Figure 11: Standard deviation plotted against Transect location.....	79
Figure 12: Standard Deviation of berm samples plotted against Transect location...80	80
Figure 13: Results of the 2-sample T-test.....	81
Figure 14: Frequency plots for winter.....	82
Figure 15: Frequency plots for summer.....	83
Figure 16: Frequency plots for fall	84
Figure 17: Littoral transport trends.....	85
Figure 18: Swell direction and frequency plots.....	88
Figure 19: QFL composition plots.....	89
Figure 20: Lithic counts.....	90
Figure 21: Cross-polarized thin section photos.....	93
Figure 22: Heavy mineral abundance.....	94
Figure 23: Pebble composition charts.....	97
Figure 24: January Pajaro coastline picture.....	98
Figure 25: July coastline photos.....	98

Figure 26: October coastline photos.....99

ACKNOWLEDGEMENTS

I would like to acknowledge the hard work and guidance that my advisor, Dr. Ivano Aiello, has put into this project; without his help this research would never have been completed.

INTRODUCTION

Beach erosion is a persistent problem for coastal communities, and as global population continues to rise, there will be an increased demand for accurate information regarding past and present trends of shoreline movement. Beaches are important features along wave-dominated coast-lines as they act as both habitats and natural buffers to coastal erosion (Hapke et al 2006). Accelerated global warming and anticipated rising sea-level make it essential to have a clearer understanding of oceanographic processes that govern the accretion or erosion of our coast, as well as small scale (meter) variability in transport within beach environments. Global sea-level has risen at a mean rate of 1.8 mm/yr over the last century, and as sea levels could continue to rise, sediment starved beaches are expected to be quickly submerged (Douglas 1997). Without a clear understanding of littoral sediment transport we cannot accurately construct a model for future changes to our coastlines (Ryan et al 1999). Grain size trends and heavy mineral depositional patterns can be used to monitor both large-and small-scale variability in transport patterns, but to date few studies have combined these parameters to trace sediment movement (*see* Yancey 1972).

1.1 Beach Dynamics along Wave-exposed coastlines

Beaches fringe about 40% of the world's coast-line, and generally consist of unconsolidated deposits of siliclastic sand and gravel on the shore (Bird 2000). Beach morphology depends on the patterns of refracting waves approaching the shore and the sediment characteristics, they fall into two general categories: dissipative and reflective beaches (Osborne & Simpson 2005, Bertin 2008, Wright et al 1979, Bird 2000). Dissipative beaches are systems where most wave energy

is expended through the process of breaking (Osborne and Simpson 2005). In cross section, morphodynamically dissipative beaches are characterized by low near-shore gradient and beach slopes (0.01 and 0.03), and are composed of unconsolidated well-sorted fine-grained sands (Bertin 2008, Osborne and Simpson 2005). Reflective beaches are characterized by steep, coarse-grained linear beach faces, well-developed berms and beach cusps, and surging breakers with high run-up (Wright et al 1979).

Seasonal changes in wave energy affect the structure of coastal environments, creating semi-permanent cusp structures and re-sorting both fine and coarse sediment from beach berms into offshore bars (Bird 2000, Masselink & Pattiaratchi 1998, Dingler 2002, Cloud 1966). Beach cusps are rhythmic shoreline features formed by swash action (Figure 1). Cusps are characterized by steep-gradient, seaward-pointing cusp horns and gentle-gradient, seaward-facing cusp embayments (Masselink & Pattiaratchi 1998). The beach sediment is commonly coarser on the cusps than in the intervening depressions between them (Cloud 1966). Cusps develop along wave dominated coast-lines and the spacing of cusps is related to the height of the waves (Cloud 1966). The swash zone is arguably the most dynamic part of the nearshore region and is characterized by large flow velocities, high turbulence levels and large suspended sediment concentrations (Elfrink & Baldock 2002, Masselink et al 2005). Nearshore bars control wave dissipation and near-shore current circulation, and offshore bars can dissipate over a third of the energy of breaking waves (Kaczmarke 2005, Sedrati & Anthony 2007). During storms, intense wave breaking on beaches drives strong offshore-directed rip currents that carry sediment seaward, resulting in offshore sandbar migration (Hoefel & Elgar 2003). Selective sorting along offshore bars removes finer material to dune anti-node faces, creating coarse grained (0.125-0.5 mm) dune crests (Landry et al 2007). Shoreward drift of coarser bar sediment

occurs during periods of low sea-level, decreased wave energy or increased tidal forcing (Bird 2000, Sedrati & Anthony 2007).

In central California, beaches are ephemeral features controlled by seasonal shifts in wave energy. Seasonal beaches, which are present in the summer months and are lost during the winter months, are common along exposed coasts with a limited offshore supply of sand (Hapke et al 2006). The coastline of central Monterey Bay is characterized by migrating berm, dune and cusp fields, symptoms of a high-energy environment where large amounts of variability occur over small spatial and temporal scales (Best & Griggs 1991, Dingler & Reiss 2001, Eittreim et al 2002). Easily eroded dunes back relatively wide, sandy beaches along the central bay, with the western boundary defined by an offshore bar which migrates on-shore during calm summer months and offshore during high energy winter conditions (Figure 1, Smith et al 2005a, Moore & Griggs 2002). Beaches along the Monterey Bay are composed of siliclastic sand derived from a mix of riverine, dune and coastal cliff sources (Moore & Griggs 2002, Best & Griggs 1991, Eittreim et al 2002). Seasonal changes in Monterey Bay coastline morphology include an increase in beach slope and mean grain size during winter months, and a shallower beach slope with well-defined berm forming during summer months (Moore & Griggs 2002, Smith et al 2005a, Dingler & Reiss 2002, Hapke et al 2006).

1.2 Littoral Transport

Along tectonically active, wave-dominated coastlines, such as the west coast of North America, the alongshore movement of sediment is characterized by littoral cells which transport sediment from rivers to near-shore sinks, such as submarine canyons or along coastal promontories (Figure 2). The California coastline is characterized by sediment-starved pocket beaches fueled by sediment

transported along the coast from distant point sources (Storlazzi & Field 2000, Eittreim 2002, Smith et al 2007, Patsch & Griggs 2008). Many pocket beaches develop within littoral cells and serve as temporary storage areas for sediment, although changes in beach slope and grain size can cause non-dissipative conditions that prompt rapid sediment removal, which is common along high angle beaches where surging breakers rapidly remove large amounts of both fine and coarse-grained sediment (Bertin et al 2008, Osborne & Simpson 2005). Streams provide the majority of sediment to California's beaches, but this component is difficult to quantify due to the storm-driven episodic nature of input, with strong variability occurring between El Niño and La Nina years (Patsch & Griggs 2008, Inman & Jenkins 1999).

Littoral sediment transport can be estimated based on alongshore-current patterns, changes in grain size parameters and mineral provenance (Chesser & Petterson 1987, Frihy et al 1995, Gao & Collins 1992). When waves break at an angle $> 30^\circ$ to the shoreline, an alongshore current, known as "littoral drift", is generated flowing parallel to the shoreline and confined to the near-shore zone between the breakers and the shoreline (Komar 1974). Littoral cells are segments of the coast with distinct sediment sources, defined longshore transport pathways, and sinks where the sediment is removed from the littoral system (Hapke et al 2006, Inman & Jenkins 1999, Komar 1976, Patsch & Griggs 2008, Sedrati & Anthony 2007). A littoral cell redistributes sand from river mouths to tidal inlets, dune fields, submarine canyons and accreting beaches, fueling the development and destruction of many beaches, deltas and coves (Frihy & Dewidar 2003, Storlazzi & Field 2000). In California the cells are bound by either prominent rocky headlands or submarine canyons that cross the continental shelf to a shallow enough depth as to intercept alongshore moving sediment (Hapke et al 2006, Figure 2). The Santa Barbara Littoral cell is the largest and most well studied cell in southern California; it transports 1.84×10^6 m³/yr sediment 225 km

from the mouth of the Santa Maria River to Mugu Submarine Canyon (Patsch & Griggs 2008).

In Monterey Bay, littoral cells are thought to act as primary transport pathways by siphoning sediment into the canyon, but the dynamics of these cells are still only partially understood (Smith et al 2007, Paull et al 2005, Greene et al 2002). Extensive studies of cross-shelf transport of sediment have established that an offshore “mud-belt” exists along the inner-shelf of Monterey Bay and is the largest sink for finer (<1 mm) terrigenous sediment (Figure 3, Eittreim et al 2002, Edwards 2002). Previous sediment budgets estimate that the head of the Monterey canyon acts as a filter for sediment, removing the majority of coarser material from the littoral system, while the finer fraction is rapidly removed to the shelf (Best & Griggs 1991, Thornton et al 2006, Smith et al 2007 2005, Eittreim et al 2002, Paull et al 2005, Smith et al 2007). Transport of both fine and coarse sediment across the head of the canyon has been implied in the past but never demonstrated, indicating that we still do not have a clear understanding of transport patterns along the Monterey Bay (see Yancy 1972, Wolf 1968).

1.3 Sediment Transport Trends

Grain size is the most fundamental property of sediment particles, affecting their entrainment, transport and deposition (Blott & Pye 2001). Grain size analysis provides important clues to sediment provenance, transport history and depositional conditions (Blott & Pye 2001). Estimates of sediment transport patterns based on spatial changes in grain size, sorting and skewness parameters have been used successfully in the past (*see* McLaren and Bowles 1985, Gao & Collins 1992), however the interpretation of littoral transport patterns using beach sediment textural parameters can be complicated by high levels of storm-induced variability of sediment supply and removal in the swash-zone (Pedreros et al

1996, Poizot et al 2007). Seasonal changes in near-shore swell energy can prompt alternations between dissipative and reflective profiles within beaches, affecting their grain size, sorting, and composition (Bertin et al 2008). The one-dimensional sediment transport approach distinguishes two potential patterns of downstream transport: sequential deposits may become either coarser, better sorted, and more positively skewed under high wave energy conditions (Case 1: “CB+”); or finer, better sorted, and more negatively skewed with a decreasing energy regime (Case 2: “FB-”) (Figure 4, Gao & Collins 1992, McLaren & Bowles 1985, Pedreros et al 1996, Poizot et al 2007, McLaren & Bowles 1985). Sorting of samples is measured by changes in the standard deviation of sample mean grain sizes.

Approximations of grain size parameters can be obtained by plotting frequency data as a cumulative frequency curve, extracting prescribed values from the cumulative percentage curve using a linear interpolation between adjacent known points on the curve and entering these into logarithmic or geometric graphical measurements, a technique known as the "Folk & Ward method" (Folk & Ward 1957). The parameters used to describe a grain size distribution are: 1) the average size, 2) the spread (sorting) of the sizes around the average, 3) the symmetry or preferential spread (skewness) to one side of the average, and 4) the degree of concentration of the grains relative to the average (kurtosis) (Blott & Pye 2001). Grain size values are plotted on the Krumbein (1941) logarithmic “phi” scale, with skewness values representing the symmetry of the frequency curve: negative skewness is a decrease in symmetry around the mean grain size, and a increase in skewness represents a decrease in curve asymmetry (Masslink & Hughes 2003, Figure 4). Generally, decreased skewness and increased sorting along the direction of transport is expected in inter-tidal environments, but because other trends are possible (Case 3A: “FB+” *see* Poizot et al 2007), a single transport trend will not always accurately describe inter-tidal sediment transport (Pedreros et al 1996). Recent studies have invalidated Case 3

trends in the intertidal environment, indicating that Case 1 and Case 2 trends are most applicable to describe littoral transport patterns (Gao & Collins 1992, Kaczmarek et al 2005, Masslink & Hughes 2003, Pedreros et al 1996, Poizot et al 2007).

As grain-size parameters are environmentally sensitive, "noise" (chaos) may be introduced by comparisons between sampling sites in different environments resulting from excessively large sampling intervals (Poizot et al 2007). To reduce sample "noise", a 2D "point-to-point" approach has been developed by Gao & Collins (1992) using the McLaren & Bowles (1985) approach to produce a residual plot of sediment transport, which can be averaged to produce a more accurate representation of net transport direction in intertidal environments (Gao & Collins 1992, Poizot et al 2007). The Gao and Collins (1992) approach has been successful in predicting transport direction in both offshore and intertidal settings, but the approach has yet to be applied to a high-energy coastal setting, such as Monterey Bay (Pedreros et al 1996, Cheng et al 2004). The Gao & Collins (1992) approach relies on the creation of transport vectors between transects and determines average transport vectors in the direction of increased sorting, or decreased sample deviation from transect means (Figure 8, Gao & Collins 1992). For the purposes of this study, the Gao & Collins (1992) modification of the traditional one-dimensional McLaren & Bowles (1985) sediment transport approach for the inter-tidal will be used, assuming that transport will occur in the direction of Case 1 (CB+) or Case 2 (FB-) trends (Gao & Collins 1992, McLaren & Bowles 1985, Pedreros et al 1996, Poizot et al 2007).

1.4 Beach Composition

Beach sediments consist of sand or gravel particles of various sizes that are derived from a mix of terrigenous and continental shelf sources (Bird 2000,

Sallenger et al 2002, Smith et al 2005a). Siliclastic sediment is generated from the erosion and fluvial transport of material from rock outcrops. The volume of fluvial sediment loads is influenced by the steepness of the hinterland, the vigor of runoff produced by rainfall and the resistance of the source rock to weathering (Bird 2000). The products of outcrop erosion are both dissolved and non-dissolved minerals and can be divided into three fractions based on Optical properties: 1) framework minerals, which make up the majority of beach sand, divided into quartz, feldspar and lithic (QFL) fractions; 2) accessory minerals, which are present in less than 5% of igneous or metamorphic rocks, but can provide information on the initial formation and subsequent geological evolution of source rocks (Harlov & Forster 2007); 3) heavy minerals, which consists of all clastic grains with specific gravities greater than $\sim 2.9 \text{ g/cm}^3$ (Carver 1971, Table 1).

Beaches along the Monterey Bay are composed of a combination of siliclastic coastal sources, aeolian dune deposits and shell fragments from inner shelf and uplifted marine sandstones (Allen 1946). North of Santa Cruz, the coast comprises coastal terraces and numerous pocket beaches at the mouths of coastal streams. At Monterey, the coast becomes granitic and the shoreline is rocky with small pocket beaches (Galliher, 1932, Dingler & Reiss 2002). Sand sources include the Salinas and Pajaro Rivers, erosion of coastal cliffs and dunes and offshore sands (Dingler & Reiss 2002).

1.5 Provenance Studies

The nature of sediment supplied to beaches by rivers depends on the types of rock that crop out along the river channel and within the catchment basin, where runoff delivers surface material formed as rock outcrops decompose or disintegrate by weathering (Bird 2000). The origin of the various kinds of beach

sediment can be determined with reference to petrological and mineralogical characteristics, and to patterns of sediment flow produced by waves and currents on the coast and in nearshore areas (Bird 2000).

The framework composition of terrigenous sediment can be used to describe the maturity of coastal deposits, as distal sediment will be composed mostly of the minerals most resistance to weathering and mechanical break-up while in transport (Masselink & Hughes 2003). Older, poly-cyclic sediment is composed of only trace amounts of sandstone or other rock fragments, which tend to erode away faster than the quartz and feldspar. Coastal provenance can be estimated by examining the proportion of quartz in framework minerals, as more mature sediment will be composed of well-sorted quartz fragments with limited amounts of the less resilient feldspar and lithic fractions (Akarish & El-Gohary 2008, Dickinson 1984).

In addition to the framework composition of sediment, heavy mineral assemblages supply valuable information to understand erosion, grain motion, and alongshore drift processes in the coastal zone (Ergin 2007). Heavy minerals are concentrated along sections of eroding beach formations, such as cusps, and have higher resistance to weathering processes than other minerals (Frihy et al 1995). Due to the high resilience of heavy mineral grains, monitoring of heavy mineral deposition can serve as an excellent tracer for alongshore transport patterns at greater distances from river sources.

Most heavy minerals are sufficiently strong mechanically to resist loss by abrasion during transport, although some will be lost during temporary alluvial storage in floodplains (Tucker 1981). The heavy mineral fraction of beach sediment is denser, and finer grained than the lighter fraction, and the concentration of heavy minerals are expected to decrease with increased grain size, following the McLaren & Bowles (1985) approach for transport in coastal environments (Ergin 2007). Yancy (1972) used heavy minerals as a tracer for

sediment movement across the Monterey Submarine Canyon, and found that garnet derived from the Salinas valley were observed all along the central Monterey Bay coastline. Yancy (1972) determined that further study was needed before cross-canyon transport could be accurately assessed.

1.6 Description of Study Area

Central California has a rugged coastline characterized by a narrow continental shelf and coastal mountains cut with high seacliffs and narrow river valleys. The distribution of sediment varies across the shelf, with the coarsest sediment accumulating in shallow depressions in the surf zone, and at the shelf break, and the fine to medium sediment deposited offshore to depths of about 20 m (Storlazzi & Wingfield 2005, Anima et al 2002, Edwards 2002, Dinger & Reiss 2002). Monterey Bay is a unique high-energy crescent shaped embayment with distinct point sources (Salinas, Pajaro and San Lorenzo rivers) and sinks (Monterey Submarine Canyon) for sediment, and less distinctive sediment sources (sea-cliff and dune erosion). The Monterey Submarine canyon is considered the largest sink for sediment in the bay, with large amounts of fine-grained material flanking coarser deposits along the axis of the canyon head (Storlazzi & Field 2000, Eitrem 2002, Smith et al 2007, Thornton et al 2006, Paull et al 2005, Mitts 2004). Sediment transport dynamics within Monterey Bay are poorly defined because the North and South bay coastlines are oriented opposite to each-other, allowing a single swell to cause erosion and deposition along different directions in different regions of the bay (Figure 3, Eitrem et al 2002, Wolf 1970, Habel & Armstrong 1978). The majority of sediment input to the bay occurs during episodic winter storms and El Niño conditions, during which the majority of fluvial input is provided from the Salinas, San Lorenzo and Pajaro rivers (Best & Griggs 1991, Farnsworth & Milliman 2003). During drier conditions with reduced

river input, erosion of cliffs and other coastal promontories fuel the development of beaches, although the exact contribution of each source is still undefined (Smith et al 2005).

Monterey Bay comprises a relatively broad, shallow continental shelf in central California deeply bisected by the Monterey Canyon system (Smith et al 2007, Figure 3). The Monterey Canyon extends from the mouth of Moss Landing Harbor at least 90 km offshore to over 3 km depth (Smith et al 2005, Figure 3). Continental shelf sedimentation rates are a function of the amount, composition and distance to source of the source material, with more distant sources recorded as more mature, clay-rich deposits (Liu et al. 2008). Shifts in drainage locations and discharge intensity can cause significant changes in the depositional patterns of terrigenous material along the inner shelf of the Monterey Bay (Epping et al. 2008, Liu et al. 2008). In the 19th century, the Salinas River emptied into the bay near the present day location of Moss Landing, but at the turn of the 20th century, the Salinas River mouth was re-directed southward in 1908 for agricultural development (Dyke & Wasson 2005).

Monterey Bay is characterized by three oceanographic seasons: The Spring upwelling (March 13th-July 17th), Fall relaxation (July 24th-November 9th), and Winter storm (November 27th-March 15th) seasons (Largier et al 1993). The largest and most frequent swell approaches the Monterey Bay from the Northwest throughout the year, with the largest waves (2-10 m) recorded between October and May (Storlazzi & Wingfield 2005). Southern swells generated by South Pacific swells impact the Monterey coastline between April and October, but wave height (0.3-3 m) is small relative to the North Pacific Swells (Storlazzi & Wingfield 2005).

The current geology of the Monterey Bay area is the result of subduction and, transpressional tectonics that have occurred over the last 65 my (Greene et al 1991, Atwater 1970). The basement rocks now exposed in the Monterey Bay

region were created by the subduction of the Farallon Plate underneath the American plate, a process that stopped in the Early Miocene to late Oligocene (Atwater 1970). The basement rocks are divided into two fault-bounded terrains (or blocks): the Salinian Block, a fragment of Granodioritic basement thought to represent the former southern continuation of the Sierra Nevada batholith, and the Franciscan Block: low temperature metamorphic blueschist facies rocks located east of the San Andreas Fault (Howell et al 1985, Page 1982). The Salinian Block is a Pre-Cretaceous 40-70 km wide and 500 km long series of terrains originally formed by subduction of the Farallon Plate under the American Plate (Howell et al 1985, Page 1982). The Salinian Block is considered to represent displaced fragments of a late Mesozoic continental plutonic arc “Granitoids” wedged between the San Andreas Fault system to the east, and the San Gregorio-Sur Nacimiento Fault zone to the southwest (Figure 3, Page 1982). The Salinian block is overlain by a sequence of Pleistocene Aeolian sediments from the Aromas Sandstone formation (Greene 1970). The Aromas “red sandstone” terrace deposits are a Quaternary heterogeneous mixture of aggrading fluvial and alluvial-fluvial fan deposits, primarily arkosic composition with high concentrations of hematite and quartz (Allen 1946). Franciscan-type metamorphic complexes presently surround the Salinian Block (Page 1982). The Salinian Block encompasses both the Salinas River Valley and the San Lorenzo and Santa Lucia Ranges, providing Hornblende assemblages as well as large quantities of Granite/Granodiorites and trace amounts of metamorphic minerals, such as Sphene, to the Salinas River (Yancy 1972, Figure 6).

The Franciscan Block is a late Jurassic to mid Cretaceous subduction complex located east of the San Andreas Fault in the Diablo range, and west of the Sur-Nacimiento Fault Zone (Figure 5, Ernst 1993). The Franciscan complex is most visible in the eastern Diablo Range, and was created during periods of subduction-zone metamorphism accompanying the descent of the Farallon plate

under the North American Plate during the mid-Cretaceous (Figure 5, Ernst 1993). The Franciscan complex is composed of remnants of the Farallon Plate and turbidites deposited in the paleo-trench and then metamorphosed. The Franciscan complex includes large amounts of serpentine, glaucophane-lawsonite, schists, slates, cherts and greywacke and is a large contributor of lawsonite and glaucophane/jadeite to the Pajaro River (Figure 7, Yancy 1972). As a consequence of active faulting and the input of bedrock material from the Diablo, La Panza and Santa Lucia Ranges, the Pajaro and Salinas Rivers transport heavy mineral assemblages, unique to each river, into the Monterey Bay (Figure 6, Yancy 1972). Spinel, garnet and hornblende has been found to be common in the Salinas watershed, while larger amounts of augite, pyroxene and glaucophane can be found in the Pajaro watershed (Yancy 1972). Additional heavy mineral input to the bay is derived from erosion of igneous rocks from the Santa Cruz mountains, although sediment is localized around the San Lorenzo River mouth and input to the central bay is low (Weber et al 1999, Hicks & Inman 1987).

1.7 Purpose of study

The purpose of this study is to determine the alongshore transport patterns of the central Monterey Bay beaches on either side of the Monterey Canyon between the Pajaro and Salinas River mouths using a combination of mineral provenance (*see* Yancy 1972) and spatial grain size trend studies (*see* Gao & Collins 1992, Kaczmarek et al 2005, Masselink & Hughes 2003, Pedreros et al 1996, Poizot et al 2007). Petrographic and grain size analysis was performed on beach sediment collected from central Monterey Bay, between the Manresa and Fort Ord Dune fields in 2009 (Figure 7). Using Gao and Collins (1992) as a reference for transect layout, sediment was collected within nine transects, covering the foreshore coastal environment in central Monterey Bay (Figures 7,

8). Petrographic and grain size analysis was used to determine potential sources for littoral sediment, and examine the relationship between fluvial and bedrock geology for the Pajaro and Salinas watersheds. Sediment was collected during the three oceanographic seasons defined within Monterey Bay to account for changes in both the on-shore (rain-fall) and offshore (wave height and direction) climate (Drake et al 2005).

Previous studies have not used grain size trends to describe littoral transport in Monterey Bay, and the goal of this study was to use both grain size trends and petrographic data to describe seasonal changes to littoral transport patterns within Monterey Bay. This study will attempt to address the following questions: *1) What are the sources for littoral/beach sediment along central Monterey Bay? 2) What are the alongshore patterns of sediment migration from the Salinas and Pajaro watersheds? 3) How do seasonal changes affect the composition of beaches within central Monterey Bay?* Grain size and petrographic data are expected to record the deposition of pyroxenes along the Pajaro River and northern Monterey Bay, between Sunset and Moss Landing State Beaches (Yancy 1972). Spene and garnet are expected to be deposited along the Salinas River State Beach from the Salinas River (Yancy 1972). Seasonal changes in both approaching swell direction and intensity are expected to affect the composition of beaches along the central Monterey Bay, with stronger NW winter swells causing southward dispersion of sediment from the Pajaro watershed along the Salinas State Beach. Sediment from the Salinas watershed is expected to be dispersed northward during periods of W-SW swell. Mixing of sediment from the Pajaro and Salinas watersheds is implied if Garnets and Pyroxenes are found within both northern and southern transects, which is expected during winter storm events when high wave energy disperses large amounts of sediment from both watersheds along the coast.

METHODS

Experimental procedures were designed to determine seasonal changes to the provenance of sediment in central Monterey Bay using a combination of petrographic and grain-size data. Sediment samples were collected from nine transects, covering the coastline between the Manresa and Fort Ord Aromas sandstone dune fields (Figure 7). Sampling was performed five times covering the late winter, early spring, summer and fall seasons in 2009 (Table 2). Sampling transects followed the procedure used by Gao & Collins (1992), and grain-size trends were calculated using a modification of the 2D method developed by McLaren and Bowles (1985). Samples were returned to Moss Landing Marine Laboratories where they were processed for grain size and petrographic analysis (40 g subsamples were used for each, see below). Particle size data was obtained using a Beckman-Coulter Laser Particle Sizer and petrographic thin sections were prepared for petrographic analysis. Transport vectors and petrographic data were used to address questions regarding sediment provenance and coastal redistribution patterns.

2.1 Sampling Strategy

Alongshore transport trends were generated from swash-zone grain size trends and the provenance of heavy minerals from the Salinas and Pajaro watersheds. CDIP Buoy #156 (stationed at the outer canyon at 36°45'0" N 122°1'12" W) was used to measure incoming swell direction, amplitude, and frequency, with plots generated from 48 hour periods around each sampling date. Due to the ephemeral nature of sediment input to the central Monterey Bay, sediment samples were collected one week after coastal storm events, signified by significant wave height greater than 10 m, high terrestrial precipitation and significant increases in wave energy. Summer samples were

collected towards the end of the Spring upwelling season to capture a representation of coastal composition during dryer inland conditions (Table 2, Drake et al 2005).

112 sediment samples were collected from a total of 28 transects using a modification of the Gao and Collins (1992) sampling method (Table 2, Figure 8). Each transect was composed of four sample sites spaced 15 m apart starting at the swash zone moving linearly towards the back-shore (Figures 1, 8). To determine the potential contribution to littoral transport from the San Lorenzo river and the Aromas sandstones in the North and South Bay, 4 additional sediment samples were collected for petrographic analysis: San Lorenzo River mouth, Seacliff State Beach, Manresa State Park, and Fort Ord State Dune field (Table 2, Figure 7). The petrographic composition of the San Lorenzo river was determined from Swash zone samples collected at the San Lorenzo River mouth and at a Seacliff State Beach site 1 km to the east of the river. Aromas samples were selected at the exposed 30 - 40 m alluvium base layer of the dunes at Manresa and Fort Ord sites to capture a representative of the roughly 183 m thick Aromas deposits, which represent Quaternary sedimentation patterns in central Monterey Bay (Allen 1946). At each sample site, the top 1 – 2 cm of beach sand was removed before taking 500 g of sample to reduce the effects of diurnal variation (Gao 1996, Storlazzi & Jaffe 2002, Clark & Osborne 1982).

In order to determine the typical mineral assemblages of the Pajaro and Salinas River channels and compare it with Yancy's analysis (1972), pebble and sediment samples were collected and identified from the Upper Pajaro and Salinas Rivers, near Aromas and Marina, California in February 2009 (Figure 7). Two sediment samples were collected from the upper Salinas and Pajaro channels for petrographic analysis (Figure 7).

2.2 Grain size analysis

Sediment samples were returned to the lab and split into two approximately 250 g aliquots, with one aliquot dried using a Precision Model G520 Series Convection oven at ~100 °C over-night or until dry. The second 250 g aliquot was kept in storage unless additional sediment was required for analysis. Wet and dry weights were measured using a Scout Pro 400 g scale tared to individual beaker weight. After drying, samples were placed in a desiccator until re-weighed and then split into coarser and finer than -1 phi fractions, with each fraction weighted again. Material finer than 2 µm was split again using a sediment splitter into two 40 g samples, one sample for petrographic analysis, and one sample for grain size analysis.

One 40 g sub-sample was analyzed using the Beckman-Coulter LS I3 320 Laser Diffraction Particle Size (LPS) Analyzer dry module (0.4 µm to 2000 µm). The Fraunhofer Optical theory was used to analyze particles much larger than the wavelength of light, or when the sediment was highly absorptive, which is typical for medium - to - very fine sand (Coulter 1994). Particle size distributions were scaled using the graphical method of Folk & Ward (1957). Statistics can be calculated either arithmetically or geometrically (logarithmically) based on either the value of a channel center or the logarithm of that value (Coulter 1994). For the purposes of this study, frequency plots were generated using log-normal (geometric) scaling. Geometric statistics were more appropriate for particle size distributions that were closer to log-normal, which was more representative of the characteristics of beach sediments (Coulter 1994, Blott & Pye 2001).

2.3 Thin section petrography

The mineral and lithic content and textural relationships within coastal sediment samples were described through petrographic analysis of 31 thin sections obtained from Swash zone samples (Table 3). Thin sections were generated only from Swash zone

samples because Swash zone samples were key representatives of littoral sediment transport and coastal deposition after periods of high terrestrial run-off (Bird 2000, Elfrink & Baldock 2002). Swash zone sediment samples were ground down to 0.020 mm thin sections using a Hillquest Thin Section machine, and final sample slides were preserved using a Norland Optical Adhesive (83H). The Optical properties of framework, accessory and heavy mineral fractions of each thin section were identified using a LEICA DM EP Petrographic microscope (Table 4). The 40x objective lens was used to identify general textural characteristics, such as sorting and angularity, while the optical characteristics were identified using the 63x objective lens with the upper polarizer (analyzer) and Amici-Bertrand lens filters. The key optical parameters used to identify minerals include pleochroism, cleavages, birefringence and extinction angle: pleochroism is the alteration of mineral color in plain polarized light (PPL) as the stage was rotated, and is caused by changes in the absorption of polarized light; cleavages are areas of weakness along the crystallographic plane where chemical bonds are weaker and the mineral is most likely to break; birefringence is a measure of difference between the fast and slow light rays as they pass through the mineral and upper polarizer; and the Extinction Angle (EA) is the measure between the cleavage direction or habit of a mineral and the angle when Cross-polarized light dims.

Mineral abundance for each thin section was described using a random-plot 200 grain point-count method: using the 40x objective lens, clasts found in or near the center of the cross-hairs were identified based on the Optical properties listed in table 4, then the slide was randomly moved and the procedure was repeated until 200 grains had been counted, providing a sufficient representation of the composition of each thin section (Figure 9, Table 4, Alekseeva & Hounslow 2004, Blott & Pye 2001). Point counts of framework minerals for each sample have been organized into quartz, feldspar and lithic fractions and plotted as ternary diagrams to generate estimates of sandstone provenance (Dickinson & Suczek 1979).

For the generation of QFL plots for each sample, sandstones are considered lithic fragments, with plagioclase and alkali feldspars grouped together with microcline in the 'feldspar' group. Foliated or microgranular metaquartzite (chert) fragments are abundant in some rocks, and have been found common in both the Salinas and Pajaro watersheds (Dickinson 1984, Yancy 1972). Severe compaction of metaquartzite fragments may develop polygonal textures within single quartz crystals, which then resemble composite or aggregate grains but are not lithic fragments, and microcrystalline quartz will not be counted as lithic fragments for this study, following the classification scheme of Dickinson (1984). Classification of lithic fragments was restricted to microcrystalline aphanitic materials containing no crystals larger than the matrix limit (0.0625 mm), with larger crystals counted as separate mineral grains (Dickinson 1984). Feldspars were identified based on twin lamellae (both Albite and Carlsbad), perfect cleavage intersecting between 93-94° and low birefringence colors (with the exception of orthoclase, which was distinguished from quartz based on cleavage angles) (Figure 20). For the purpose of this study, blueish-green pleochroism and a range of extinction angles between 35-130° identify the common amphiboles, including the heavy minerals hornblende and glaucophane (Table 4). Additional chain-silicate heavy minerals, such as sphene, were identified by orthorhombic (three unequal axes at right angles) structure and high birefringence colors (Table 4).

2.4 Upper Watershed Pebble Analyses

Pebble samples from the upper Pajaro and Salinas River channels were collected from or near point-bar deposits, representing the most likely location of deposition within the river channel (Boggs 2006). Nineteen pebbles were collected from the point-bar of the Salinas River channel near Marina, CA, and sixteen pebbles were collected from the Pajaro River channel near Aromas, CA (Figure 7). Intrusive igneous rocks were identified by phaneritic textures, and include granites and diorites (Mottana et al 1978). Extrusive

igneous rocks were identified by aphanitic, glassy or porphyritic textures, and include andesite and basalt. Granodiorite was identified based on higher quartz and plagioclase feldspar content, distinguishes it from granite rocks (Mottana et al 1978). Basalt was identified based on fibrous hornblende and feldspar masses inbedded in a very fine grained mafic texture. Andesite was identified based on felsic, porphyritic texture with very little quartz. Arkose fragments were identified by their aphanitic texture with very fine grained silicious matrix and microscopic bedding structures. Pegmatite fragments were identified by their coarse-grained, quartz and mica rich texture with interlocking phaneritic grains. Diorite fragments were identified by their dark grey-to-black phaneritic texture with plagioclase feldspar, hornblende prisms and tabular biotite with trace amounts of pyroxene. Dacite was distinguished from diorite because of its aphanitic texture. Arenite was identified as a clastic sedimentary rock with trace amounts of fossils and rounded to sub-rounded rock fragments.

2.5 Grain size trends

Sediment transport vectors were determined from samples collected between dune and river transects based on the methods of Gao and Collins (1992). The estimation of transport vectors involves the measurement of changes in skewness and average grain size of samples between transects. Dimensionless trend vectors were attributed to the site with the higher sorting coefficient (a decrease in the variance between the mean grain size between the two sites), and were calculated within a critical maximum distance (D_{cr}) between transects so that $D_{cr} \sim 1$ km (Figure 8). A final transport direction between transects was calculated by averaging the trend vectors between transect sample locations (Figure 8, Gao & Collins 1992, Pedreros et al 1996). This study relies on Gao & Collins (1992) 2D “vector” interpretation of the likely inter-tidal sediment trends presented originally by McLaren & Bowles (1985), which uses one of two trends, Case 1 (CB+) and Case 2 (FB-), to describe the most probable indication of sediment movement within

a near-shore environment (Gao & Collins 1992, Masslink and Hughes 2003, McLaren & Bowles 1985, Pedreros et al 1996,). Transport between sites A and B was likely if both skewness and grain size decrease or increase along with improved sediment sorting (Gao & Collins 1992, Figure 8). Two additional trends, CB- and FB+, were considered only if transport direction was supported by heavy Mineral counts from Swash zone samples (Poizot et al 2007, Yancy 1972).

An independent 2-sample “T-test” was performed to test differences in the arithmetic means and skewness of samples between Transect locations to generate an estimate of transport direction (Equation 1). For the T-test, a 95% confidence interval was assumed along with 6 degrees of freedom, comparing sediment samples between transects. The data were assumed to be independent and normally distributed. The null hypothesis is that the the means between transects were not equal. If the means between transects were significantly different, transport was in the direction of decreased sample variance from sample mean (improved sorting) (Gao & Collins 1992, Pedreros et al 1996, Poizot et al 2007).

$$t = \frac{\mu_A - \mu_B}{S_{\bar{x}}}$$

Equation 1: Paired-sample t-test to determine if differences exist between the means of transect A and B. S_x refers to the grand standard deviation and was calculated according to Equation 2. Null hypothesis was that there were no differences between the means of two independent samples. For the purposes of this project, the means reflect independent sample locations within transects A and B.

$$S_{x1x2} = \sqrt{\left(\frac{(S_{x1})^2 + (S_{x2})^2}{2}\right)}$$

Equation 2: Grand Standard Deviation from Transect 1 to Transect 2 (x_1, x_2). S = standard deviation.

RESULTS

In this section, grain size and petrographic data are presented from the January - March (winter), July (summer) and October (fall) sampling seasons performed in 2009. Grain size data (mean, median, mode, skewness and standard deviation) are presented from winter, summer and fall Pajaro and Salinas Transects first to detail seasonal textural variations (Table 5). Grain size data are compared between swash-zone and fore-dune samples and dimensionless trend vectors are plotted between Pajaro and Salinas transects; seasonal shifts in these patterns are highlighted for each season (Table 6). The framework, accessory and heavy mineral composition is detailed for Pajaro and Salinas transects, along with the oceanographic conditions for each season (Tables 7-9). Finally grain size and petrographic data are presented from samples collected in the upper Pajaro and Salinas channels (Table 5D, 7D, 11). The data collected from samples in the San Lorenzo River and Aromas Sandstones are listed separately from the Pajaro and Salinas data (Tables 5D, 7D, 10).

3.1 Grain Size Data

The average grain size of sediment found along the central Monterey Bay coastline decreased between winter and fall seasons, with the coarsest material found during winter surveys along the Salinas State Beach (Table 5A-5C, Figure 10). The highest percentage of fine-sand (26.38% between 125 & 250 μm) and coarse-sand (31.1% between 500 & 1000 μm) was recorded from Pajaro transect samples during the October survey (Table 5A-5C). The average grain size of Pajaro transect sediment decreasing between winter and summer transects (Table 5A-5C). The finest sediment was found from within the October transect 1 km north of the Pajaro River Mouth (PRN), and

the coarsest sediment was found from sediment collected at the berm within the July Salinas River Mouth (SR4) transect (Table 5A-5C, Figure 11).

The highest standard deviation was recorded in the October transects, and the lowest standard deviation was recorded during winter surveys (Table 5A-5C, Figure 11). The mean grain size and standard deviation of Pajaro berm sediment decreased between winter and summer seasons, with the coarsest berm sediment recorded 1 km north of the Pajaro River Mouth (Table 5A-5C, Figure 12). The grain size of Salinas berm sediment increased along with a decreased standard deviation between winter and fall seasons, with the coarsest berm sediment recorded from the berm surrounding the Salinas River mouth during the July survey (Table 5A-5C, Figure 12). Two-sample t-tests between the means of adjacent transects produced the t-values during July surveys, and the highest t-values during winter surveys (Table 6, Figure 13). Sediment collected during the October surveys was highly positively skewed with the lowest values of kurtosis (frequency-curve peak) compared to sediment from winter and summer surveys (Table 5A-5C, Figures 14-16). During winter and summer surveys, Pajaro sediment was more positively skewed than Salinas sediment, with a trend of increasing skewness between PR1 and PR3 (Figures 14-16, Table 5A-5B). During the October survey, sediment along the Salinas State Beach was more positively skewed than sediment along the Pajaro beach, with a trend of decrease skewness from SR1 to SR5 transects (Table 5C, Figure 14).

3.2 Vector Trends

Net transport vectors between swash-zone and fore-dune samples were fitted to Case 1 and Case 2 trends between Pajaro and Salinas transects, producing seasonally-averaged southward transport trends between Pajaro transects and northward transport trends between Salinas transects (Table 6, Figure 17). Changes in the skewness, grain size and standard deviation indicated southern transport between winter PR1 and PR3 transects (Table 6, Figure 17). Winter Salinas sediment did not produce conclusive trends

for SR2-SR5 transects, but changes between SR2 and SR1 support Case 2 northern transport trends (Table 6, Figure 17). Northern transport between PR4 and PR3 is demonstrated during both winter and summer surveys, but a southern transport between is plotted between PR3 and PR4 during the October survey (Table 6, Figure 17). No trend was found between PR2 and PR1, and between SR4 and SR5 during July surveys (Table 6, Figure 17). July Salinas trends indicate a northern transport between SR4 and SR2, with a southern transport between SR1 and SR2 (Table 6, Figure 17B). A shift from southern to northern transport is plotted between PR1 and PR2 when comparing the July surveys with the October surveys, but consistent southern transport is plotted between PR2 and PR4, and SR4 to SR5 during the October surveys (Table 6, Figures 17B-17C). Case 1 or Case 2 trends were not able to generate estimates between October SR3 and SR4 and SR5 surveys.

The dominant swell direction (observed during ~ 80% of days between January and March) was from 292.5° to the Northwest during the Winter 2009 sampling season (Figure 18). Between July 1st and July 31st, the dominant swell originated from 292.5° NW, but 1-1.5 m waves were observed from 225° SW during ~ 60% of days in between July 1st and July 31st (Figure 18). Between October 1st and October 31st, the dominant swell originated from 292.5° NW, and wave height peaked between 4 and 5 m from swell approaching from 270° W (Figure 18).

3.3 Petrographic Data

Sediment within Pajaro transects was composed of mostly quartz, with the highest quartz values recorded from the swash zone of PR1 during the October survey (Table 7). The abundance of quartz increased in both Salinas (33.2% to 39.9%) and Pajaro (39.2% to 49%) sediment between winter and fall surveys (Table 7, Figure 19). The highest abundance of feldspar (including both potassium and plagioclase) was found along the Salinas State Beach during the July surveys, and the abundance of feldspars did not

significantly decrease (30.3% to 29.5%) between July and October surveys (Table 7). The highest abundance of lithic fragments were found along the Salinas State Beach during the July surveys, and the abundance of lithic fragments within the central Monterey Bay did not significantly increase (21.8% to 23.9%) between winter and fall surveys (Table 7). Intrusive rock fragments were the most common lithic fragment found along the central Monterey Bay, with highest amounts found along the Salinas State Beach (Table 8, Figure 20). Higher amounts of sandstone fragments were found from Pajaro transects, with the highest amount of sandstones found within the swash zone of PR4 during the October surveys (Figure 20C).

The accessory mineral fraction of sediment collected from the swash zones of central Monterey Bay transects was composed of chlorite, hematite, biotite, opal and hornblende, with the highest concentration of both chlorite and hornblende found from Swash zone samples collected from the PR1 transect (Figure 21, Table 9). The heavy mineral fraction of central Monterey Bay Swash zone samples was composed of garnet, glaucophane, jadeite, titanite / sphene, rutile, clinopyroxene and orthopyroxene (Figure 21, Table 9). The highest concentration of heavy minerals was found from the swash zone sample within the winter PR1 transect, and the lowest concentration was found from the swash zone sample within the SR4 July transect (Table 9, Figure 22). The concentration of heavy minerals did not significantly decrease (15.2% to 11.4% of total minerals counted) from winter to summer surveys and there was no significant increase (11.4% to 15.7%) between summer and fall surveys (Table 9). Pyroxene was the most common heavy mineral identified from the Pajaro transect samples, with the highest concentration found from the swash zone of the winter PR2 transect (Table 9, Figure 22). The number of pyroxenes found within Salinas transects increased (24.7%) between winter and fall transects, with the highest pyroxene counts found from the fall SR5 swash-zone (Table 9). Garnet and sphene were the most common heavy minerals found from Salinas samples, with the highest concentration found from the swash zone of the winter SR4 transect (Table 9, Figure 22). Pyroxene was found in the swash zone of both Pajaro and

Salinas transects in all seasons (Table 9, Figure 22). Trace amounts of garnet (a average of 4% of total composition) were found in the swash zone of February PR1, July PR4 and October PR1 transects (Table 9). Garnet was found in the swash zones of winter January SR4, July SR3 - SR1, October SR5 and SR3 Salinas transects (Table 9). The Salinas transects contained higher (6.8% vs 4.2%) amounts of garnet then found along Pajaro transects, and the amount of garnets increased (7.1 - 9.1 %) between winter and summer Salinas transects (Table 9).

3.4 Upper Salinas and Pajaro data

Two sediment samples were collected from the upper Pajaro and Salinas channels and analyzed with thin-section petrography to determine their grain size and heavy mineral composition (Figure 7, Tables 5D, 10, 11). The average grain size of upper Pajaro channel sediment was higher then Salinas channel samples, and the Salinas channel had higher standard deviation, skewness and kurtosis (Table 5D). The Salinas channel had higher amounts of fine-sand, medium-sand and coarse-sand then the Pajaro channel (Table 5D). The Pajaro channel had a higher lithic content then the Salinas channel, which was mostly composed of higher amounts of quartz and feldspar (Table 7D, Figure 19).

The accessory mineral fraction of sediment collected from the upper Pajaro and Salinas channels was composed of hornblende and biotite, with the highest amount of accessory minerals found from the Salinas River channel (Table 10). The heavy mineral fraction of the upper Pajaro River sample is composed of chloritoid, clinopyroxene and orthopyroxene (Table 10). The heavy mineral fraction of the upper Salinas River sample is composed of garnet, glaucophane, chloritoid, epidote, clinopyroxene and orthopyroxene (Table 10). Orthopyroxene is the most commonly counted heavy mineral in both upper channel samples (Table 10).

Nineteen pebbles were collected from the point-bar of the Salinas River channel near Marina, CA, and sixteen pebbles were collected from the Pajaro River channel near Aromas, CA (Figure 23, Table 11). Granodiorite was the most common pebble found in the Salinas channel, with trace amounts of diorite, dacite, granite, arenite, basalt and arkose sandstones also identified (Figure 23). Basalt fragments were the most common pebble found from the Pajaro channel along with trace amounts of granodiorite, andesite and arkose sandstones (Figure 23, Table 11).

3.5 Aromas Sandstone and San Lorenzo River

The average grain size, framework, accessory and heavy mineral composition of sediment from the Manresa and Fort Ord dune sites is recorded from February 2010 samples taken at the base of each dune. The Aromas sandstone unit at the Fort Ord Dune field had a higher grain size, standard deviation and kurtosis than measured from the Manresa Dune field (Table 5D). The Manresa Dune sediment was composed of higher amounts of fine-to-medium sized sand particles than the Fort Ord Dune sample (Table 5D). The Fort Ord Dune sample had higher amounts of framework minerals (quartz, feldspar and lithic fragments) than the Manresa Dune sample (Table 7D). The Manresa Dune sample was mostly composed of lithic fragments and the Fort Ord Dune sample, which was mostly composed of quartz (Table 7D). The accessory mineral fraction of the Manresa Dune sample were composed of hematite, hornblende, glauconite, biotite and opal; no glauconite or biotite was identified in the Fort Ord sample (Table 10). Hornblende was the most common accessory mineral identified in each sample (Table 10). The heavy mineral fraction of the Aromas Sandstone samples is composed of chloritoid, clinopyroxene and orthopyroxene, with the highest amounts of heavy minerals found in the Manresa sample (Table 10). Trace amounts of garnet (1.2%) and augite (6.1%) were identified from the Manresa dune sample, but not in the Fort Ord sample

(Table 10). Clinopyroxene and orthopyroxene were common (27% & 50% of total heavy minerals counted) heavy minerals in both Aromas Sandstone samples (Table 10).

The average grain size, framework, accessory and heavy mineral composition of samples collected from the San Lorenzo River mouth (SLRM1) and 1 km south-east of the San Lorenzo River mouth (SLRM2) is recorded from October 2009 samples. The grain size and kurtosis increased between SLRM1 and SLRM2 Swash zone samples (Table 5D). SLRM1 had the highest quartz and fine-to-medium sand sized sediment of San Lorenzo samples, and half of the grains counted in SLRM2 were classified as lithic fragments (Tables 5D & 7D). The accessory mineral fraction of SLRM1 sediment is composed of hornblende, hematite and biotite, with hornblende the most common (Table 10). The only accessory mineral identified from SLRM2 sediment is glauconite (Table 10). The heavy mineral fractions of both SLRM1 and SLRM2 are composed of chloritoid, clinopyroxene and orthopyroxene (Table 10). Orthopyroxene was the most common heavy mineral in both SLRM1 and SLRM2 samples (Table 10).

DISCUSSION

During the winter 2009 surveys, both the Pajaro and Salinas coastlines were characterized by broad, gently sloping profiles with little-to-no visible berms, composed mostly of fine-grained feldspar and lithic fragments, which has been observed during high-energy winter months when storm-waves deposit coarser berm sand into offshore bars (Figures 10, 19 & 24, Dingler & Reiss 2002). High angle sloping berms were present along the Pajaro and Salinas coastlines during the July sampling season, and transects along the Salinas State Beach covered both cusp and horn structures (Figure 25). During the October sampling season, the beach adjacent to the Pajaro River Mouth was characterized by a small berm and a gradual sloping profile, consistent with transitional oceanographic energy regimes (Figure 26, Dingler & Reiss 2002). The Salinas beach morphology was similar to the Pajaro with the exception of a large berm that blocked the mouth of the Salinas River from the ocean (Figure 26).

The combination of petrographic and grain-size data offers us an in-depth look at the sources as well as the seasonal variability in the transport patterns of coastal sediment in central Monterey Bay. The composition of beaches in the central Monterey Bay is defined by the lithic and heavy mineral assemblages of the Pajaro and Salinas Rivers. The lithic composition of transect sediment can be interpreted as a shift from recycled to volcanic arc provenance between the Pajaro and Salinas sediment, as Salinas transects are composed of higher amounts of volcanic rock fragments than found within Pajaro transects (Dickinson & Suczek 1979). The results of the littoral transport trends together with grain size and petrographic data sets are discussed separately for the Pajaro and Salinas transects. In general, grain-size data suggests a year-round southward transport of sediment from the Pajaro River mouth. Petrographic and grain-size data also suggests that seasonal shifts imply changes in swell energy and direction cause a localized northward transport of sediment from the Salinas River Mouth. The data from this study

supports the hypothesis that beach sediment sources switch from river to offshore bars between winter and summer conditions (Bird 2000, Masselink & Pattiaratchi 1998, Dingler 2002, Cloud 1966). Wave height and direction are interpreted qualitatively in relation to the general orientation of the central Monterey Bay coastline to determine the potential direction of littoral transport.

The distribution of heavy minerals in both transects provided further evidence of littoral sediment provenance. Garnet was not found from samples collected in the upper Pajaro River channel, and only trace amounts were found in the lower fluvial deposits of the Aromas sandstones, so garnet is assumed to be a signature distinct to the Salinas watershed and serves as a good tracer of Salinas River sediment (Tables 9 & 10). Pyroxenes are not a common occurrence within the Salinas watershed (both river and beach sediments), but common in sediments collected from Pajaro transects. The amount of heavy minerals found along both Pajaro (22.5% to 10.8%) and Salinas transects (7.83% to 12%) varies between winter and summer seasons (Table 9). In general, sediment collected from Salinas transects was coarser with higher amounts of igneous rock fragments and garnet than found along Pajaro transects (Table 9). The trace (~4% of total heavy minerals counted) amounts of garnet found within Pajaro transects in winter and fall seasons indicates the possibility of limited northward transport of Salinas material, or input of sediment from sources outside of the Pajaro or Salinas watersheds, but garnet is not present in sufficient quantities to provide conclusive evidence of cross-canyon transport (Table 9). Overall, the distribution of heavy minerals along The central Monterey Bay beaches suggests a year-round supply of pyroxenes, chert and hornblende from terrigenous sources. The main sources for heavy minerals are the Salinas and Pajaro watersheds, although petrographic and grain size data suggest that the Aromas sandstone samples at Fort Ord and Manresa are an additional possible source.

Increases in the abundance of pyroxenes (orthopyroxene, clinopyroxene, augite and jadeite) relative to total mineral counts within the Salinas Beach transects during the summer suggest either the deposition of heavy minerals from Aromas sandstone sources,

or the resorting of material by offshore bar progradation. Sediment deposited in offshore bars and promontories between the tributaries of the Monterey Bay Submarine Canyon can be a coastal source of selected types of minerals having different provenances, and presents a scenario of possible cross-canyon transport which would explain the increases in summer pyroxenes within Salinas transects.

4.1: Seasonal changes in grain-size

Changes in the sorting of beach sediment was recorded in order to determine the effect of seasonal shifts of wave energy on the beaches of central Monterey Bay. Seasonal shifts in the variance (sorting) between transect grain-sizes shows that in Monterey Bay, variability in the composition of coastal sediment is related to episodic winter storm events. Winter storms create large amounts of river discharge, which distribute poorly sorted sediment along beaches near the river mouths. Sorting is expected to improve between winter and summer seasons due to the re-sorting of coastal sediment by waves (Bird 2000, Dingler & Reiss 2001, Hoefel & Elgar 2003). High seasonal variance in the grain size of beach sediment around the Pajaro and Salinas river mouths has been recorded before and after El Niño storm events, and seasonal changes in the variance can be used to identify changes between on and offshore sediment sources (Bird 2000, Dingler & Reiss 2001). Increases in the mean grain size and variance of mean grain sizes between Pajaro and Salinas transects from winter to summer seasons correlate with the seasonal on-shore movement of offshore bar deposits (Figure 13, Tables 5 & 6, Bird 2000, Sedrati 2007, Landry et al 2007, Kaczmarek et al 2005).

Offshore bars are well-sorted river-derived medium-to-coarse quartz and feldspar-rich sand, and the increase in quartz and feldspar between winter and summer Pajaro and Salinas transect sediments can be explained by the movement of these coarser sediments from the offshore bars to the beach (Bird 2000, Sedrati 2007, Tables 5 & 7). Despite the removal of fine-grained sediment to off-shore bars during winter months, the grain size of

beach sediment is expected to increase during the summer as the coarser off-shore bar dune crests are re-deposited along the foreshore environment (Landry et al 2007, Hoefel & Elgar 2003, Figure 1). The shoreward movement of coarse grained (0.125-0.5 mm) offshore sediment during periods of decreased wave energy has been observed in previous studies (see Frihy & Dewidar 2003, Hoefel & Elgar 2003) and even though offshore bars are typically well sorted (see Landry et al 2007), the mixing of coarse-grained sediment deposited along the dune crests of offshore bars with the finer grained beach sediment could account for the increased variance in grain sizes observed between winter and summer Pajaro and Salinas transects.

The winter coastline was characterized by a gently sloping beach composed of a homogenous mix of river sediment composed of higher amounts of heavy minerals, and lower variance between the mean grain sizes of transects than samples collected in July and October (Figures 13 & 24, Tables 5 & 7). As berm facies developed between 30 and 45 m from the swash zone along Pajaro and Salinas transects between the winter and summer surveys, the standard deviation from the mean grain size increased between transect samples collected 30 m from the swash zone, indicating that the sediment was becoming more poorly sorted (Figures 12 & 25, Table 5). The development of poorly sorted berms within summer Pajaro and Salinas transects correlates with the re-deposition of offshore bar sediment along developing berm facies, as less energetic oceanographic conditions (wave height and period) re-distributes bar sediment along the coastline (Hoefel & Elgar 2003). Sediment collected during the October survey was a mix of offshore and river sources, as variance in grain sizes were lower than summer, but higher than winter surveys and heavy mineral abundances increased, indicating an increase in river sediment sources (Figure 13, Tables 6 & 7).

4.2 Littoral Transport Trends

For the winter sampling season, the results of the grain size analysis showing a southward littoral drift of sediment between Pajaro transects occurred during high frequency northwest swells (Figures 17 & 18). Despite a local northward transport of sand between winter SR2 and SR1, vector analysis of the majority of winter and fall Salinas transects is inconclusive (Figures 17 & 18, Table 6). Despite the inconclusive result of the majority of vector analysis performed between Salinas transects, the trace amounts (~2-8% of total heavy minerals counted) of garnet found within the Pajaro transects in winter and fall sampling seasons indicates northward transport of sediment derived from the Salinas watershed, or input of sediment from sources outside of the Pajaro or Salinas watersheds, such as sea-cliff erosion (Table 9). The Salinas River seems the most likely source of Pajaro transect garnets because higher amounts of garnet have been found around the Salinas River mouth and the upper Salinas River channel during the high discharge winter season, and the scarcity of garnets (~ 0.6% of Aromas sandstone totals) from San Lorenzo and Aromas Sandstone samples (Tables 9 & 10).

As described before, the July transect sediment samples were coarser and more poorly sorted (higher standard deviation and variance between mean grain sizes than winter and fall samples) indicating that summer sediment supply could be from offshore bars instead of direct deposition from the Salinas and Pajaro rivers, but the occurrence of a dominant W-SW swell and the results of the grain size trends previously documented suggest that littoral drift can transport sediment northward locally along the Salinas coastline (Figures 17 & 18). Overall, grain size and heavy mineral data from the summer transects indicate the possible mixing of Pajaro and Salinas sediment as W to SW swells generate southward transport along the Pajaro coastline and northward transport localized along the Salinas coastline (Figure 17). W to SW swells are common during the summer in Monterey Bay, and besides local variations due to headland promontories and the presence of the submarine canyon, the 2009 summer swells hit the south-bay coastline

approximately at a angle of $\sim 240^\circ$, which would be sufficient to fuel northern transport along the Salinas State Beach (Storlazzi & Wingfield 2005, Komar 1974, Figures 17 & 18).

Grain size trends supported weakly by wave data suggest two littoral transport patterns in central Monterey Bay: A year-round north bay (or “Pajaro”) cell funneling sediment from the Pajaro River Mouth southward; and a seasonal south bay (or “Salinas”) cell which, over time, might produce a net northward transport of sediment from the Salinas River when W-SW swells dominate. Currently estimated Salinas and Pajaro cell littoral transport patterns require a north - northwest breaking wave angle between 330 and 280 degrees, which is common in the Monterey Bay (Storlazzi & Wingfield 2005). Northward littoral transport of sediment from the Salinas River is supported by summer grain size trends, past evidence of the deposition of lithic arenites derived from the Salinian block along the Monterey Submarine Canyon axis, and garnets found along the Pajaro coastline between January and October 2009 transects (Mitts 2002, Table 9).

Grain size, heavy mineral data and previous studies of sediment deposition along the head of the Monterey Bay Submarine Canyon (*see* Mitts 2002) suggest that littoral drift moves sediment from the Pajaro and Salinas Rivers into the tributaries around the head of the Monterey Submarine Canyon. The Monterey submarine canyon receives over 320,000 m³/yr of littoral sand and gravel, and sediment transport can be generated by episodic storm events which can re-suspended sediment trapped along canyon promontories (Chesser & Peterson 1987, Smith et al 2007, Smith et al 2005). The deposition of large assemblages of heavy minerals along offshore promontories has been observed in previous studies (*see* Frihy & Dewidar 2003), and the coastal distribution of heavy minerals along Monterey Bay suggests similar depositional patterns along the Monterey submarine canyon (Table 9, Figure 22). Seasonal storm-waves may re-suspend sediment trapped along canyon tributaries, allowing sediment to bypass the canyon axis, and the high residence times of sediments in tributary promontories around the canyon

head delays the episodic removal of river sediment down the canyon axis (Chesser & Peterson 1987, Smith et al 2007, Smith et al 2005). The transport of sediment around the canyon axis has been suggested in previous studies (*see* Smith et al 2005, Xu et al 2004, Yancy 1972), but to date no direct evidence exists to support or deny the possibility of cross-canyon transport.

4.3: Upper Watershed Analysis

During the Summer and Fall seasons, both the upper Pajaro and Salinas River channels were found to be completely dry, despite outflow at the Pajaro River Mouth, and ample water dammed by a large berm at the Salinas River Mouth. The central Monterey Bay is dotted with large patches of farmland and the draining of the upper watershed could be caused by the high water demands of the extensive irrigation network. Despite the lack of flow in the upper watersheds, heavy minerals, dominated by amphiboles and pyroxenes, were found from samples collected along point-bar deposits from the dried channels (Table 10).

Extrusive igneous rocks, basalt and andesite, were found common among the dried Pajaro River bed, while intrusive igneous (granodiorite) and sedimentary (breccia and conglomerates) rock fragments were common deposits along the Salinas River Channel (Table 10, Figure 23). Most mafic rocks, including basalt, are composed of high amounts of pyroxene (primarily orthopyroxene), as well as amphiboles (primarily hornblende), which supports the high amounts of pyroxene identified along the Pajaro coastline. Both the upper Pajaro and Salinas River channel sediment samples were dominated by chert, hornblende and pyroxenes (Table 10). Hornblende and biotite are minerals commonly found in granodiorites, which were common among the rock fragments identified along the upper river channel. Granodiorites are plutonic igneous rocks similar to granites, but contain more plagioclase, biotite and hornblende than true granites. The large amount of granodiorite fragments found in the upper Salinas channel

explains the large amount of plagioclase feldspar that dominates Salinas Beach material (Figure 23, Table 7). A basalt pebble was identified in the Salinas River channel, which could be the source of the pyroxene identified from channel and river mouth thin sections (Figure 23). The pyroxenes (dominated by orthopyroxene) found in the Salinas channel sediment is most likely eroded from Pleistocene and Pliocene marine sedimentary rocks which may contain basalt (*see* Page 1982), such as the breccia and conglomerate pebbles found in the Salinas channel.

4.4: Seasonal changes in composition

The composition of framework mineral (quartz, feldspar and lithic, “QFL”) is an indication of both maturity and provenance of beach sediment, and wave-exposed sections of the coastline go through many cycles of fluvial discharge and sorting by significant littoral currents each year (Akarish & El-Gohary 2008, Dickinson 1984). Within central Monterey Bay, the relative percentages of QFL, and the type of lithic fragments, in beach sediment were used to establish river provenance: intrusive lithics are commonly found near the Salinas River Mouth, and sandstone fragments are common in sediment near the Pajaro river mouth (Figures 19 & 20, Table 8). The composition and amount of lithic fragments is the most important compositional difference between the two rivers. The dominance of intrusive igneous fragments in the Salinas River samples supports year-round input of Gabilan range material, while the Pajaro has higher amounts of sandstone lithic fragments that are likely derived from paleo-turbidite deposits from the remnants of the Farallon Plate along the Franciscan complex (Ernst 1993, Figure 20). The Pajaro watershed includes volcanic rock fragments from the exposed outcrops of the Diablo range, although the Diablo range is not likely to contribute significant sediment to the Salinas watershed (Yancy 1972). There is little seasonal variance in the QFL composition of central Monterey Bay sediment and the majority of sediment can be classified between volcanic-arc and recycled origin provenances (*see* Dickinson &

Suczek 1979), which fits the mix of volcanic input from the Salinas watershed and sandstone from the Pajaro watershed (Figure 19).

Similarly to the changes in grain size trends, the abundance of heavy minerals near both the Salinas and Pajaro River mouths might reflect seasonal changes in both river discharge and wave energy. The highest abundance of total heavy minerals found within Pajaro transects was found during the winter season (Table 9). The highest abundance of heavy minerals along the Salinas State Beach was found during the summer, when the upper Salinas River was dried out; indicating the possibility of input of heavy minerals from offshore bars (Table 9).

Between July and October 2009 sampling season, the Salinas River Mouth was found to be completely cut off from the ocean by a large berm, yet 11-21% of all heavy minerals found from Swash zone samples collected in October were identified as pyroxenes (Table 9, Figure 25). Sediment collected from transects north of the Salinas River Mouth have roughly half the pyroxene concentration of Pajaro transect sediment, but pyroxene within Salinas transects is persistent throughout the year and varies with season; the highest concentrations of pyroxene are found during the summer and fall seasons (Figure 22, Table 9). A previous study has found pyroxene only near the Pajaro River mouth (*see* Yancy 1972), but this study has found large (>25% total heavy minerals counted) assemblages of both clinopyroxene and orthopyroxene within summer Salinas transects that rivals assemblages counted around the Pajaro River mouth during high discharge seasons (Figure 22, Table 9). Pyroxene was found within both Pajaro and Salinas transects in all seasons, and these results contradict Yancy's 1972 study which found pyroxene (in the form of Jadeite) only along the Pajaro coastline (*see* Yancy 1972), and used this mineral as a indication of provenance from the Pajaro watershed within the central Monterey Bay. The diversity of pyroxene types and common occurrence of both orthopyroxene and calcic-clinopyroxene is also unique to this study, as Yancy's (1972) study relied on glaucophane and jadeite as a indication of Pajaro River provenance.

The relatively high occurrence of pyroxene along the Salinas State Beach suggests three possible scenarios: 1) pyroxene is transported down the coast from the Pajaro River mouth, and re-deposited along the Salinas State Beach; 2) the pyroxene deposited along the Salinas State Beach is from trace amounts (~5%, *see* Table 11) of basalt found from upper Salinas River channel samples; 3) pyroxene is derived from sea-cliff erosion of the Fort Ord Aromas Sandstone. Seasonal southward transport of Pajaro material is supported by littoral transport trends between Pajaro transects (not Salinas transects) and the abundance of pyroxene along the Pajaro coastline (Figures 17 & 18). The south coast pyroxene could have originated from erosion of the basalt pebbles found in the upper Salinas watershed, but the trace amount of basalt (~5%, *see* Table 11) is unlikely to provide enough pyroxene to the Salinas coastline to solely account for the high amounts found during summer transects. The third scenario, the erosion of the Aromas sandstone dunes, is a viable scenario to explain Salinas pyroxene distributions; however significant dune erosion has only been monitored during the winter season, which would not explain the increase in Salinas transect pyroxenes between winter and summer transects (Hapke et al 2006, Dingler & Reiss 2001, Smith et al 2005, Tables 9 & 10).

4.5: Littoral contributions from other sources: the Aromas Sandstones and San Lorenzo River

Twenty-five percent of the heavy minerals counted from the San Lorenzo River channel were identified as pyroxenes, which represents the highest abundance outside of the Pajaro River (Table 10). Pyroxene abundance increased to 44% of total heavy minerals 1 km east of the San Lorenzo River Mouth (*see* Table 10), demonstrating the resilient nature of both orthopyroxene and clinopyroxene to intense reworking by waves along the Seabright State Beach. Alongshore transport from the San Lorenzo River mouth is eastward, however very little longshore dispersion of river sediment has been recorded, even after flood events (Hicks & Inman 1987). Construction of the Santa Cruz

harbor in 1964 blocked the majority of south-eastern littoral transport to the central bay, and sediment from the San Lorenzo River is mostly trapped in the local delta and along Cowell Beach (Hicks & Inman 1987). Despite the known resilience of heavy minerals (*see* Frihy et al 1995) both the distance, intense wave action along the Santa Cruz coastline, and the Santa Cruz Harbor blockage makes it unlikely that littoral input from the San Lorenzo river could account for the additional pyroxenes along the Salinas River coastline.

Previous lithologic and petrographic studies have detailed the framework and accessory composition of the Aromas sandstones (*see* Allen 1946, Dupre 1975, Dupre & Tinsley 1980), but to date few studies have examined the heavy mineral composition of Aromas deposits within the Fort Ord and Manresa dune fields (Allen 1946, Dupre & Tinsley 1980). The base of the Aromas unit exposed at the Fort Ord and Manresa dune fields is composed of sand-sized particles with limited biotite and abundant feldspar and lithic fragments, which is similar to previous estimates of the composition of the Aromas deposits (Table 7D, Allen 1946). Previous petrographic analysis of north and south bay coastal Aromas deposits have found high amounts of hematite, quartz and garnet, but little-to-no trace of pyroxenes or other metamorphic heavy minerals (Allen 1946, Dupre & Tinsley 1980). The limited number of Aromas sandstone samples collected during this study can be considered good representations of the 30-40 m basal unit of the Aromas sandstone, which is a representative unit of the entire Aromas unit (*see* Allen 1946), but the large amount of pyroxene found is unique to this study. Given the poorly-sorted nature of alluvium deposits (*see* Dupre & Tinsley 1980), the low sample size (one sample for Manresa and Fort Ord dunes) and limited previous heavy mineral analysis of the Aromas sandstone units (*see* Allen 1946, Dupre & Tinsley 1980), it is unclear if the petrographic counts reported in this study are representative of the composition of the dune deposits along the north and south coastline.

If the samples collected during this study are representative of the Aromas sandstone deposits, the high rates of coastal erosion at the Manresa and Fort Ord dune

fields could account for the additional metamorphic counts found within winter and fall Salinas transects (Thornton et al 2006). The large amount (38% of heavy mineral composition) of pyroxenes (dominantly clinopyroxene) found from the Aromas Sandstone sampled at a outcrop in the Manresa State Dune Field can be redeposited along the Salinas River State Beach if southward littoral transport is monitored between Pajaro transects, as observed during this study (Figure 16, Table 10). The Fort Ord Dune Field has very little pyroxene, but large amounts of chert, which could account for the high abundance (12-37%) of the re-crystallized quartz found along the beaches of the Central Monterey Bay (Tables 9 & 10). Given the isolated nature of San Lorenzo sediment, the Aromas sandstones seems the most likely additional source of pyroxenes to the central Monterey Bay coastline.

4.6: Conclusions & Future Study

The lithic and heavy mineral composition of both the Pajaro and Salinas transects describes unique sources of sediment for each river: erosion of detrital basalt-bearing sandstone units likely part of the Franciscan complex exposed in the Pajaro watershed provides large amounts of pyroxene into the Pajaro river, and erosion of granodiorite and granite outcrops along the Santa Lucia range provides garnet to the Salinas watershed. The discovery of pyroxene near the Salinas River mouth is unique to this study and is likely derived from a combination of three possible sources: 1) Pajaro & Salinas Rivers, 2) offshore bars and 3) Aromas Sandstone. The coastal concentration of heavy minerals varies with season, with the highest amounts of Pajaro pyroxenes found during the winter and fall seasons, and the highest amount of Salinas pyroxenes found during the summer. The fluvial heavy mineral abundances are complemented by input from the Aromas Sandstones and during the low-energy summer season, progradation of offshore bars results in a coarse-grained, poorly mixed coastal composition.

Heavy mineral abundance and grain-size data suggest two littoral transport patterns within Monterey Bay: A year-round “Pajaro” cell that transports sediment southward along the coast from the Pajaro River Mouth, and a seasonal “Salinas” cell that disperses sediment locally from the Salinas River Mouth which, over time, transports sediment northward during summer W-SW swell conditions. The Gao & Collins “2D Vector” approach agreed with heavy mineral data when averaged across multiple transects, but there were high amounts of variability between individual transects (particularly between Salinas transects) and many of the Salinas transects did not fit either Case 1 or Case 2 trends (Figure 17). The results of this study suggest that the Gao & Collins (1992) approach should not be used as the only proxy of littoral transport, and that either heavy mineral or nutrient tracers are required to confirm the trends implied by grain size vectors. The distribution of heavy minerals along central Monterey Bay suggests two provenances which generally agree with previous estimates (*see* Yancy 1972): Salinian block material is eroded into the Salinas River, and Franciscan block material into the Pajaro River, where it is transported southward by NW/W swells. Small scale seasonal variations are implied by these trends, but the transport patterns are largely persistent throughout the year. It remains unclear if the Pajaro and Salinas river sediment mixes, but the heavy mineral and grain size data demonstrates the possibility of cross-canyon transport of sediment stored in along submarine canyon promontories during winter storm events.

This study has demonstrated how the erosion and accretion of beaches is controlled by seasonal shifts in the littoral transport of sediment and has suggested the interaction of littoral cells across a deep canyon sink. Future coastal morphology models should consider the possibility of sediment transport across off-shore canyons and other sinks as additional sources of sediment which can act as buffers against coastal erosion. Future studies should focus on a clearer understanding of cross-canyon sediment transport patterns. The results of this study do not conclusively prove that the Salinas and Pajaro littoral cells are interacting across the axis of the Monterey Submarine canyon, but

grain size and heavy mineral data cannot rule it out, and provide modest support for the idea. The depositional patterns of sediment along the Monterey Bay submarine canyon have been well documented (*see* Edwards 2002, Smith et al 2007, Smith et al 2005, Mitts 2002), but no studies have been performed to examine the potential transport of heavy minerals across the canyon axis. Up-canyon migration of sand-waves in response to tidal currents has been demonstrated in the Monterey Submarine Canyon using morphometric modeling (*see* Innocenti et al 2009) and future studies should focus on establishing the composition of these sand waves, and their possible interaction with river sediment deposited along canyon tributaries. In addition to canyon transport, a more detailed petrographic study of the Aromas sandstone units along central Monterey Bay would be a useful tool to establish a more complete understanding of sediment sources in Monterey Bay.

LITERATURE CITED

Akarish, A.I.M., El-Gohary, A.M., Petrography and Geochemistry of the Lower Paleozoic Sandstones, East Sinai, Egypt: Implications for Provenance and Tectonic Setting, *African Earth Sciences* (2008), doi: 10.1016/j.jafrearsci.2008.04.002

Alekseeva, Veronika A., Hounslow, Mark W. 2004. Clastic sediment source characterization using discrete and included magnetic particles – their relationship to conventional Petrographic methods in early Pleistocene fluvial glacial sediments, Upper Don River Basin (Russia). *Physics and Chemistry of the Earth* 29. 961-971.

Allen, J.E. 1946. *Geology of the San Juan Bautista Quadrangle California*: California Division of Mines Bull. 133.

Andersen, David W., Rymer, Michael J. 1983. Tectonics and Sedimentation along faults of the San Andreas System. *Pacific Section of Society of Economic Paleontologists and Mineralogists*.

Anima, R.J., Eittreim, S.L., Edwards, B.D., Stevenson, A.J., 2002. Nearshore morphology and late Quaternary geologic framework of the northern Monterey Bay Marine Sanctuary, California. *Marine Geology* 181. 35-54.

Arnal, Robert E., Dittmer, Eric., Shumaker, Evelyn. 1973. Sand transport studies in Monterey Bay, California. Technical Publication 73-5. Moss Landing Marine Laboratories.

- Atwater, Tanya. 1970. Implications of Plate Tectonics for the Cenozoic Tectonic Evolution of Western North America. *Geological Society of America Bulletin* 81. 3513-3536.
- Bayram, Atilla., Magnus, Larson., Hanson, Hans. 2007. A new formula for the total longshore sediment transport rate. *Coastal Engineering* 54. 700-710.
- Bertin, Xavier, Castelle, Bruno., Chaumillon, Eric., Butel, Remi., Quique, Robin. 2008. Longshore transport estimation and inter-annual variability at a high-energy dissipative beach: St. Trojan beach, SW Oleron Island, France. *Article in Press: Continental Shelf Research*
- Bird, Eric. 2000. *Coastal Geomorphology: An Introduction*. Wiley publishing, West Sussex PO19 9UD, England.
- Blott, Simon J. And Pye, Kenneth. 2001. GRADISTAT: A grain size distribution and statistics package for the analysis of Unconsolidated Sediments. *Earth Surface Processes and Landforms* 26. 1237-1248.
- Boggs, Sam. 2006. *Principles of Sedimentology and Stratigraphy*. 4th Edition. Pearson Prentice. New Jersey.
- Carver, Robert E. 1971. *Procedures in Sedimentary Petrology*. Wiley-Interscience, New York.
- Cheng, Peng., Gao, Sue., Bokuniewicz, Henry. 2004. Net sediment transport patterns of the Bohai Strait based on grain size trend analysis. *Estuarine, Coastal and Shelf Science* 60. 203-212.

Chesser, Steve A., and Peterson, C.D. 1987. Littoral cells of the Pacific Northwest coast. Coastal Sediments. Am. Soc. Civ. Eng 87. New York, NY, United States.

Clark, Ross A., and Osborne, R.H., 1982. Contribution of Salinas River sand to the beaches of Monterey Bay, California, during the 1978 Flood Period; Fourier grain-shape analysis. Journal of Sedimentary Petrology 52(3). 807-822.

Cloud, Preston E. Jr. 1966. Beach Cusps: Response to Plateau's Rule? Science, New Series. 154(3751). 890-891.

CNDR: California-Nevada River Forecast Center. http://www.cnrfc.noaa.gov/monthly_precip_2009.php

Coulter Corporation. 1994. Coulter Corporation, Coulter LS Series Product Manual PN 7222061A, Coulter Corporation, Miami, Florida, US.

Dickinson, W.R., Beard, L.S., Brakenridge, G.R., Erjavec, J.L., Ferguson, R.C. 1983. Provenance of North American Phanerozoic sandstones in relation to tectonic setting. Geological Society of America Bulletin 94(2). 222-235.

Dickinson, W.R., and Suczek, C.A. 1979. A plate tectonic and sandstone compositions. Bull. Am. Assoc. Pet Geol 63. 2164-2182

Dingler, John R., and Reiss, T.E. 2001. Changes to Monterey Bay beaches from the end of the 1982-83 El Niño through the 1997-98 El Niño. Marine Geology 181. 249-263.

Drake, Patrick T., McManus, M.A., Storlazzi, C.D. 2005. Local wind forcing of the Monterey Bay area inner shelf. *Continental Shelf Research* 25. 397-417

Dupre, William R. 1990. Quaternary Geology of the Monterey Bay Region, California. *Geology & Tectonics of the Central California coastal region, San Francisco to Monterey. Pacific Section, AAPG.* 185-191.

Dupre, William R. 1975. Maps showing geology and liquefaction potential of the Quaternary deposits in Santa Cruz county, California: U.S. Geol. Survey Misc. Field Studies Map, MF-643, 2 sheets, scale 1:62,500

Dupre, W.R., and Tinsley, J.C. III. 1980. Maps showing the Quaternary geology and liquefaction potential of parts of northern Monterey and southern Santa Cruz Counties, California: U.S. Geol. Survey Misc. Field Studies Map MF-1199, 2 sheets, scale 1:62,500

Dyke, Eric Van, and Wasson, Kerstin. 2005. Historical Ecology of a Central California Estuary: 150 Years of Habitat Change. *Estuaries* 28(2). 173-198.

Edwards, Brian D. 2002. Variations in Sediment Texture in the Northern Monterey Bay National Marine Sanctuary continental shelf. *Marine Geology* 181. 83-100.

Elfrink, B. and Baldock, T. 2002. Hydrodynamics and sediment transport in the swash zone: a review and perspectives, *Coast. Eng.* 45. 149-1

Eittriam, Stephen L., Xu, J.P., Noble, Marlene., Edwards, B.D. 2002. Towards a sediment budget for the Santa Cruz shelf. *Marine Geology* 181. 235-248

Epping, U. A., J.-B. Stuut, et al. (2008). "Variations in sediment provenance during the past 3000 years off the Tagus River, Portugal." *Marine Geology* in press.

Ergin, Mustafa, Keskin, Seref, Dogan, A.U., Kadioglu, Y.K., Karakas, Zehra. 2007. Grain size and Heavy mineral distribution as related to hinterland and environmental conditions for modern beach sediments from the Gulfs of Antalya and Finike, eastern Mediterranean. *Marine Geology* 240. 185-196.

Ernst, W. G. 1993. Metamorphism of Franciscan tectonostratigraphic assemblage, Pacheco Pass area, east-central Diablo Range, California Coast Ranges. School of Earth Sciences, Stanford University, Stanford, California 94305-2210.

Farnsworth, Katherine L., and Milliman, J.D. 2003. Effects of climatic and anthropogenic change on small mountainous rivers: the Salinas River example. *Global and Planetary Change* 39. 53-64.

Folk R.L., and Ward W.C. 1957. Bronzos River bar: a study in the significance of grain size parameters. *Journal of Sedimentary Petrology* 27. 3-26.

Frihy, Omran E. Lotfy, and M.F., Komar, P.D. 1995. Spatial variations in Heavy minerals and patterns of sediment sorting along the Nile Delta, Egypt. *Sedimentary Geology* 97. 33-41.

Frihy, Omran E. and Dewidar, K.M. 2003. Patterns of erosion/sedimentation, Heavy mineral concentration and grain size to interpret boundaries of littoral sub-cells of the Nile Delta, Egypt. *Marine Geology* 199. 27-43.

- Gao, Shu. 1996. A FORTRAN program for grain-size trend analysis to define net sediment transport pathways. *Computers and Geosciences* 22(4). 449-452.
- Gao, Shu, and Collins, Michael. 1992. Net sediment transport patterns inferred from grain-size trends, based upon definition of "transport vectors." *Sedimentary Geology* 80. 47-60.
- Greene, H.G., Maher, N.M., Paull, C.K. 2002. Physiography of the Monterey Bay National Marine Sanctuary and implications about continental margin development. *Marine Geology* 181. 55-82.
- Griggs, Gary B. and Best, Tim C. 1991. A sediment budget for the Santa Cruz Littoral Cell, California. *Society for Sedimentary Geology Special Publication* 46.
- Habel, J.S. and Armstrong, G.A. 1978. Assessment and atlas of shoreline erosion along the California coast: State of California Department of Boating and Ocean Development, Sacramento, CA 277.
- Hapke, Cheryl J., Reid, David., Richmond, Bruce M., Ruggiero, Peter. and List, Jeff. 2006. National Assessment of Shoreline Change Part 3: Historical Shoreline Change and Associated Coastal Land Loss Along Sandy Shorelines of the California Coast. USGS Open-File Report 2006-1219.
- Hanson, Randall T. 2003. Geohydrologic Framework of Recharge and Seawater Intrusion in the Pajaro Valley, Santa Cruz and Monterey Counties, California. U.S. Geological Survey Water-Resources Investigations Report 03-4096

Harlov, Daniel E., Forster, Hans-Jürgen. 2007. The role of accessory minerals in rocks: Petrogenetic indicators of metamorphic and igneous processes. *Lithos* 95, vii-x.

Hicks, D. Murray and Inman, Douglas L. 1987. Sand Dispersion from an Ephemeral River Delta on the Central California Coast. *Marine Geology* 77. 305-318.

Hoefel, Fernanda, Elgar, Steve. 2003. Wave-Induced Sediment Transport and Sandbar Migration. *Science* 299. 1885-1887.

Howell, D.G., Jones, D.L., and Schermer, E.R. 1985. Tectonostratigraphic terranes of the circum-Pacific region: in Howell, D.G., ed., Tectonostratigraphic terranes of the circum-Pacific region, Circum-Pacific council for energy and mineral resources, Earth science series, number 1: Circum-Pacific Council for Energy and Mineral Resources, Houston, Texas. 3-30.

Ingersol, Raymond V. and Christopher A. Suczek. 1979. Petrology and Provenance of Neogene sand from Nicobar and Bengal Fans, DSDP Sites 211 and 218. *Journal of Sedimentary Petrology* 49. 1217-1228.

Inman, D.L., Jenkins, S.A., 1999. Climate change and the periodicity of sediment flux of small California Rivers. *Journal of Geology* 107, 251-270.

Innocenti, C., Taramelli, A., Besio, G., Pascoletti., Disperati, L., Aiello, I.W. 2009. Prediction of the Dynamic Behaviour and Migration Rates of Sand Waves in the Monterey Canyon System of California. In-Press. AGU Fall Meeting, abstract #EP43A-0650

Kaczmarek, Leszek M, Ostrowski, Rafael., Pruszek, Zbigniew., Rozynski, Grzegorz. 2005. Selected problems of sediment transport and morphodynamics of a multi-bar nearshore zone. *Estuarine, Coastal and Shelf Science* 62. 415-425.

Komar, Paul D. 1974. Evaluation of wave-generated longshore current velocities and sand transport rates on beaches. *Beach and Nearshore Sedimentation*, Society of Economic Paleontologists and Mineralogists: Special Publication 24.

Komar, Paul D., Inman, Douglas L. 1970. Longshore Sand Transport on Beaches. *Journal of Geophysical Research* 75(30). 5914-5928.

Krumbein, W.C. 1941 Measurement and geological significance of shape and roundness of sedimentary particles. *Journal of Sedimentary Research*; v. 11; no. 2; p. 64-72

Landry, J. Blake, Hancock, Matthew J., Mei Chiang C. 2007. Note on sediment sorting in a sandy bed under standing water waves. *Coastal Engineering* 54. 694 - 699

Largier, J.L., Magnell, B.A., Winant, C.D. 1993. Subtidal Circulation Over the Northern California Shelf. *Journal of Geophysical Research*. v.98 (C10). p.147-179

Lewis, Roger C., Coale, Kenneth H., Edwards, Brain D., Marot, Marci, Douglas, Jocelyn N., Burton, Erica J. 2002. Accumulation rate and mixing of shelf sediments in the Monterey Bay National Marine Sanctuary. *Marine Geology* 181. 157-169

Liu, J. P., C. S. Liu, et al. (2008). "Flux and fate of small mountainous rivers derived sediments into the Taiwan Strait." *Marine Geology* 256: 65-76.

Masselink, Gerhard, and Hughes, M.G. 2003. Introduction to coastal processes and geomorphology. Oxford University Press.

Masselink, Gerhard., Evans, Darren., Hughes, Michael G., Russell, Paul. 2005. Suspended sediment transport in the swash zone of a dissipative beach. *Marine Geology*. 216 (3). 169-189.

Masselink, Gerhard., and Pattiaratchi, C.B. 1998. Morphological evolution of beach cusps and associated swash circulation patterns. *Marine Geology* 146. 93-113.

McLaren, Patrick., and Bowles, Donald. 1985. The Effects of Sediment Transport on grain-size distributions. *The Society of Economic Paleontologists and Mineralogists* 55 (4) 457-470.

Mitts, Patrick J. 2003. Deposition and Provenance of modern coarse sediment in Monterey Submarine Canyon. Thesis presented to the Faculty of Moss Landing Marine Laboratories and San José University.

Moore, Laura J., and Griggs, Gary B. 2002. Long-term cliff retreat and erosion hotspots along the central shores of the Monterey Bay National Marine Sanctuary. *Marine Geology* 181. 265-283.

Mottana, Annibale, Crespi, Rodolfo, Liborio, Giuseppe. 1978. *Rocks and Minerals*. Simon & Schuster inc publishing, New York.

Morton, Andrew C. 1991. Geochemical studies of detrital Heavy minerals and their application to provenance research. British Geological Survey, Keyworth, Nottingham NG12 5GG, UK.

Nesse, William D. 2000. *Introduction to Mineralogy*. New York Oxford University Press.

Osborne, Philip D., and Simpson, David P. 2005. Cross-Shore Variation of Grain Size on Beaches. *Encyclopedia of Coastal Science*. Springer Publishing. 353-354.

Page, Benjamin M. 1982. Migration of Salinian Composite Block, and the disappearance of fragments. *American Journal of Science* 282. 1694-1734.

Paull, Charles K., Mitts, Patrick., Ussler III, William., Keaten, Rendy., Greene, H.G. 2005. Trail of sand in upper Monterey Canyon: Offshore California. *Geological Society of America* 117(9/10). 1134-1145.

Patsch, K.B, and Griggs, Garry. 2008. A sand budget for the Santa Barbara Littoral Cell. *Marine Geology* 252. 50-61.

Pedreiros, R. H.L., and Michel, H.D.1996. Application of grain size trend analysis for the determination of sediment transport pathways in intertidal areas. *Marine Geology* 135. 35-49.

Poizot, Emmanuel, Mear, Yann., Biscara, Laurie. 2007. Sediment trend analysis through the variation of granulometric parameters: A review of theories and applications. *Earth-Science Review* 1-28.

Ryan, Holly, Gibbons, Helen., Hendley II, J.W., Stauffer, P.H., 1999. El Niño Sea-Level rise wreaks havoc in California's San Francisco Bay Region. *USGS Fact Sheet* 175-99.

- Sallenger, Asbury H. Jr., Krabill, William, Brock, John, Swift, Robert, Manizade, Serdar, Stockdon, Hilary. 2002. Sea-cliff erosion as a function of beach changes and extreme wave runup during the 1997-1998 El Niño. *Marine Geology* 181. 279-297.
- Sedrati, Mouncef., and Anthony, E.J. 2007. Storm-generated morphological change and longshore sand transport in the intertidal zone of a multi-barred macrotidal beach. *Marine Geology* 244. 209-229.
- Schwartz, Maruice L. *Encyclopedia of Coastal Science*. 2006. Berlin: Springer publications. 353 - 354.
- Smith, Douglas P., Rikk Kvitek, Rikk., Iampietro, P.J., Wong, Kendra. 2007. Twenty-nine months of geomorphic change in upper Monterey Canyon (2002-2005). *Marine Geology* 236. 79-94.
- Smith, Douglas P., Ruiz, Genoveva, Kvitek, Rikk, Iampietro, Pat J. 2005. Semiannual patterns of erosion and deposition in upper Monterey Canyon from serial multibeam bathymetry. *Geological Society of America Bulletin*; v117. 1123-1133.
- Smith, Douglas P., Gref, Karen., Hofmann, Alex., Turrini-Smith, Leslie. 2005a. Are "Stable Shorelines" and "Broad Beaches" Mutually Exclusive Management Goals Along Southern Monterey Bay? The Watershed Institute. Report No. WI-2005-09.
- Storlazzi, C.D., and Field, M.E. 2000. Sediment distribution and transport along a rocky, embayed coast: Monterey Peninsula and Carmel Bay, California. *Marine Geology* 170. 289-316

Storlazzi, C.D. and Jaffe, B.E. 2002. Flow and sediment suspension events on the inner shelf of central California. *Marine Geology* 181. 195-213.

Storlazzi, C.D. And Wingfield, Dana K. 2005. Spatial and Temporal Variations in Oceanographic and Meteorologic Forcing Along the Central California Coast, 1980-2002. Scientific Investigations Report 2005-5085.

Thorton, Edward B., Sallenger, Abby., Sesto, J.C., Egley, Laura., McGee, Timothy., Parsons, Rost. 2006. Sand mining impacts on long-term dune erosion in southern Monterey Bay. *Marine Geology* 229. 45-58.

Tucker, Maurice E. 1981. *Sedimentary Petrology*.

USACE. 1984. *Shore Protection Manual*. Department of the Army, U.S. Corps of Engineers, Washington, DC 20314.

Wolf, Stephen C. 1970. Coastal Currents and mass transport of surface sediments over the shelf regions of Monterey Bay, California. *Marine Geology* 8, 321-336.

Wright, L.D., Chappell, J., Thom, B.G., Bradshaw, M.P., Cowell, P. 1979. Morphodynamics of reflective and dissipative beach and inshore systems: Southeastern Australia. *Marine Geology* 32 (1-2). 105-140.

Xu, J.P., Noble, M.A., Rosenfield, L.K. 2004. In-situ measurements of velocity structure within turbidity currents: *Geophysical Research Letters*. V.31. L09311.

Yancey, Thomas E. 1972. Major Heavy mineral Assemblages and Heavy mineral Provinces of the Central California Coast Region. Geological Society of America Bulletin 83. p. 2099-2104.

APPENDIX: TABLES

Table 1: Heavy mineral Specific Gravities

Mineral ID	S.G. (g/cm ³)		Average S.G.
	Min	Max	
Chlorite	2.6	3.3	2.95
Biotite	2.7	3.3	3
Tremolite	2.99	3.48	3.235
Hornblende	3.02	3.59	3.305
Garnet	3.1	4.2	3.65
Ca-Clinopyroxene	3.19	3.56	3.375
Orthopyroxene	3.21	3.96	3.585
Jadeite	3.24	3.43	3.335
Epidote	3.38	3.49	3.435
Augite	3.40	3.60	3.5
Chloritoid	3.46	3.8	3.63
Titanite / Sphene	3.48	3.60	3.54
Glaucophane	3.05	3.50	3.275

Table 1: List of Common heavy minerals expected along the central Monterey Bay coastline and their Specific Gravities (S.G.)

Table 2: Transect location and Dates

Station ID	UTM		Sampling Dates		
	Easting (m)	Northing (m)	Winter	Summer	Fall
SL1	587928	4091291			10/17/09
SL2	588415	4091143			10/17/09
MD	601742	4087051			9/20/09
PR1	605766	4079262	2/22/09	7/11/09	10/23/09
PR2	606246	4078567	1/29/09	7/11/09	10/23/09
PR3	606587	4077687	2/24/09	7/11/09	10/23/09
PR4	606921	4076797	2/24/09	7/11/09	10/23/09
SR1	607245	4070720		3/22/09	7/11/09
SR2	607060	4069740	2/22/09	7/11/09	10/21/09
SR3	606845	4068774	2/22/09	7/11/09	10/21/09
SR4	606660	4067800	1/29/09	7/11/09	10/21/09
SR5	606586	4066298		3/22/09	7/11/09
FD	605149	4057664			9/20/09

Table 2: Location of beach transects and sampling dates. Locations based on UTM 10N coordinate grid. Station ID is based on distance from river mouth, and are ~ 1km apart. SL1 = San Lorenzo River Mouth, SL2 = Seacliff State Beach 1km south of SL1, MD = Sunset / Manresa Dunes, PR1 = 1 km north of Pajaro River Mouth, PR2 = Pajaro River Mouth, PR3 = 1 km south of Pajaro River Mouth, PR4 = 2 km south of Pajaro River Mouth, SR1 = 3 km north of Salinas River Mouth, SR2 = 2 km north of Salinas River Mouth, SR3 = 1 km North of Salinas River Mouth, SR4 = Salinas River Mouth, SR5 = 1 km South of Salinas River Mouth, FD = Ft. Ord Dune Field Sample.

Table 3: Location of Swash zone samples

Sample ID	Easting (m)	Northing (m)
SLRM1	587928	4091291
SLRM2	588415	4091143
MD	601742	4087051
PR1	605751	4079456
PR2	606246	4078567
UPR	620808	4083990
PR3	606587	4077687
PR4	606921	4076797
SR1	607245	4070720
SR2	607060	4069740
SR3	606845	4068774
SR4	606660	4067800
USR	612110	4059882
SR5	606586	4066298
FD	605149	4057664

Table 3: Location of swash zone thin sections. Locations based on UTM 10N coordinate grid. SLRM1 = San Lorenzo River mouth swash zone sample. SLRM2 = swash zone sample 1 km east of San Lorenzo River Mouth.

Table 4: Optical properties

Mineral Name	Formula	EA	Cleavage	Habit	Pleochroism	Bi-refringence	Optic Sign	Relief
Quartz	SiO ₂	30-90	None	Tetrahedral	None	0.009	U (+)	low-moderate
Plagioclase Feldspar	NaAlSi ₃ O ₈	45-102	93-94	Twinning	None	0.007-0.013	B (+),	low (+) to (-)
Potassium Feldspar	KAlSi ₃ O ₈	40-70	90	Anhedral	None	None	B(+)	low (-)
Chert	SiO ₂	UD	None	Microcrystal	None	0.009	U (+)	low-moderate
Hematite	Fe ₂ O ₃	none	none	Hexagonal	Red-redish brown	None	U (-)	Moderate-high
Tridymite	SiO ₂	40-90	None	Orthorhombic	None	0.002-0.004	B (+)	Moderate-High
Tremolite	Ca ₂ (Mg, Fe) ₃ Si ₈ O ₂₂	62-88	56, 124	Columnar	None	0.027-0.017	B (-)	Moderate-High
Titanite	CaTiO ₅	17-40	Prismatic	Octahedral	weak yellow	0.005-0.007	B (+)	Very High (+)
Omphacite	(Ca,Na)(Mg,Fe,A)	56-84	87, 93	Euhedral 4-8	none-greenish blue	0.012-0.028	B (+)	High (+)
Orthopyroxene	(Mg, Fe) ₂ Si ₂ O ₆	50-132	88, 92	Euhedral 4-8	None-weak	0.006-0.022	B (+)	Moderate
Jadeite	NaAlSi ₂ O ₆	60-96	87-93	fibrous	None	0.006-0.021	B (+)	Moderate-High
Hornblende	(Ca,Na) ₂₋₃ (Mg,Fe)	35-130	56, 124	Prismatic	Yellow/green-brown	0.018-0.025	B (+)	Moderate-High
Epidote	CaAl ₂ (OH)SiO ₄	14-40	Perfect	Columnar	Yellowish-green	0.01-0.05	B (+),	High (+)
Calcic Clinopyroxene - Diopside	CaMgSi ₂ O ₆	25-90	87, 93	Stubby 4-8	None-weak	highly variable	B (+)	High (+)
Calcic Clinopyroxene - Augite	(Ca,Mg,Fe ²⁺ ,Fe ³⁺)	60-110	87, 93	Prismatic	pale green, blue-brown	0.028-0.060	B (+)	High (+)
Chloritoid	Fe ₂ Al ₃ O ₂ (SiO ₄) ₂	55-88	90	Hexagonal	Green-blue grey	0.010-0.012	B (+)	High (+)

Table 4: Optical properties table. EA = Extinction angle, the angle between the length or a prominent cleavage in a mineral and a vibration direction. Cleavage is a measure of the angle between weak chemical bonds along crystallographic planes. Habit refers to the structure of the mineral. Pleochroism is the colors that are minerals display when rotated under plane light. Birefringence is a measurement of the retardation of light as it passes through a mineral and is reported in units of nanometers. Optical sign is a record of the number of rays that light is split into as it passes through anisotropic minerals. Optical sign is recorded as Uniaxial positive and negative (U+, U-) or Biaxial positive and negative (B+,B-). Relief is the degree to which mineral grains stand out from the background mounting medium. Minerals with low and negative relief do not stand out, while minerals with positive or high relief are clearly visible (Nesse 2000).

All mineral identification from 2009 samples is based on this table.

Table 5(A): Winter Grain Size Data

Sample ID	Mean	Median (d50)	Mode	S. Dev	Skewness	Kurtosis	% Fine Sand (125-250 um)	% Medium Sand (250-500 um)	% Coarse Sand (500-1000 um)	% V.Coarse Sand (1000-2000um)
PR1D	520	507	471	1.54	0.055	-0.145	3.21	45.6	43.4	7.8
Average PR1	520	507	471	1.54	0.055	-0.145	0	0	100.0	0
PR2A	252	253	145	1.32	-0.089	-0.507	48.2	51.4	0.4	0
PR2B	350	338	296	1.66	0.450	0.700	25.4	50.9	21.3	2.3691
PR2C	302	288	269	1.66	0.379	2.08	34.0	53.3	9.5	3.1561
PR2D	367	342	324	1.66	0.755	0.564	21.1	66.2	7.0	5.653
Average PR2	318	305	259	1.57	0.374	0.710	32	55.4	9.6	2.8
PR3A	297	303	324	1.43	-1.12	8.09	26.1	66.6	7.3	0.0191
PR3B	279	286	296	1.40	1.14	5.35	32.2	62.4	5.4	0
PR3C	255	259	269	1.39	-1.59	9.85	43.3	52.5	4.2	0
PR3D	268	274	269	1.41	-1.46	8.90	37.04	58.1	4.9	0
Average PR3	275	280	290	1.40	-0.755	8.05	34.7	59.9	5.4	0.0
PR4A	333	330	324	1.54	0.008	3.90	19.9	65.4	12.1	2.602
PR4B	295	299	296	1.34	-0.34	-0.04	27.4	69.6	3.0	0
PR4C	300	296	296	1.42	0.54	0.90	30.1	62.8	7.0	0.0483
PR4D	313	303	296	1.61	0.20	1.83	30.6	52.2	15.0	2.2419
Average PR4	310	307	303	1.48	0.102	1.65	27.0	62.5	9.3	1.2
Average Pajaro	356	350	330	1.50	-0.06	2.56	23.5	44.5	31.1	1.0
SR1A	444	430	390	1.5	-0.08	2.02	5.61	57.55	32.4	4.442
SR1B	437	410	391	1.56	0.50	0.19	6.91	60.83	26.2	6.0392
SR1C	426	416	391	1.45	0.25	0.81	4.98	64.43	28.1	2.498
SR1D	500	485	391	1.7	-0.27	1.18	6.00	44.9	39.7	9.4211
Average SR1	452	435	391	1.55	0.103	1.05	5.87	56.9	31.6	5.6
SR2A	592	586	517	1.57	-0.06	-0.34	1.94	35.4	48.6	14.0649
SR2B	522	506	429	1.55	0.08	-0.21	3.10	45.6	42.9	8.4698
SR2C	485	465	429	1.54	0.22	-0.09	4.07	52.1	37.2	6.6259
SR2D	540	518	429	1.66	0.03	-1.9	4.29	42.7	39.4	13.6524
Average SR2	535	519	451	1.58	0.069	-0.62	3.35	43.9	42.0	10.7
SR3B	674	684	751	1.55	-0.23	-2.0	1.17	24.6	54.1	20.1633
SR3C	1013	1072	1197	1.47	-0.95	1.15	0.254	5.20	37.7	56.8533
SR3D	1053	1206	1314	1.59	-1.56	2.04	1.07	9.5	19.1	70.4194
Average SR3	913	987	1087	1.54	-0.916	0.411	0.832	13.1	36.9	49.1
SR4A	669	704	905	1.68	-0.33	-0.50	3.02	26.7	45.2	25.1238
SR4B	560	520	429	1.72	0.03	0.18	3.52	42.9	35.6	17.9769
SR4C	611	616	623	1.55	-1.9	-0.26	1.72	31.8	51.9	14.5699
SR4D	789	870	1091	1.69	-0.57	-0.41	1.75	20.3	38.5	39.3919
Average SR4	658	678	762	1.66	-0.695	-0.25	2.50	30.4	42.8	24.3
SR5D	450	429	391	1.5	0.38	0.10	5.64	58.8	94.8	5.1496
Average SR5	450	429	391	1.5	0.38	0.10	5.64	58.8	94.8	5.1
Average Salinas	601	610	616	1.57	-0.211	0.137	3.6	40.6	49.6	19.0

Table 5(B): Summer Grain Size Data

Sample ID	Mean	Median (d50)	Mode	S. Dev	Skewness	Kurtosis	% Fine Sand (125-250 um)	% Medium Sand (250-500 um)	% Coarse Sand (500-1000 um)	% V.Coarse Sand (1000-2000um)
PR1A	267	273	269	1.38	-1.38	7.51	37.05	59.08	3.9	0
PR1B	327	315	324	1.51	0.979	1.86	23.91	65.22	7.5	3.38
PR1C	326	306	296	1.62	0.196	3.00	27.2	55.04	14.9	2.86
PR1D	327	298	245	1.73	0.599	-0.16	34.67	42.53	18.6	4.25
Average PR1	312	298	284	1.56	0.099	3.05	30.7	55.47	11.2	2.6
PR2A	296	295	296	1.45	-.18	3.64	29.7	62.03	8.2	0.04
PR2B	326	311	296	1.53	.82	1.01	26.5	60.1	10.8	2.59
PR2C	322	302	269	1.59	.8	.53	31.53	53.06	12.6	2.82
PR2D	395	389	391	1.63	-.11	.87	16.77	51.11	29.0	3.16
Average PR2	335	324	313	1.55	.33	1.51	26.12	56.58	15.1	2.2
PR3A	327	312	296	1.53	1.01	1.62	24.88	63.81	7.9	3.38
PR3B	297	294	296	1.41	.81	2.8	29.44	65.55	3.7	1.33
PR3C	423	415	391	1.49	.17	.14	7.93	60.21	29.5	2.38
PR3D	540	539	517	1.55	-.13	-.13	3.71	39.36	48.5	8.46
Average PR3	397	390	375	1.49	.47	1.11	16.49	57.23	22.4	3.9
PR4A	273	281	296	1.38	-1.43	7.18	33.0	61.96	5.0	0
PR4B	244	252	269	1.43	-.84	2.8	44.92	46.6	8.5	0
PR4C	299	298	296	1.47	-.39	4.72	29.1	61.53	3.6	5.74
PR4D	435	434	429	1.68	-.34	1.41	12.29	46.8	35.2	5.74
Average PR4	313	316	322	1.49	-.75	4.03	29.83	54.22	13.1	2.9
Average Pajaro	339	332	323	1.52	.04	2.42	25.79	55.88	15.5	2.9
SR1B	473	442	391	1.61	0.363	-0.240	6.28	53.26	31.8	8.71
SR1C	578	562	391	1.70	0.025	-0.801	4.09	38.95	38.5	18.41
SR1D	485	398	296	2.01	0.285	-1.200	18.05	39.83	19.7	22.46
Average SR1	512	467	359	1.77	0.224	-0.747	9.48	44.01	30.0	16.5
SR2B	539	530	471	1.54	-0.038	-0.148	2.79	41.78	46.8	8.639
SR2C	450	432	391	1.52	0.323	0.128	5.53	58.12	31.8	4.5907
SR2D	408	358	324	1.76	0.734	-0.159	16.89	54.8	17.4	10.8652
Average SR2	466	440	395	1.60	0.340	-0.0597	8.4	51.57	32.0	8.0
SR3B	453	439	429	1.50	.22	.32	4.8	57.68	33.3	4.1825
SR3C	599	571	471	1.63	.18	-.72	1.80	38.6	41.7	17.9432
SR3D	305	303	296	1.35	.43	1.42	24.66	70.71	4.6	0.03
Average SR3	452	438	399	1.50	0.278	0.341	10.4	55.7	26.5	7.4
SR4A	1,055	1,192	1,584	1.59	-1.50	2.13	1.46	7.41	23.8	67.2848
SR4B	868	1,031	1,584	1.78	-0.863	-0.230	2.86	17.61	27.6	51.933
SR4C	731	830	1,314	1.89	-1.13	5.14	3.11	25.44	32.4	39.0708
SR4D	1,309	1,349	1,584	1.24	-0.542	-0.362	0.	0.	12.8	87.2286
Average SR4	991	1,101	1,517	1.62	-1.01	1.67	1.86	12.62	24.1	61.4
SR5B	620	629	825	1.65	-0.133	-0.665	2.68	33.12	44.2	20.0444
SR5C	529	485	391	1.66	0.285	-0.681	3.88	47.99	33.6	14.4936
SR5D	658	674	391	1.82	-0.115	-1.11	3.71	34.41	30.5	31.4062
Average SR5	603	596	535	1.71	0.012	-0.820	3.43	38.51	36.1	22.0
Average Salinas	605	608	641	1.64	-0.031	0.077	6.72	40.47	29.7	23.1

Table 5(C): Fall Grain Size Data

Sample ID	Mean	Median (d50)	Mode	S. Dev	Skewness	Kurtosis	% Fine Sand (125-250 um)	% Medium Sand (250-500 um)	% Coarse Sand (500-1000 um)	% V.Coarse Sand (1000-2000um)
PR1A	268	270	269	1.45	-0.577	5.26	39.1	53.95	6.9	0.021
PR1B	247	248	245	1.31	-0.111	-0.474	50.53	48.59	.9	0
PR1C	277	279	296	1.33	-0.147	-0.462	35.96	62.96	1.1	0
PR1D	301	290	269	1.62	-0.166	5.91	32.73	52.04	12.9	2.34
Average PR1	273	272	270	1.43	-0.250	2.56	39.58	54.39	5.4	.6
PR2A	275	280	296	1.45	-0.816	5.59	34.81	57.48	7.7	0.0179
PR2B	415	391	324	1.78	-0.094	0.315	18.18	42.54	32.0	7.266
PR2C	304	287	269	1.7	0.305	1.33	34.72	44.79	17.5	2.986
PR2D	337	322	296	1.62	0.181	2.14	24.14	56.38	16.5	2.985
Average PR2	333	320	296	1.64	-0.106	2.34	27.96	50.3	18.4	3.3
PR3A	404	394	391	1.47	0.338	0.728	8.21	65.8	23.6	2.431
PR3B	346	336	324	1.5	0.682	1.21	19.29	65.77	12.1	2.831
PR3C	333	325	324	1.5	0.695	1.27	22.48	64.45	10.5	2.575
PR3D	375	367	356	1.62	-0.252	1.82	18.27	52.64	26.8	2.284
Average PR3	364	356	349	1.52	0.366	1.26	17.06	62.17	18.2	2.5
PR4A	305	307	324	1.37	0.349	2.19	24.37	70.93	4.0	0.735
PR4B	325	324	324	1.4	0.518	2.12	19.7	72.39	6.7	1.221
PR4C	340	334	324	1.56	-0.310	5.76	19.35	63.58	14.3	2.721
PR4D	373	370	356	1.69	-0.247	1.46	20.19	49.04	27.4	3.353
Average PR4	336	334	332	1.5	0.078	2.88	20.9	63.99	13.1	2.0
Average Pajaro	326	320	312	1.52	0.022	2.26	26.38	57.71	13.8	2.1
SR2A	506	474	391	1.63	0.223	-0.389	4.97	48.98	34.8	11.21
SR2B	480	462	429	1.51	0.190	0.314	3.35	54.29	36.8	5.539
SR2C	465	444	391	1.53	0.326	0.059	4.69	56.06	33.4	5.825
SR2D	439	413	391	1.57	0.423	0.036	7.56	58.62	27.6	6.173
Average SR2	472	448	400	1.56	0.291	0.005	5.14	54.49	33.2	7.2
SR3A	426	413	391	1.52	0.241	0.312	7.55	60.48	28.4	3.555
SR3B	646	640	517	1.66	-0.054	-0.584	1.46	31.51	45.5	21.50
SR3C	579	527	391	1.8	0.128	-0.944	4.88	41.95	29.8	23.32
SR3D	668	689	1,091	1.78	-0.172	-0.942	3.24	31.92	34.6	30.20
Average SR3	580	567	598	1.69	0.036	-0.540	4.28	41.46	34.6	19.6
SR4A	642	650	825	1.63	-0.170	-0.540	1.95	30.77	46.2	21.07
SR4B	514	491	429	1.58	0.153	-0.254	3.54	47.65	39.3	9.513
SR4C	444	425	391	1.51	0.337	0.224	5.18	60.19	30.3	4.333
SR4D	604	594	429	1.68	-0.035	-0.692	3.03	36.15	40.7	20.11
Average SR4	551	540	518	1.6	0.071	-0.316	3.43	43.69	39.1	13.8
SR5A	459	440	391	1.53	0.247	0.031	5.32	56.38	33.2	5.150
SR5B	802	906	1,091	1.73	-0.707	-0.220	2.54	19.08	36.3	42.09
SR5C	453	415	356	1.68	0.398	-0.361	9.96	52.96	27.3	9.804
SR5D	432	394	356	1.65	0.633	0.026	9.75	59.06	22.3	8.859
Average SR5	536	539	549	1.65	0.143	-0.131	6.89	46.87	29.8	16.5
Average Salinas	535	523	516	1.62	0.135	-0.245	4.94	46.63	34.2	14.3

Table 5(D): San Lorenzo, Upper Salinas and Pajaro , Aromas Sandstone Grain Size Data

Sample ID	Mean	Median (d50)	Mode	S. Dev	Skewness	Kurtosis	% Fine Sand (125-250 um)	% Medium Sand (250-500 um)	% Coarse Sand (500-1000 um)	% V.Coarse Sand (1000-2000um)
SLRM1	478	460	429	1.58	0.103	-0.201	6.15	50.5	36.4	6.95
SLRM2	753	829	905	1.69	-0.918	1.34	2.83	17.2	46.4	33.6
MD	264	281	296	1.54	-2.86	15.5	29.9	52.6	17.5	0
FD	528	558	568	1.83	-2.72	17.2	2.85	32.04372	55.2	9.94
USR	340	339	324	1.81	-1.63	11.2	19.4	50.7	26.7	3.3
UPR	439	443	429	1.70	-1.73	9.55	4.44	51.0	40.0	4.6

Table 5: Grain size data for Pajaro (PR1-PR4) and Salinas (SR1-SR5) transects during (A) Winter 2009, (B) Summer 2009 and (C) Fall 2009. (D): Grain size data for samples collected at the San Lorenzo River Mouth (SLRM1) and 1 km south of the San Lorenzo River Mouth (SLRM2) are listed along with data for the Pajaro (UPR) and Salinas (USR) channel samples is listed with Aromas sandstone dune samples collected from the Manresa (MD) and Fort Ord Dunes (FD). Mean, Median and modes reported in μm . Skewness and Kurtosis are reports of the symmetry of grain size distribution around the mean grain sizes.

Table 6(A): Winter Grain Size Trend & Variance Data

Sub-sample	A	B	C	D	Trend	T-value
PR1	FB+	In	In	In	In	58.49
PR2	FB+	FB-	FB-	FB-	FB-, S	5.110
PR3	CP+	CB+	CB+	FB-	CB+,S	-4.377
PR4	FB+	FB+	CP+	CP-	In	-16.51
SR1	CP+	CB+	CP+	CP+	FB-(CP+), N	-9.377
SR2	In	CP-	CB-	CB-	In	22.59
SR3	In	FP+	FP+	FP+	In	3.385
SR4	In	In	NA	FB+	In	79.86
SR5	In	In	In	In	In	NA

Table 6(B): Summer Grain Size Trend & Variance Data

Sub-sample	A	B	C	D	Trend	T-value
PR1	CP+	CP+	FB-	CB+	S (FB-,CB+)	-2.601
PR2	CP-	FB+	CB+	CB-	In	-7.205
PR3	FB-	FP-	FB-	FP-	FB-, S	9.928
PR4	In	CP+	CP+	CP+	CP+, N	-22.66
SR1	In	CB+	FB-	FB-	FB-,S	6.458
SR2	In	FB-	CP+	FB+	N (FB-)	1.991
SR3	In	CP-	CP-	CP-	FB-, N	-68.27
SR4	In	FB+	FB+	FP+	In	46.95
SR5	In	In	In	In	In	In

Table 6(C): Fall Grain Size Trend & Variance Data

Sub-sample	A	B	C	D	Trend	T-value
PR1	CP+	CP-	CP-	CB-	FB-, N	-6.893
PR2	CP+	FB-	CB-	CP-	FB-, S	-3.500
PR3	FB-	FB-	CP+	FP+	FB-, S	3.317
PR4	CP+	CB+	CP-	CB-	CB+, S	-15.744
SR2	FB-	CP+	CP+	CP+	FB-, N	-11.722
SR3	CP+	FB-	FB+	FB+	In	3.105
SR4	FB-	CP-	FB+	FB-	FB-, S	1.606
SR5	In	In	In	In	In	In

Table 6: Grain size trend and variance data for Pajaro (PR1-PR4) and Salinas (SR1-SR5) transects during (A) Winter, (B) Summer and (C) Fall seasons. Transect sub-samples A-D are spaced 15 m apart from the foredune “A” to swash zone “D” (*see* Figure 8, Gao & Collins 1992). Net “downcoast” trends are comparisons between a northern and southern transect (ex: comparing mean, standard deviation and skewness from SR2A to SR3A produces SR2A trend). North or South trends are generated based on Case 1 (sediment becomes coarser, better sorted and more positively skewed, “CB+”) or Case 2 (sediment becomes finer, better sorted and more negatively skewed, “FB-”). A Northward trend is attributed between 2 transects if CP+ or FP- trends are observed (ex: Fall PR1A - PR2A trend). “In” trends are inconclusive. T-values are calculated based on equation 1, based on 6 degrees of freedom and a p-value of 0.05. Mean grain sizes between two adjacent transects are significantly different if T-test value is less than 2.45.

Table 7(A): Winter Framework Mineral counts

Sample ID	Total Count	%Q	%F	%L
PR3	157	48.41%	28.66%	22.93%
PR1	156	32.05%	33.33%	34.62%
PR2	143	37.06%	37.76%	25.17%
SR4	155	30.32%	36.77%	32.90%
SR3	130	41.54%	43.08%	15.38%
SR5	177	27.68%	36.16%	36.16%

Table 7(B): Summer Framework Mineral counts

Sample ID	Total Count	%Q	%F	%L
SRN3D	155	49.03%	38.06%	12.90%
SRN2D	165	35.15%	44.24%	20.61%
SRN1D	144	48.61%	36.11%	15.28%
SRMD	194	29.90%	23.71%	46.39%
SRS (MD)	181	41.99%	40.33%	17.68%
PRND	174	40.23%	25.86%	33.91%
PRMD	183	31.69%	31.15%	37.16%
PRS1D	173	30.64%	37.57%	31.79%
PRS2D	167	39.52%	34.13%	26.35%

Table 7(C): Fall Framework Mineral counts

Sample ID	Total Count	%Q	%F	%L
Ft. Ord	189	35.98%	34.92%	29.10%
MD	129	39.53%	28.68%	31.78%
PR1D	153	51.63%	30.07%	18.30%
PR2D	142	48.59%	26.76%	24.65%
PR3D	167	48.50%	26.95%	24.55%
PR4D	171	47.37%	17.54%	35.09%
SR2D	173	46.24%	26.59%	27.17%
SR3D	181	33.70%	26.52%	39.78%
SR4D	181	37.02%	29.83%	33.15%
SR5D	171	42.69%	33.92%	23.39%
UPR	176	38.07%	14.77%	47.16%
USR	167	42.51%	29.94%	27.54%

Table 7(D): San Lorenzo, Aromas sandstone and upper Pajaro and Salinas channel framework Mineral counts

Sample ID	Total Count	%Q	%F	%L
UPR	159	31.45%	16.35%	52.20%
USR	156	38.46%	32.05%	29.49%
FD	173	31.21%	38.15%	30.64%
MD	114	31.58%	32.46%	35.96%
SLR1	166	40.96%	29.52%	29.52%
SLR2	191	24.08%	23.56%	52.36%

Table 7: Framework Mineral counts for (A) winter, (B) summer and (C) fall Swash zone samples (PR1D = PR1 swash zone). Pajaro (UPR), Salinas (USR) and San Lorenzo channel (SLRM1) samples are listed separately with Fort Ord (FD) and Manresa Dune (MD) samples. SLRM2 = sample 1 km south of SLRM1. Chert fragments were counted as Quartz and Feldspars counted both Plagioclase and Potassium. Lithics included intrusive, extrusive and sandstone fragments.

Table 8(A): Winter Lithic Counts

Winter 2009	Intrusive	Extrusive	Chert	Sandstone
PR1	33	9	3	12
PR2	16	12	18	8
PR3	17	9	22	10
SR3	50	16	8	4
SR4	30	15	10	6
SR5	51	7	6	6

Table 8(B): Summer Lithic Counts

Summer 2009	Intrusive	Extrusive	Chert	Sandstone
PR 1	23	15	5	21
PR 2	30	18	10	20
PR 3	21	24	10	10
PR 4	17	23	13	3
SR 1	9	7	14	4
SR 2	18	12	13	4
SR 3	9	7	13	6
SR 4	69	16	9	5
SR 5	20	8	18	4

Table 8(C): Fall Lithic Counts

Fall 2009	Intrusive	Extrusive	Chert	Sandstone
PR 1	11	11	7	6
PR 2	20	11	11	4
PR 3	12	11	12	18
PR 4	6	23	6	31
SR 2	23	17	4	7
SR 3	52	8	8	12
SR 4	44	7	0	5
SR 5	16	14	4	10

Table 8: Lithic counts for (A) winter, (B) summer and (C) fall transects.

Table 9(A): Winter Accessory & heavy mineral counts

Winter 2009	PR1		PR2		PR3		SR3		SR4		SR5	
heavy minerals	N	% Total	N	% Total	N	% Total	N	% Total	N	% Total	N	% Total
Chlorite	10	18.87%	8	17.02%	6	17.14%	7	43.75%	2	10.00%	5	45.45%
Chloritoid	0	0.00%	0	0.00%	0	0.00%	0	0.00%	0	0.00%	0	0.00%
Hornblende	19	35.85%	12	25.53%	11	31.43%	5	31.25%	11	55.00%	5	45.45%
Garnet	1	1.89%	0	0.00%	0	0.00%	1	6.25%	3	15.00%	0	0.00%
Glaucofane	3	5.66%	3	6.38%	3	8.57%	0	0.00%	0	0.00%	0	0.00%
Sphene / Titanite	0	0.00%	0	0.00%	0	0.00%	0	0.00%	4	20.00%	0	0.00%
Biotite	0	0.00%	0	0.00%	0	0.00%	1	6.25%	0	0.00%	0	0.00%
Tremolite	0	0.00%	24	51.06%	15	42.86%	0	0.00%	0	0.00%	0	0.00%
Jadeite (Pyroxene)	0	0.00%	0	0.00%	0	0.00%	2	12.50%	0	0.00%	1	9.09%
Clinopyroxene	20	37.74%	0	0.00%	0	0.00%	0	0.00%	0	0.00%	0	0.00%
<i>Total Pyroxene</i>	20	37.74%	0	0.00%	0	0.00%	2	12.50%	0	0.00%	1	9.09%
Total HM	53	26.50%	47	23.50%	35	17.50%	16	8.00%	20	10.00%	11	5.50%
Accessory Minerals	N	% Total	N	% Total	N	% Total	N	% Total	N	% Total	N	% Total
Glauconite	2	25.00%	2	22.22%	2	40.00%	0	0.00%	0	0.00%	0	0.00%
Hematite	0	0.00%	1	11.11%	0	0.00%	0	0.00%	1	4.76%	0	0.00%
Opal	0	0.00%	0	0.00%	0	0.00%	0	0.00%	12	57.14%	6	85.71%
Tridymite	0	0.00%	0	0.00%	0	0.00%	0	0.00%	2	9.52%	0	0.00%
Total Accessory	2	1.00%	3	1.50%	2	1.00%	0	0.00%	15	7.50%	6	3.00%

Table 9(B): Summer Accessory & heavy mineral counts

Summer 2009	PR1		PR2		PR3		PR4		SR1		SR2		SR3		SR4		SR5	
heavy minerals	N	% Total	N	% Total	N	% Total	N	% Total	N	% Total	N	% Total	N	% Total	N	% Total	N	% Total
Chlorite	0	0.00%	1	5.88%	0	0.00%	5	16.1%	0	0.00%	0	0.00%	0	0.00%	0	0.00%	1	6.25%
Chloritoid	3	12.5%	0	0.00%	0	0.00%	0	0.00%	5	12.2%	3	10.00%	0	0.00%	0	0.00%	0	0.00%
Hornblende	9	37.5%	5	29.4%	7	29.2%	5	16.1%	19	46.3%	11	36.7%	21	46.7%	4	36.4%	7	43.8%
Garnet	0	0.00%	0	0.00%	2	8.33%	0	0.00%	3	7.32%	2	6.67%	6	13.3%		0.00%	0	0.00%
Glaucophane	0	0.00%	0	0.00%	0	0.00%	0	0.00%	0	0.00%	0	0.00%	0	0.00%	1	9.09%	0	0.00%
Sphene / Titanite	0	0.00%	0	0.00%	0	0.00%	0	0.00%	1	2.44%	0	0.00%	0	0.00%	0	0.00%	0	0.00%
Biotite	2	8.33%	4	23.5%	3	12.5%	8	25.8%	6	14.6%	1	3.33%	6	13.3%	6	54.5%	5	31.3%
Tremolite	0	0.00%	0	0.00%	0	0.00%	0	0.00%	0	0.00%	8	26.7%	2	4.44%	0	0.00%	0	0.00%
Jadeite (Pyroxene)	0	0.00%	0	0.00%	1	4.17%	5	16.1%	0	0.00%	0	0.00%	5	11.1%	0	0.00%	0	0.00%
Clinopyroxene	10	41.7%	7	41.2%	0	0.00%	0	0.00%	0	0.00%	0	0.00%	5	11.1%	0	0.00%	3	18.8%
Orthopyroxene	0	0.0%	0	0.00%	11	45.8%	8	25.8%	7	17.1%	0	0.00%	0	0.00%	0	0.00%	0	0.00%
<i>Total Pyroxene</i>	<i>10</i>	<i>41.7%</i>	<i>7</i>	<i>41.2%</i>	<i>12</i>	<i>50.0%</i>	<i>13</i>	<i>41.9%</i>	<i>7</i>	<i>17.1%</i>	<i>0</i>	<i>0.00%</i>	<i>5</i>	<i>11.1%</i>	<i>0</i>	<i>0.00%</i>	<i>0</i>	<i>0.00%</i>
Epidote	0	0.00%	0	0.00%	0	0.00%	0	0.00%	0	0.00%	5	16.7%	0	0.00%	0	0.00%	0	0.00%
Total HM	24	12.00%	17	8.50%	24	12.00%	31	15.50%	41	20.50%	30	15.00%	45	22.50%	11	5.50%	16	8.00%
Accessory Minerals	N	% Total	N	% Total	N	% Total	N	% Total	N	% Total	N	% Total	N	% Total	N	% Total	N	% Total
Glaucanite	1	33.3%	0	0.00%	2	33.3%	2	20.00%	3	30.00%	0	0.00%	1	5.88%	0	0.00%	0	0.00%
Hematite	0	0.00%	0	0.00%	1	16.7%	0	0.00%	0	0.00%	0	0.00%	0	0.00%	0	0.00%	0	0.00%
Opal	0	0.00%	0	0.00%	0	0.00%	0	0.00%	0	0.00%	0	0.00%	10	58.8%	0	0.00%	0	0.00%
Tridymite	0	0.00%	0	0.00%	0	0.00%	0	0.00%	1	10.00%	0	0.00%	0	0.00%	0	0.00%	1	100.00%
Total Accessory	1	0.50%	0	0.00%	3	1.50%	2	1.00%	4	2.00%	0	0.00%	11	5.50%	0	0.00%	1	0.50%

Table 9(C): Fall Accessory & heavy mineral counts

Fall 2009	PR1		PR2		PRS3		PR4		SR3		SR4		SR5	
heavy minerals	N	% Total	N	% Total	N	% Total	N	% Total	N	% Total	N	% Total	N	% Total
Chlorite	0	0.00%	0	0.00%	0	0.00%	0	0.00%	0	0.00%	0	0.00%	4	14.3%
Chloritoid	4	9.76%	4	8.33%	3	9.68%	2	8.70%	1	5.26%	1	4.76%	0	0.00%
Hornblende	12	29.3%	10	20.8%	8	25.8%	4	17.4%	7	36.8%	6	28.6%	12	42.9%
Garnet	1	2.44%	0	0.00%	0	0.00%	0	0.00%	1	5.26%	0	0.00%	2	7.14%
Biotite	4	9.76%	2	4.17%	6	19.4%	3	13.0%	3	15.79%	3	14.3%	1	3.57%
Augite	3	7.32%	3	6.25%	0	0.00%	2	8.70%	0	0.00%	0	0.00%	0	0.00%
Omphacite	0	0.00%	0	0.00%	0	0.00%	0	0.00%	0	0.00%	2	9.52%	0	0.00%
Jadeite	0	0.00%	0	0.00%	3	9.68%	1	4.35%	0	0.00%	0	0.00%	0	0.00%
Clinopyroxene	5	12.2%	13	27.1%	6	19.4%	4	17.4%	2	10.5%	1	4.76%	2	7.14%
Orthopyroxene	12	29.3%	16	33.3%	3	9.68%	7	30.4%	5	26.3%	5	23.8%	7	25.0%
<i>Total Pyroxene</i>	<i>17</i>	<i>41.5%</i>	<i>29</i>	<i>60.4%</i>	<i>12</i>	<i>38.7%</i>	<i>12</i>	<i>52.2%</i>	<i>7</i>	<i>36.8%</i>	<i>6</i>	<i>28.6%</i>	<i>9</i>	<i>32.1%</i>
Epidote	0	0.00%	0	0.00%	2	6.45%	0	0.00%	0	0.00%	3	14.3%	0	0.00%
Total HM	41	20.50%	48	24.0%	31	15.5%	23	11.5%	19	9.5%	21	10.5%	28	14.0%
Accessory Minerals	N	% Total	N	% Total	N	% Total	N	% Total	N	% Total	N	% Total	N	% Total
Glauconite	3	50%	2	25.00%		0.00%	4	44.4%	0	0.00%	0	0.00%	0	0.00%
Hematite	3	50%	4	50.00%	2	25.00%	2	22.2%	0	0.00%	0	0.00%	1	50%
Total Accessory	6	3.00%	6	3.00%	2	1.00%	6	3.00%	0	0.00%	0	0.00%	1	0.50%

Table 9(D): Seasonal Averages

Sample	Winter HM count	Percent of total	Summer HM count	Percent of total	Fall HM count	Percent of total
PR1	53	26.50%	24	12.00%	41	20.50%
PR2	47	23.50%	17	8.50%	48	24.00%
PR3	35	17.50%	24	12.00%	31	15.50%
SR3	16	8.00%	45	22.50%	19	9.50%
SR4	20	10.00%	11	5.50%	21	10.50%
SR5	11	5.50%	16	8.00%	28	14.00%
total	182		137		188	
average percents		15.17%		11.42%		15.67%

Table 9: Heavy and accessory mineral counts for (A) winter, (B) summer and (C) fall 2009 transects. N = number of minerals counted. %Total heavy minerals are based on total number of heavy minerals counted for each site, and total HM % is based on a total count of 200 grains. %Total accessory minerals are based on total number of accessory minerals counted for each site, and total accessory is based on a total count of 200 grains. Seasonal variation in total heavy mineral abundance is compared in table 9D, with percents based on total count of 200 grains. Transects SR1 & SR2 are excluded from averages because they were not included in winter and fall totals.

Table 10: San Lorenzo, Aromas and Upper Pajaro & Salinas Mineral counts

2009 Source Study	SLR1		SLR2		MD		UPR		USR		FD	
heavy minerals	N	% Total	N	% Total	N	% Total	N	% Total	N	% Total	N	% Total
Chlorite	0	0.00%	0	0.00%	0	0.00%	0	0.00%	0	0.00%	0	0.00%
Chloritoid	2	6.06%	1	12.5%	3	3.7%	1	3.0%	3	6.8%	3	14.3%
Hornblende	5	15.2%	0	0.0%	17	21.0%	5	15.2%	7	15.9%	1	4.8%
Garnet	0	0.00%	0	0.00%	1	1.23%	0	0.00%	4	9.09%	0	0.00%
Glaucofane	0	0.00%	0	0.00%	0	0.00%	0	0.00%	1	2.27%	0	0.00%
Chert	13	39.4%	3	37.5%	15	18.5%	9	27.3%	11	25.0%	10	47.6%
Sphene / Titanite	0	0.00%	0	0.00%	0	0.00%	0	0.00%	0	0.00%	0	0.00%
Rutile	0	0.00%	0	0.00%	0	0.00%	0	0.00%	0	0.00%	0	0.00%
Biotite	4	12.12%	0	0.00%	6	7.41%	3	9.09%	8	18.18%	0	0.00%
Tremolite	0	0.00%	0	0.00%	0	0.00%	0	0.00%	0	0.00%	0	0.00%
Omphacite	0	0.00%	0	0.00%	0	0.00%	0	0.00%	0	0.00%	0	0.00%
Augite	0	0.00%	0	0.00%	5	6.17%	0	0.00%	0	0.00%	0	0.00%
Clinopyroxene	2	6.06%	1	12.5%	18	22.2%	3	9.09%	2	4.55%	3	14.3%
Orthopyroxene	7	21.2%	3	37.5%	16	19.8%	12	36.4%	7	15.9%	4	19.0%
<i>Total Pyroxene</i>	<i>9</i>	<i>27.3%</i>	<i>4</i>	<i>50.0%</i>	<i>39</i>	<i>48.1%</i>	<i>15</i>	<i>45.5%</i>	<i>9</i>	<i>20.5%</i>	<i>7</i>	<i>33.3%</i>
Epidote	0	0.00%	0	0.00%	0	0.00%	0	0.00%	1	2.27%	0	0.00%
Total HM count	33	16.5%	8	4.00%	81	40.5%	33	16.5%	44	22.0%	21	10.5%
Accessory Minerals	N	% Total	N	% Total	N	% Total	N	% Total	N	% Total	N	% Total
Hematite	1	3.03%	0	0.00%	2	2.47%	0	0.00%	0	0.00%	2	9.52%
Glauconite	0	0.00%	1	12.50%	2	2.47%	0	0.00%	0	0.00%	0	0.00%
Opal	0	0.00%	0	0.00%	1	1.23%	0	0.00%	0	0.00%	4	19.05%
Total Accessory	1	3.03%	1	12.50%	5	6.17%	0	0.00%	0	0.00%	6	28.57%

Table 10: Heavy mineral counts from Swash zone samples San Lorenzo river mouth (SLRM1), 1 km east of San Lorenzo River mouth (SLRM2); dune samples from Manresa (MD) and Fort Ord (FD); and channel samples from the Salinas (USR) and Pajaro (UPR) Rivers

Table 11: upper Pajaro and Salinas channel pebbles

Rock	Extrusive / Intrusive?	Pajaro Count	Pajaro % Total	Salinas Count	Salinas % Total
Dacite	Extrusive	0	0.00%	1	5.26%
Diorite	Intrusive	0	0.00%	1	5.26%
Granidorite	Intrusive	2	12.50%	8	42.11%
Granite	Intrusive	0	0.00%	1	5.26%
Basalt	Extrusive	9	56.25%	1	5.26%
Arenite	Sedimentary	0	0.00%	1	5.26%
Arkose	Sedimentary	2	12.50%	2	10.53%
Breccia	Sedimentary	0	0.00%	1	5.26%
Conglomerate	Sedimentary	0	0.00%	2	10.53%
Pegmatite	Hypabyssal Igneous	0	0.00%	1	5.26%
Andesite	Extrusive	3	18.75%	0	0.00%

Table 11: Total counts of pebbles collected from the upper Pajaro and Salinas channels. % Totals are based on 16 total Pajaro pebbles and 19 total Salinas pebbles collected.

FIGURES

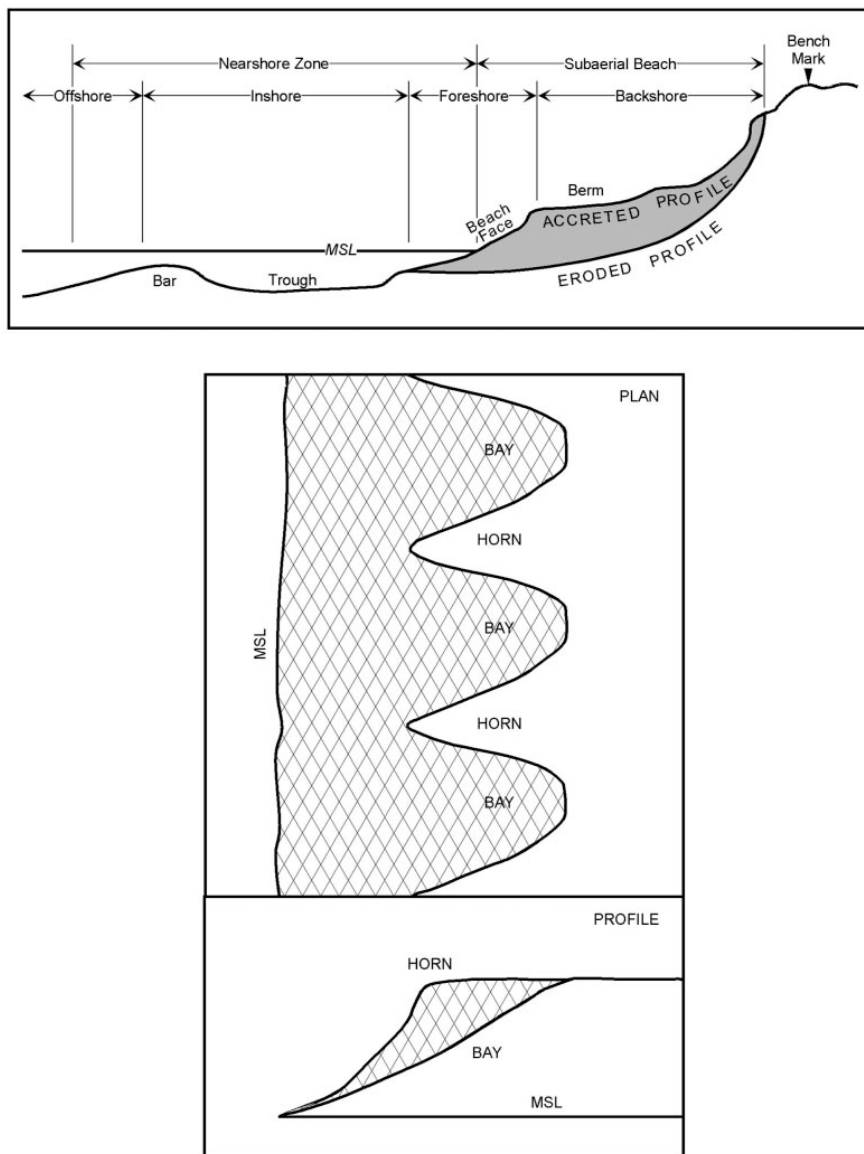


Figure 1: Beach terminology and seasonal changes in beach morphology. (Top) General profile. (Bottom) General profile of Beach cusps (Dingler & Reiss 2002).

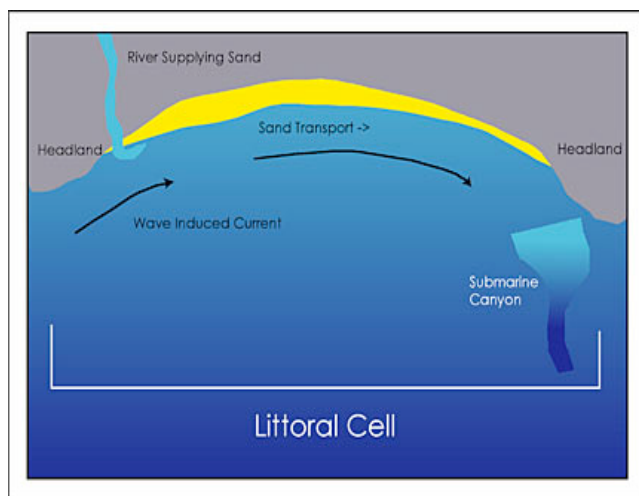


Figure 2: General littoral cell pattern commonly observed along the California coast. Sediment from rivers and erosional coastal features is redistributed down the coast. The majority of terrigenous input into a cell is lost along headlands, canyons or broader continental margins. Image taken from Washington Department of Ecology webpage: http://www.ecy.wa.gov/programs/sea/swces/research/sediment_budget.htm

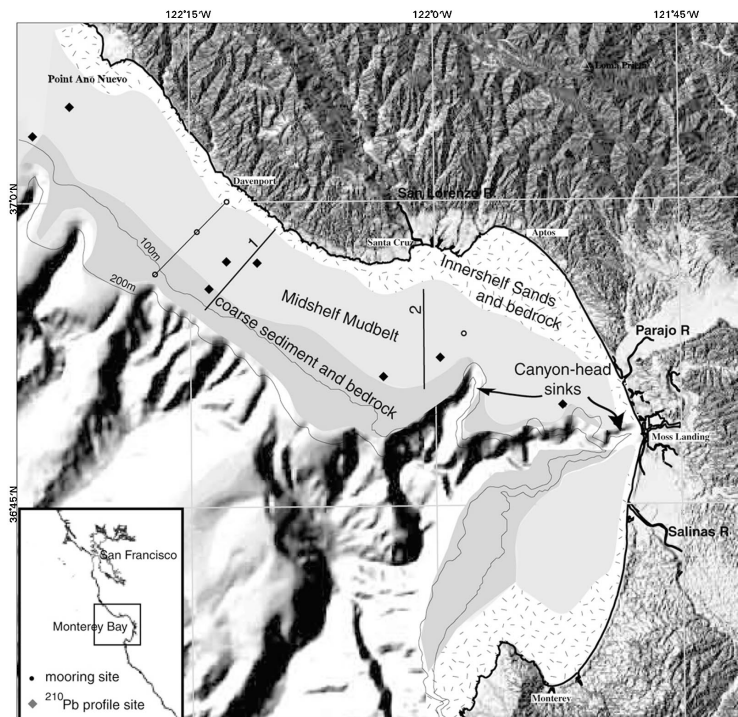


Figure 3: Generalized sediment-type provinces derived from maps in Edwards (2002) and Eittrheim et al (2002).

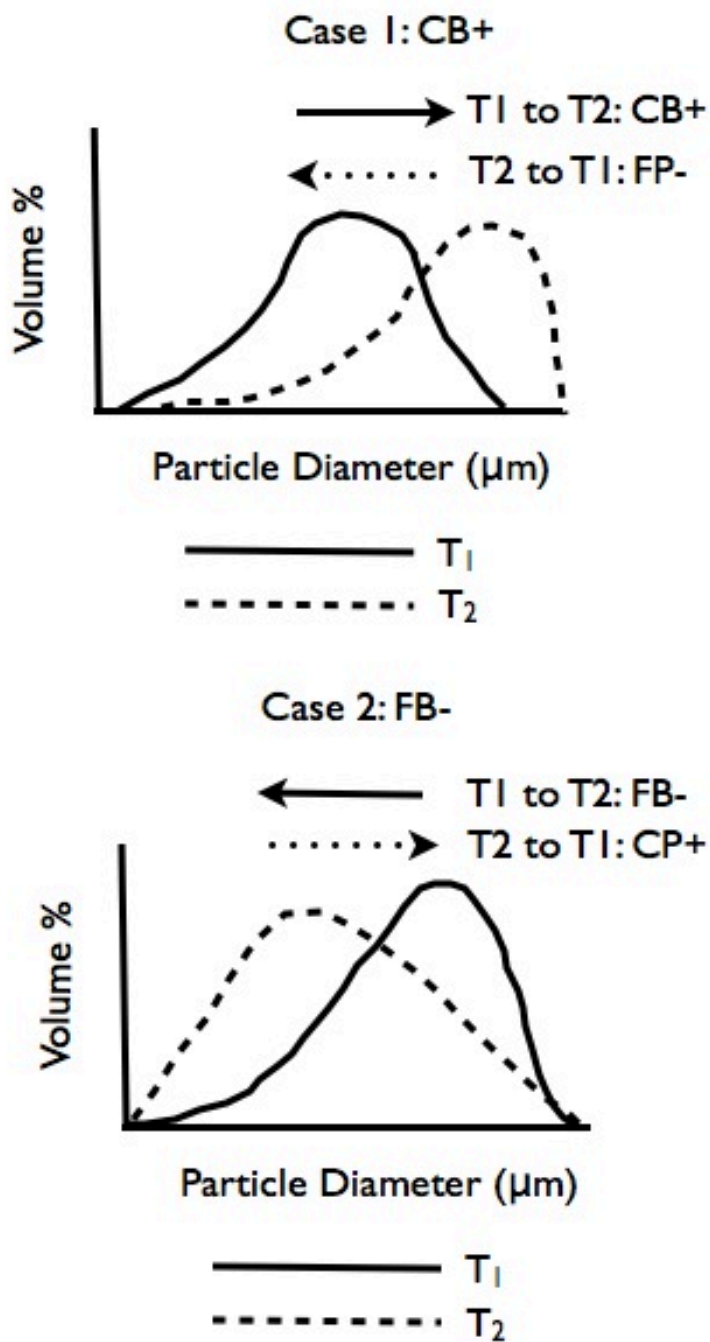


Figure 4: Diagrammatic summary of resulting grain size distributions relating deposits in the direction of transport between two transects (T1 & T2) given select combinations of wave energy and grain size (McLaren & Bowles 1985).

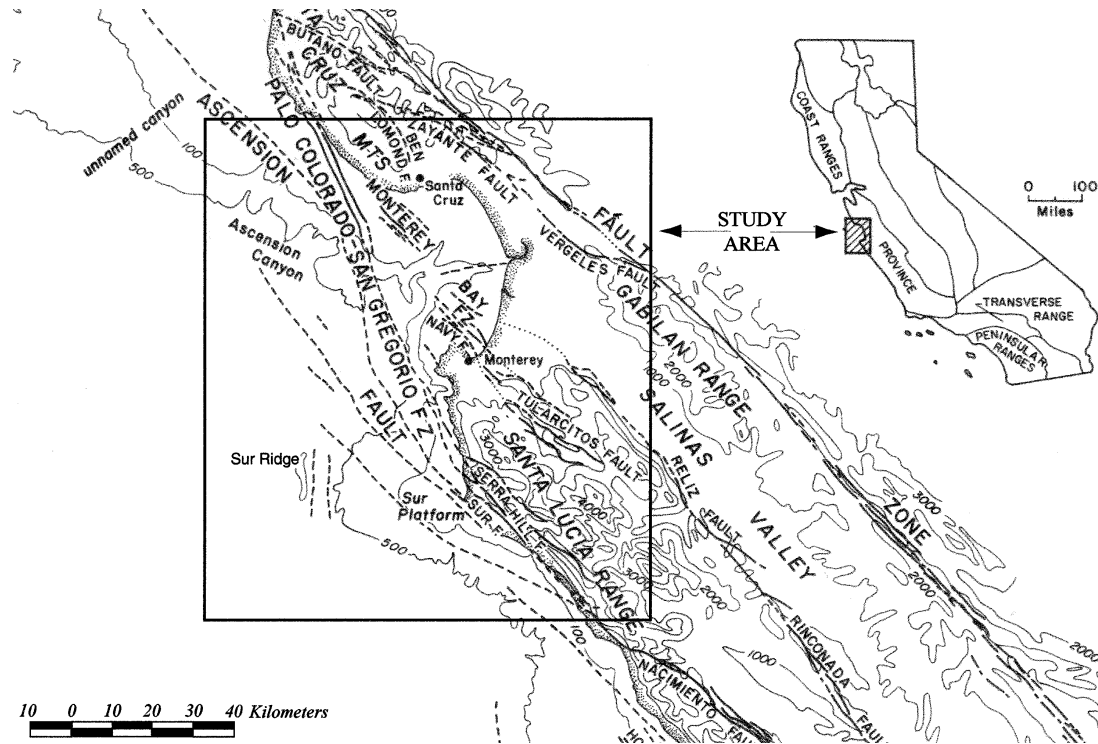


Figure 5: Map of fault blocks surrounding the Monterey Bay area (boxed in area). Salinian Block is bounded by San Andreas Fault to the east and the San Gregorio-Sur Nacimiento Fault zone to the southwest. Franciscan block is bound by San Andreas to the east and San Gregorio fault zone to the east (Greene et al 2002).



Figure 6: Aerial map of the Pajaro and Salinas Watersheds showing nearby mountain ranges. Large amounts of sphene, garnet and hornblende are eroded into the Salinas Watershed from the Gabilan and Santa Lucia Range (Yancy 1972). Augite, pyroxene and glaucophane are commonly eroded from the Diablo Range into the Pajaro Watershed (Yancy 1972, Image courtesy of Google).

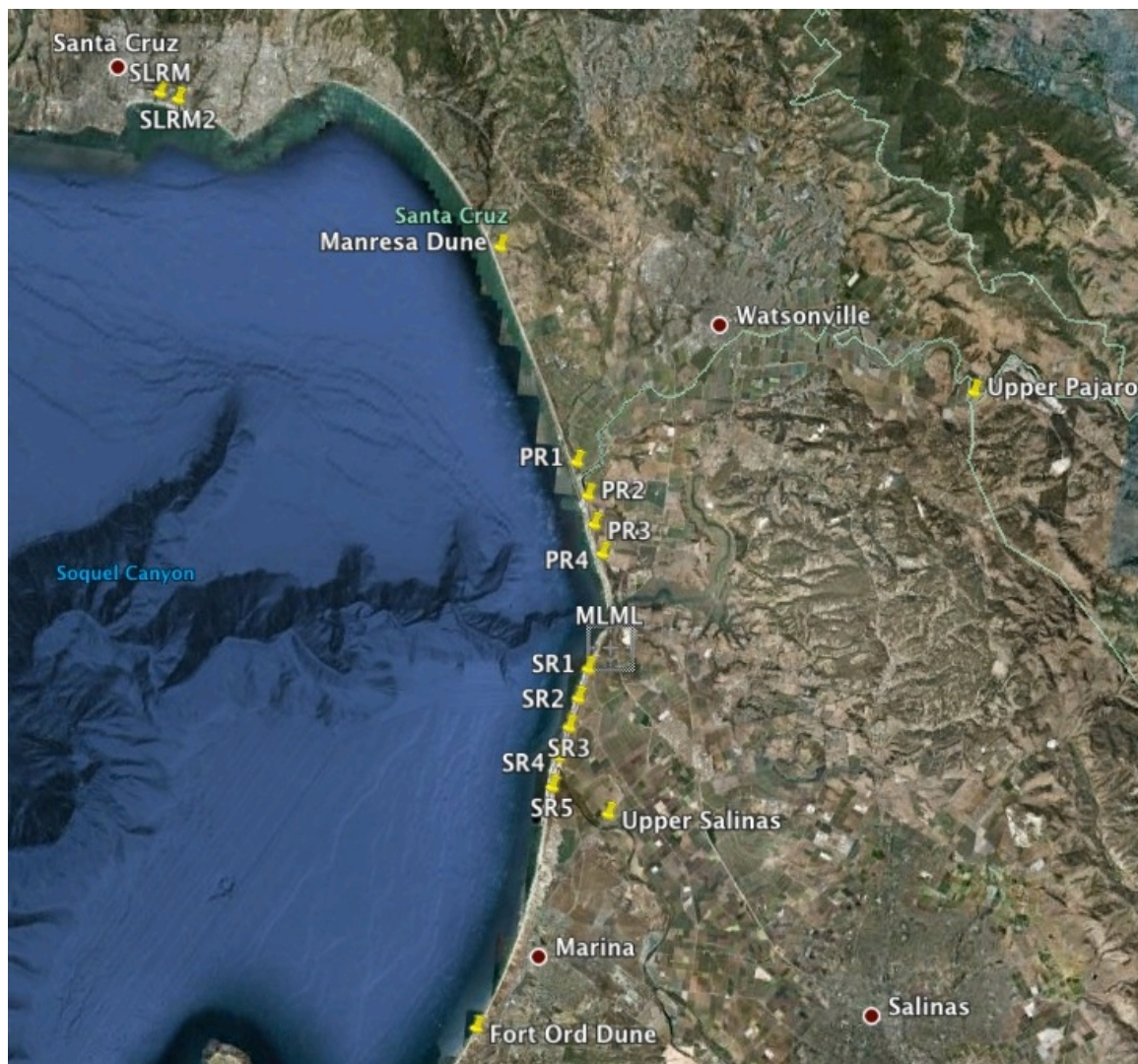


Figure 7: Aerial map of central Monterey Bay showing Pajaro (PRM1-PRM4) and Salinas (SR1-SR5) transects. Transects are spaced approximately 1 km apart.

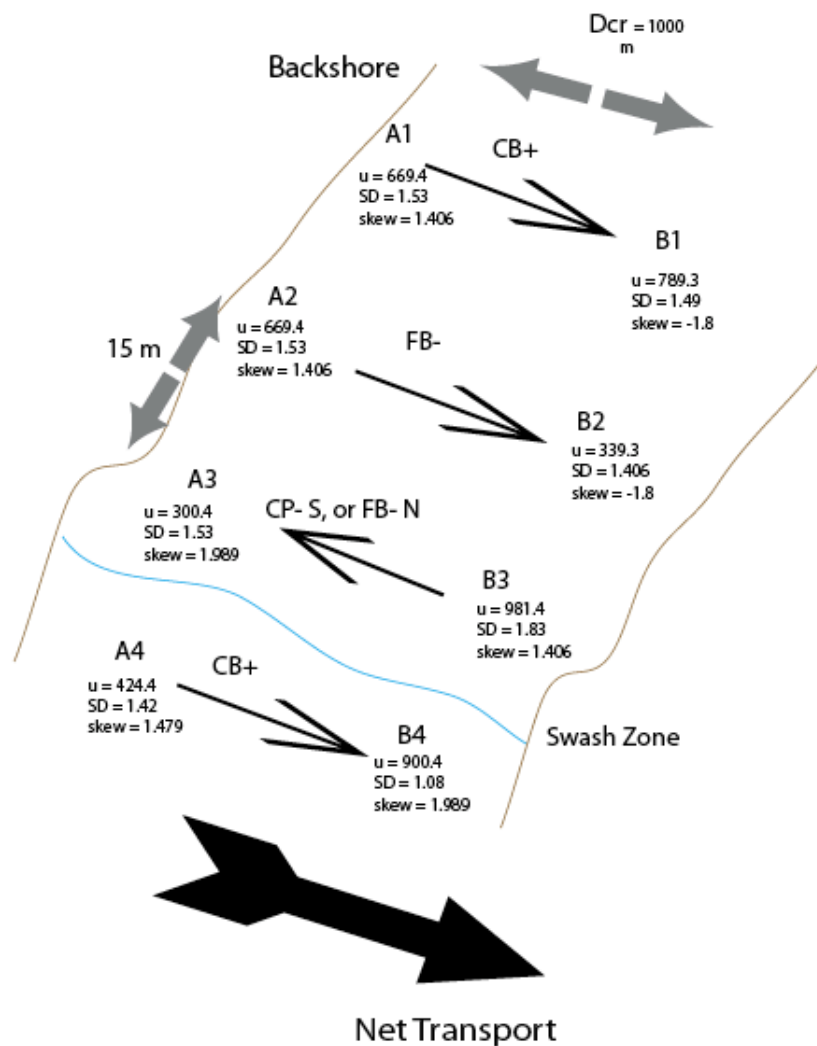


Figure 8: Diagram of arbitrary sample transects A and B, with incorporated Gao and Collins (1992) trend (small arrows) and net transport (large arrow) vectors. Each transect contains four samples starting at the swash zone and moving at 15 m intervals to the backshore. Net transport between transects A and B is averaged from trend vectors estimated between sample sites of different transects. Transport estimated to be in the direction of decreasing grain size and skewness. Figure is not to scale, as spacing between transects is ~ 1 km, but spacing between within Transect locations (A1 to A2) is 10 m. Diagram is not to scale. Trend vectors calculated based on mean grain size (u), skewness ($skew$) and sorting / standard deviation (SD). Sediments in the transport direction can either be finer with no increase in skewness (FB-) or coarser with no decrease in skewness (CB+) (Gao & Collins 1992).

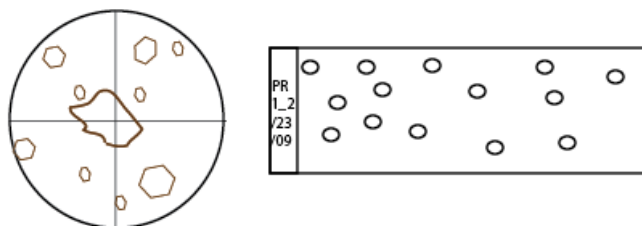


Figure 9: Random point-count procedure for thin section analysis. Circles on the right represent the random nature of clast selection. After each mineral is identified, the stage is moved at random and the clast closest to the center of the cross-hairs under the 40x objective lens were selected for identification (left). This procedure was repeated 200 times for each thin section.

Figure 10(A): Pajaro Grain Size Trends

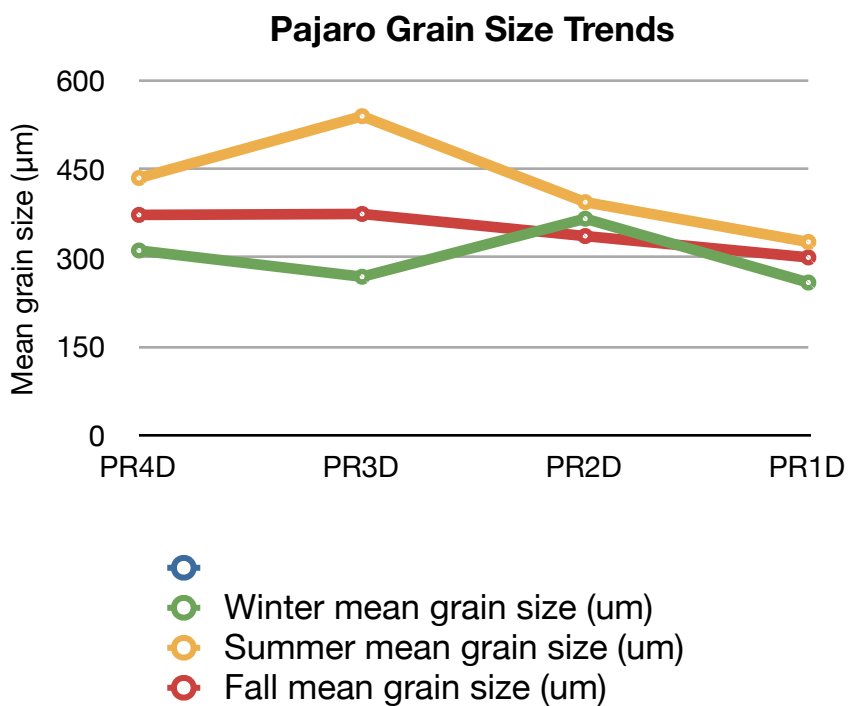


Figure 10(B): Salinas Grain Size Trends

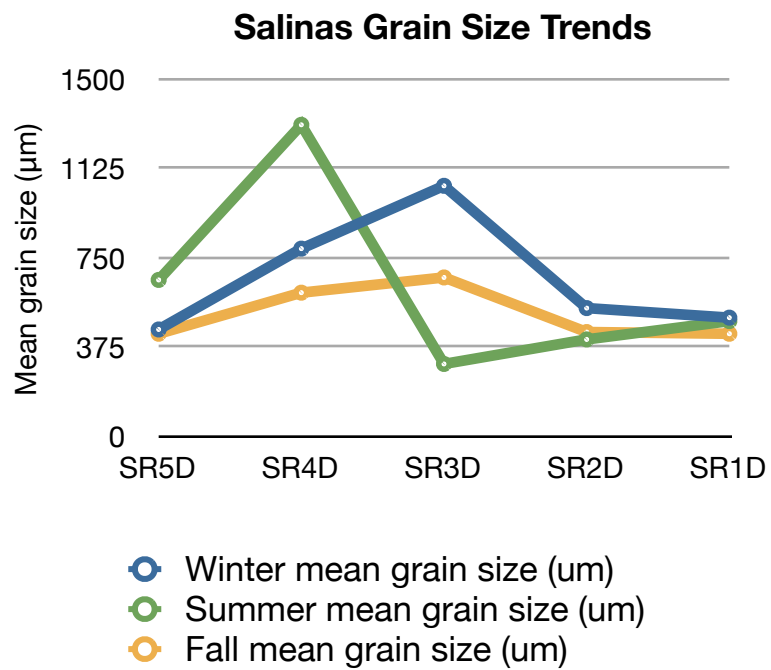


Figure 10: Grain size plotted against Transect location from (A) Pajaro and (B) Salinas River mouths for Winter, Summer and Fall seasons.

Figure 11(A): Pajaro Sorting

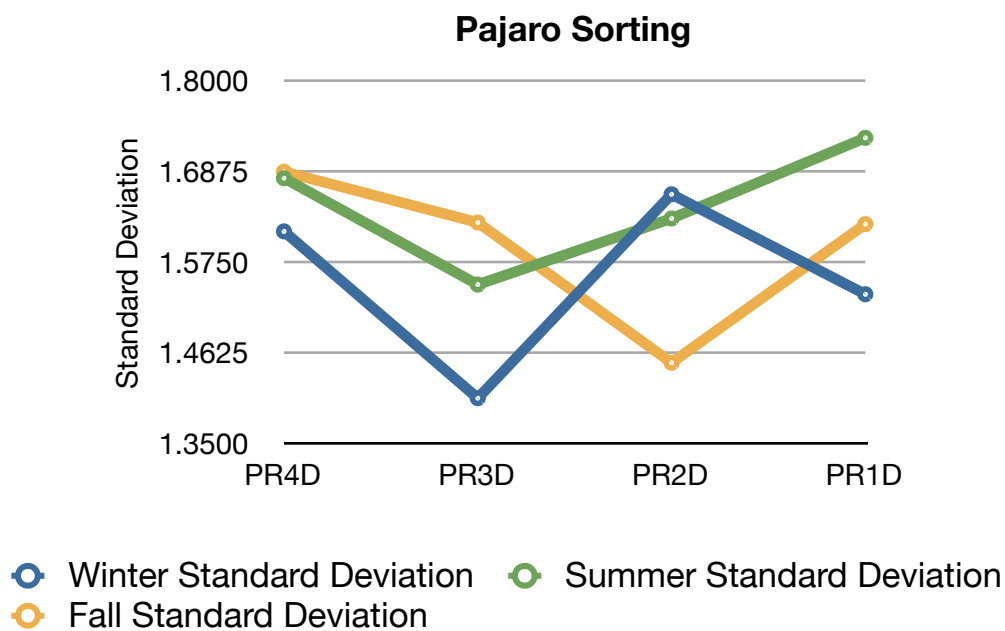


Figure 11(B): Salinas Sorting

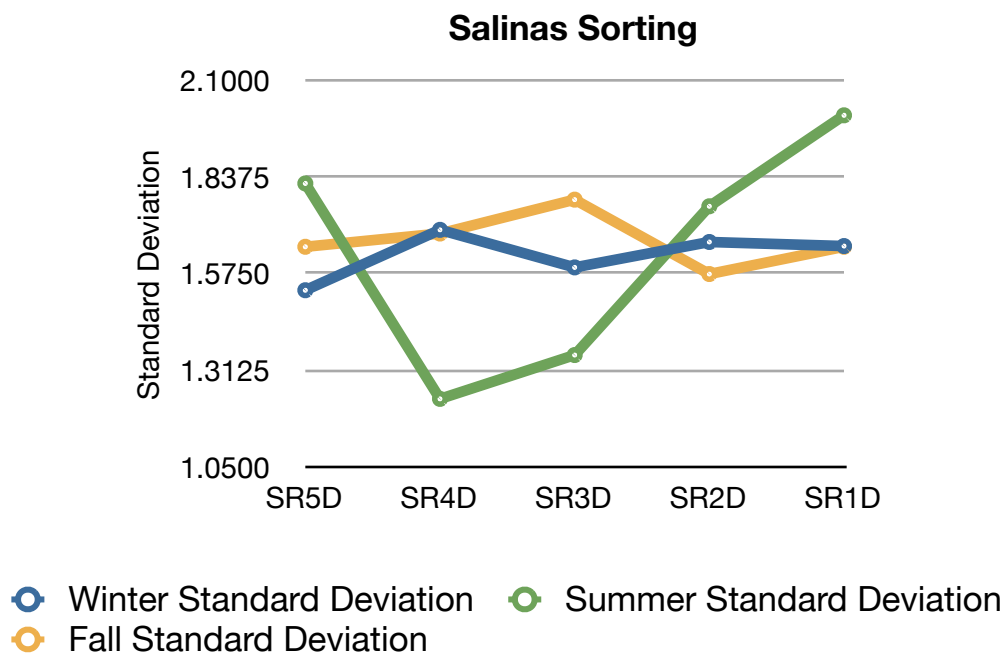


Figure 11: Standard deviation plotted against Transect location from (A) Pajaro and (B) Salinas River mouths for Winter, Summer and Fall seasons.

Figure 12(A): Salinas Berm Sorting Trends

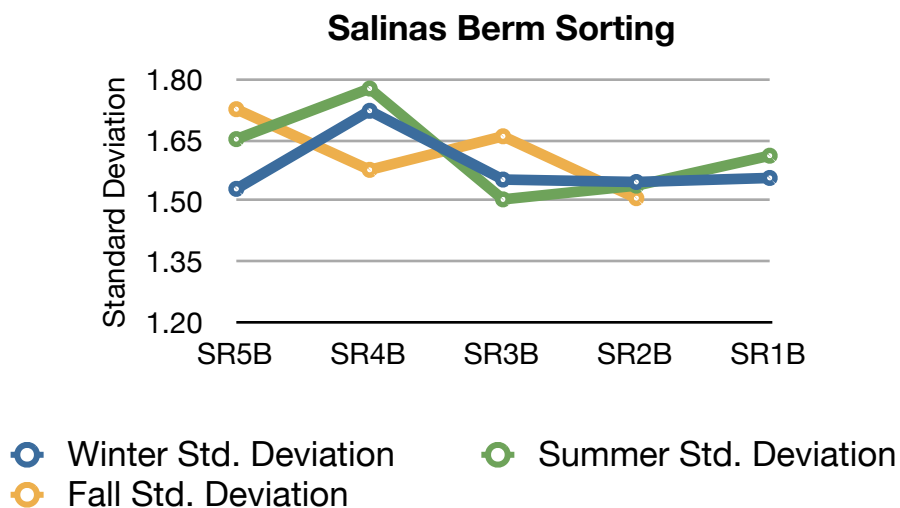


Figure 12(B): Pajaro Berm Sorting Trends

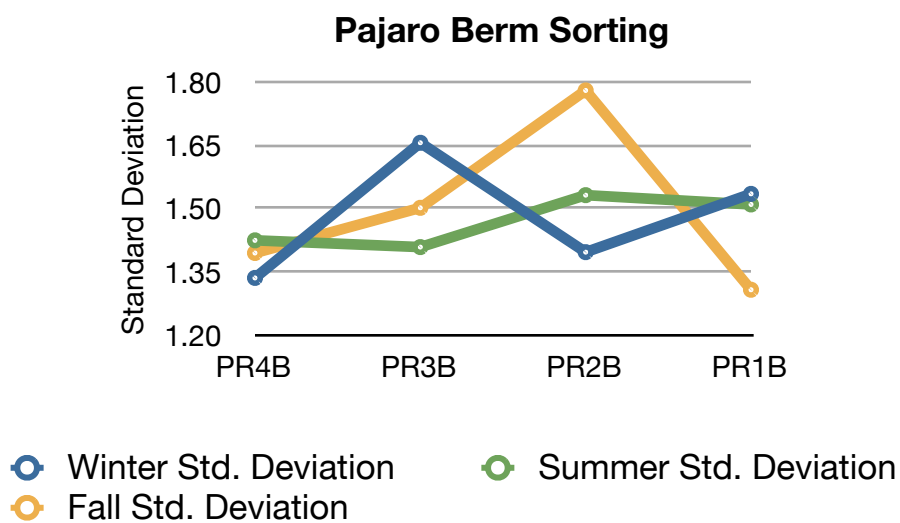


Figure 12: Standard Deviation of berm samples plotted against Transect location from (A) Salinas and (B) Pajaro River mouths for Winter, Summer and Fall seasons. As the deviation increases, the sorting decreases.

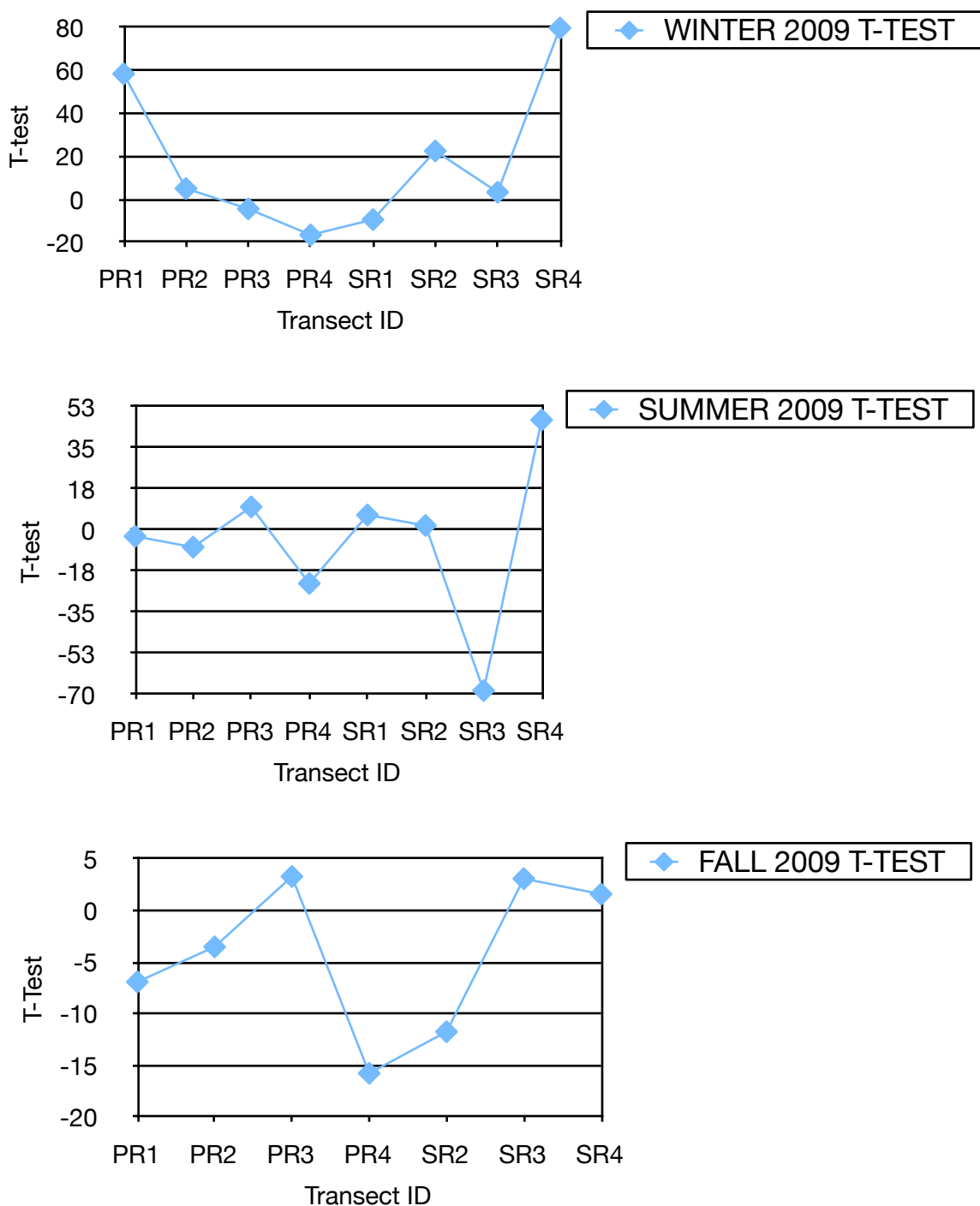


Figure 13: Results of the 2-sample T-test performed between transects for Winter - Fall sampling seasons. The T-test has 6 degrees of freedom with a p-value of 0.05 and a critical value of 2.45. All data less than 2.45 are considered to be significant. Transect T-tests compare downcoast transects, so a Northern transect to it's closest southern one (ie: PR1 is compared to PR2 to produce the first data point).

Figure 14(A): Winter Pajaro grain size frequency curve

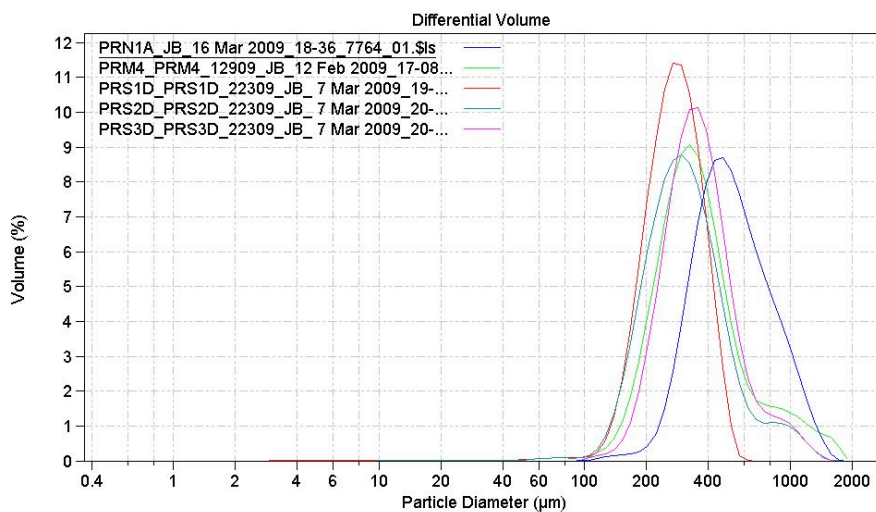


Figure 14(B): Winter Salinas grain size frequency curves

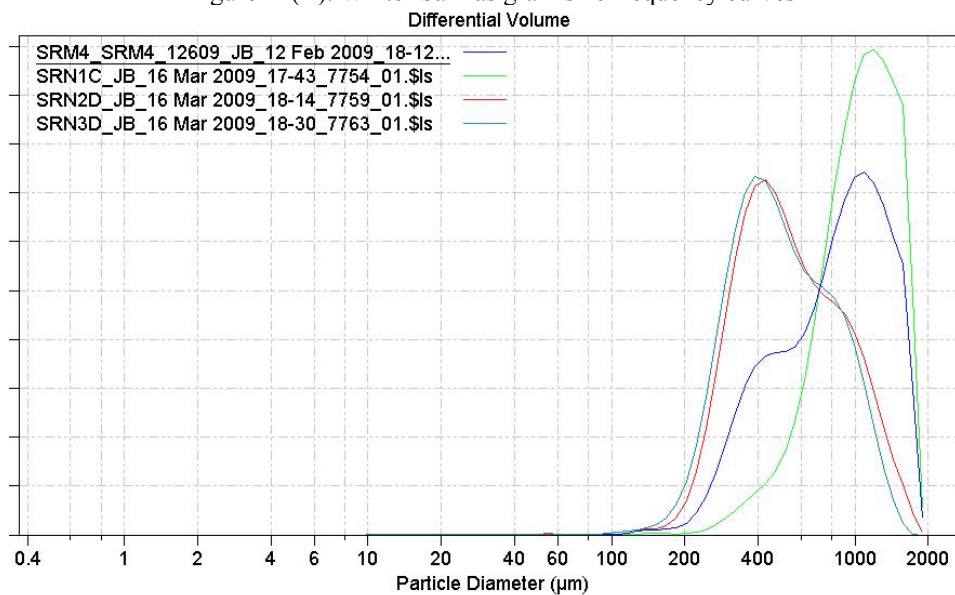


Figure 14: Frequency plots for Swash zone samples collected from winter transects. (A) Winter Pajaro transect grain size distributions. PRN1 = PR1, PRM4 = PR2, PRS1D = PR3, PRS2D = PR3, PRS3D = PR4. Changes in the grain size frequency plots reflect changes in the amount of coarse and fine grains. (B) Winter Salinas transect grain size distributions. SRM4 = SR4, SRN1 = SR3, SRN2D = SR2, SRN3D = SR1.

Figure 15(A): Summer Salinas grain size frequency plots

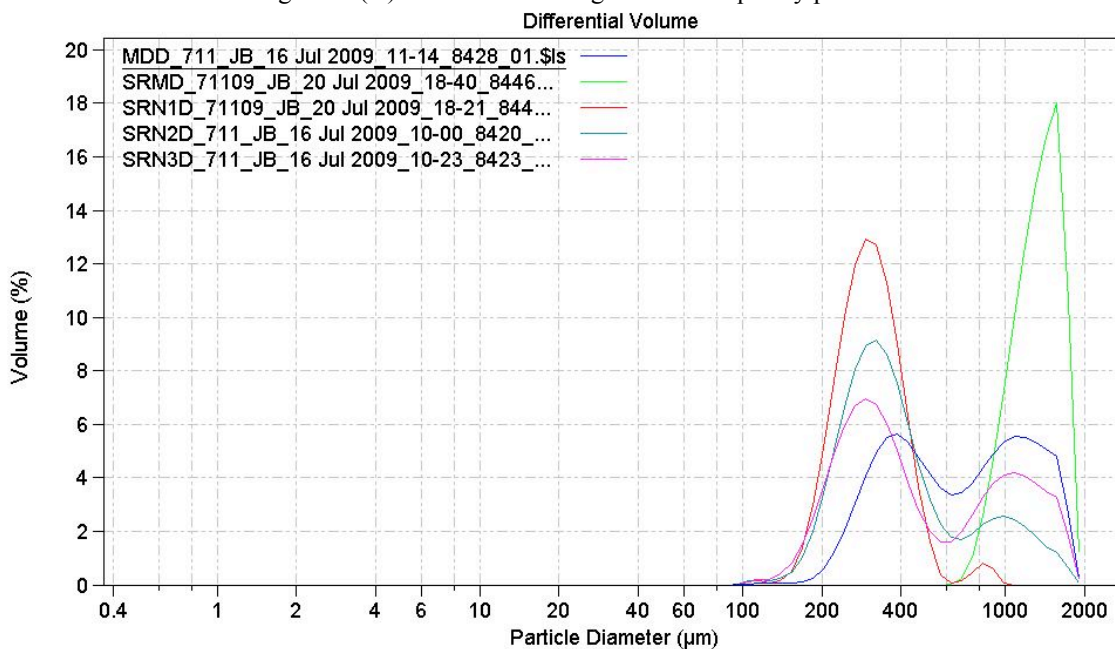


Figure 15(B): Summer Pajaro grain size frequency plot

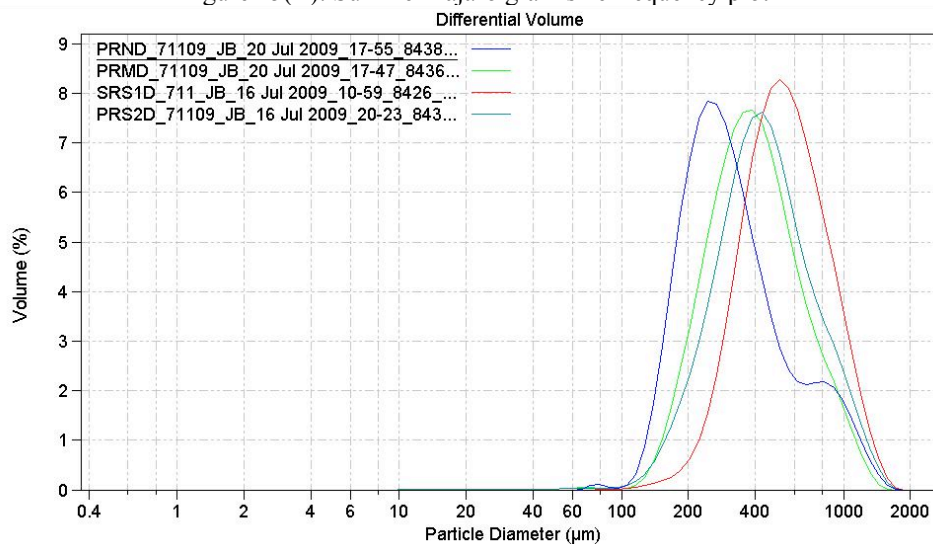


Figure 15: Summer Salinas (A) and Pajaro (B) River Mouth transect grain size distributions. Each overlay represents the swash zone grain size distributions for each transect. Pajaro transects: PRND = swash zone sample 1 km north of the Pajaro River mouth. PRMD = swash zone sample from the Pajaro River mouth, SRS1 was mislabeled and = Swash zone samples 1 km south of the Pajaro River mouth, PRS2D = swash zone sample 2 km south of Pajaro River mouth. Salinas transects: MDD = swash zone sample 1 km south of the Salinas River mouth, SRMD = swash zone sample from Salinas River mouth, SRN1D = swash zone sample 1 km north of the Salinas River mouth, SRN2D = swash zone sample 2 km north of the Salinas River mouth, SRN3D = swash zone sample 3 km north of the Salinas River mouth.

Figure 16(A): Fall Pajaro grain size frequency plots

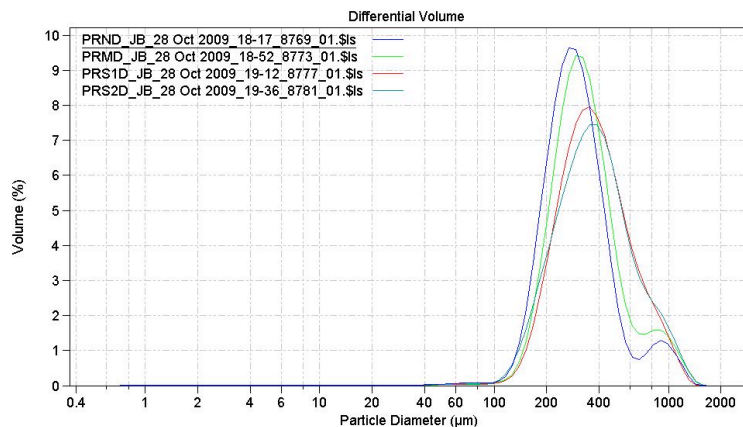


Figure 16(B): Fall Salinas grain size frequency plots

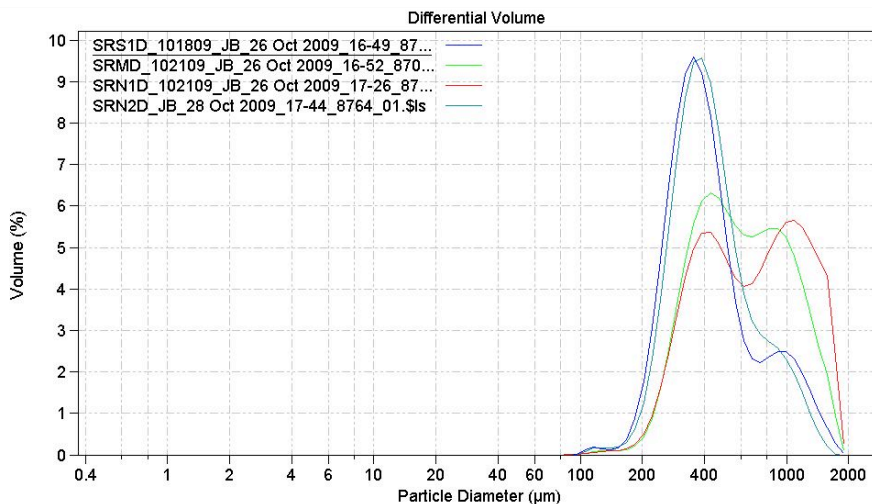


Figure 16: Fall Pajaro (A) and Salinas (B) River Mouth transect grain size distributions. Each overlay represents the swash zone grain size distributions for each transect. Pajaro transects: PRND = swash zone sample 1 km north of the Pajaro River mouth. PRMD = swash zone sample from the Pajaro River mouth, PRS1D = Swash zone samples 1 km south of the Pajaro River mouth, PRS2D = swash zone sample 2 km south of Pajaro River mouth. Salinas transects: MDD = swash zone sample 1 km south of the Salinas River mouth, SRMD = swash zone sample from Salinas River mouth, SRN1D = swash zone sample 1 km north of the Salinas River mouth, SRN2D = swash zone sample 2 km north of the Salinas River mouth.

Figure 17(A): Winter 2009 Grain Size Trends

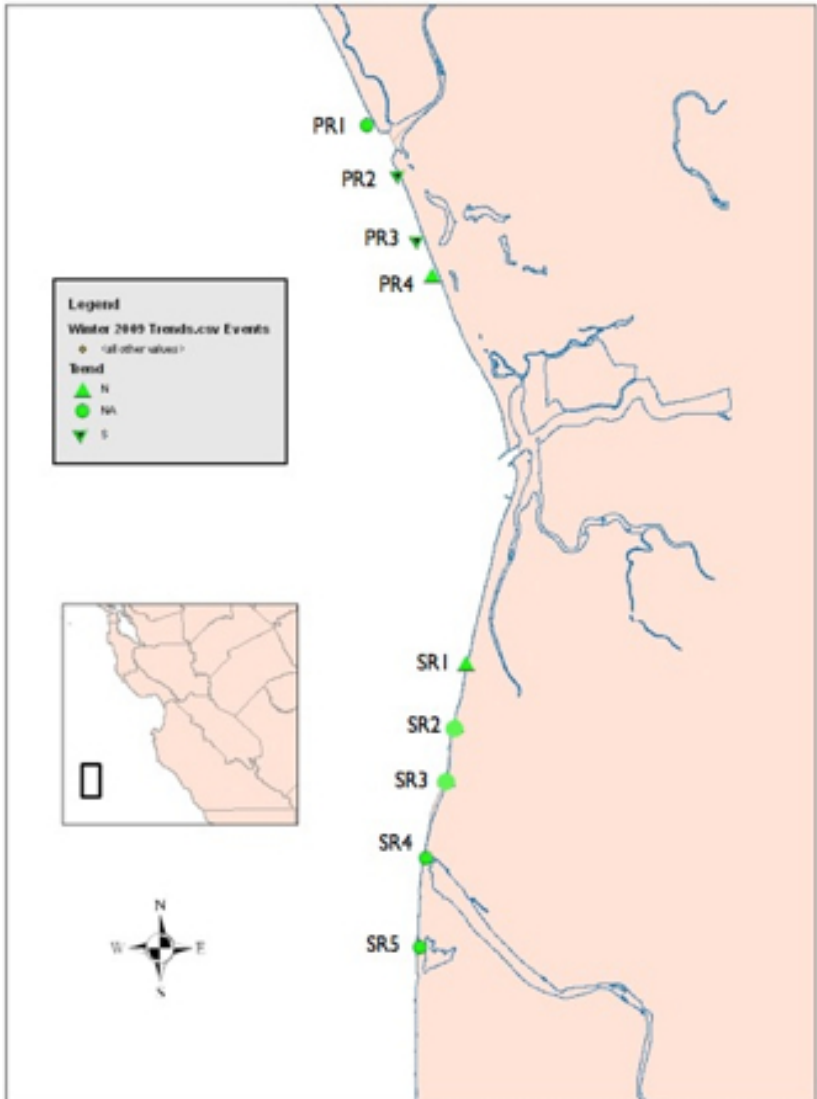


Figure 17(B): Summer 2009 Grain Size Trends

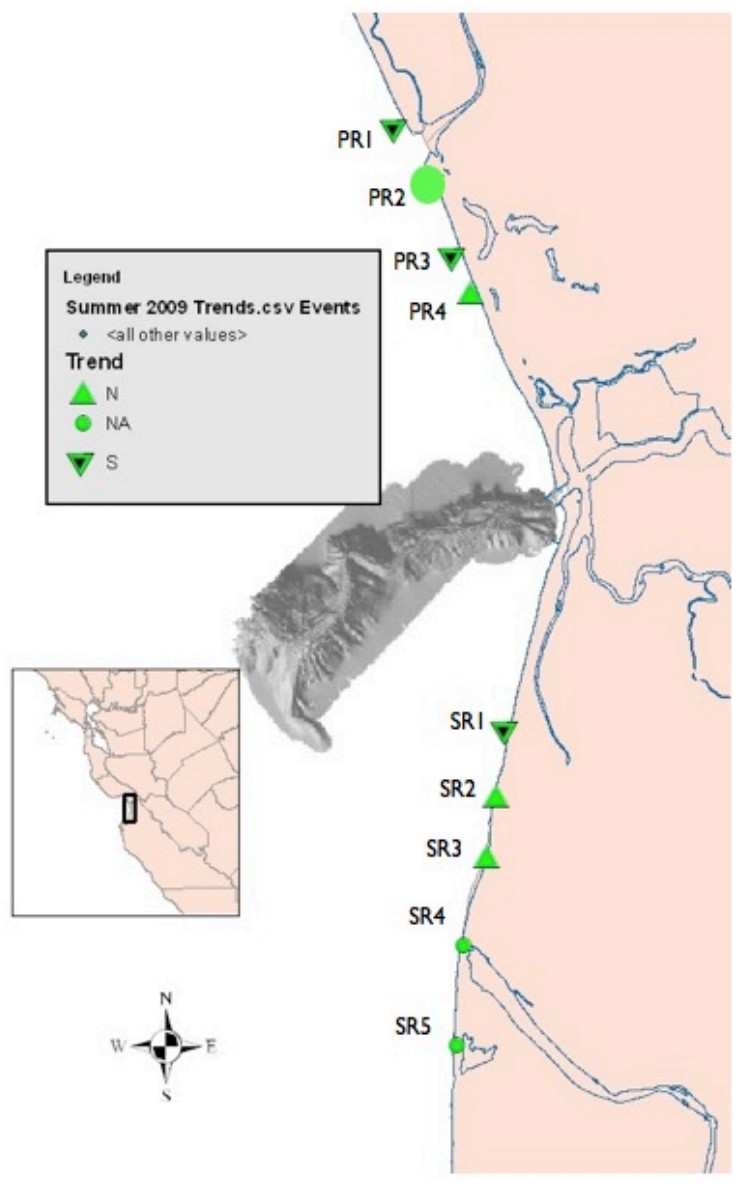


Figure 17(C): Fall 2009 Grain Size Trends

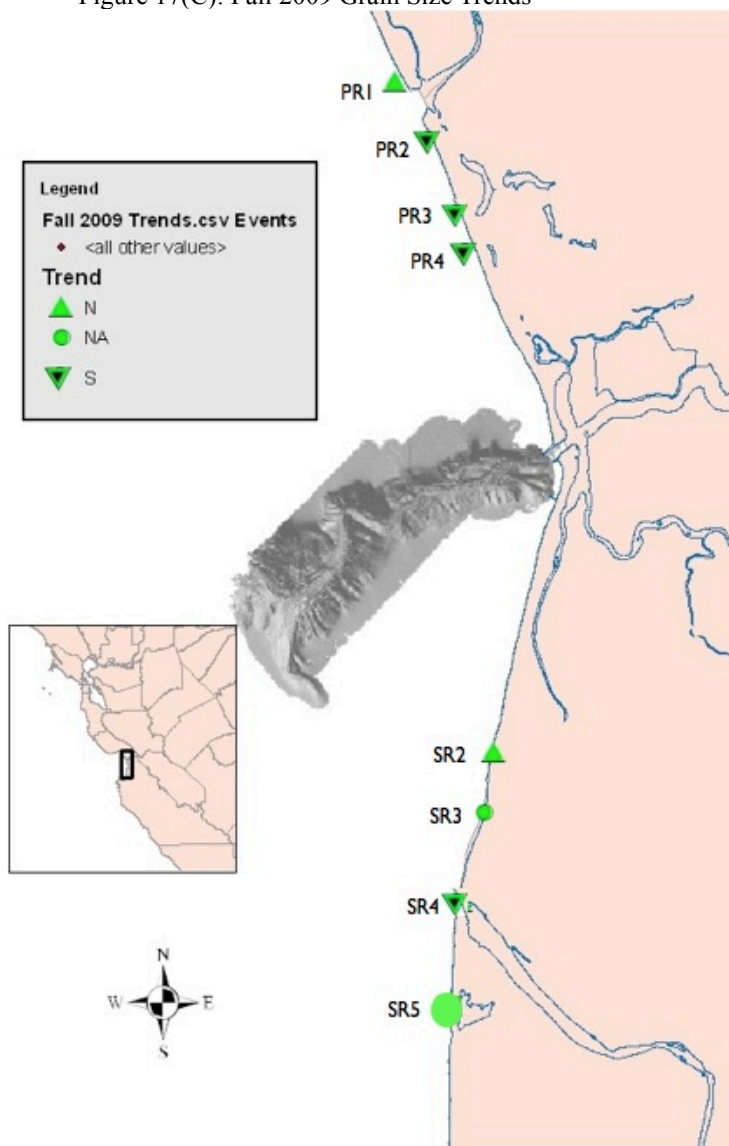


Figure 17: Transect locations and trends for samples collected in (A) Winter 2009, (B) Summer 2009 and (C) Fall 2009 samples. Arrows indicate transport direction. Circle points do not have a recognizable trend attributed to them, according to the Gao & Collins (1992) methodology.

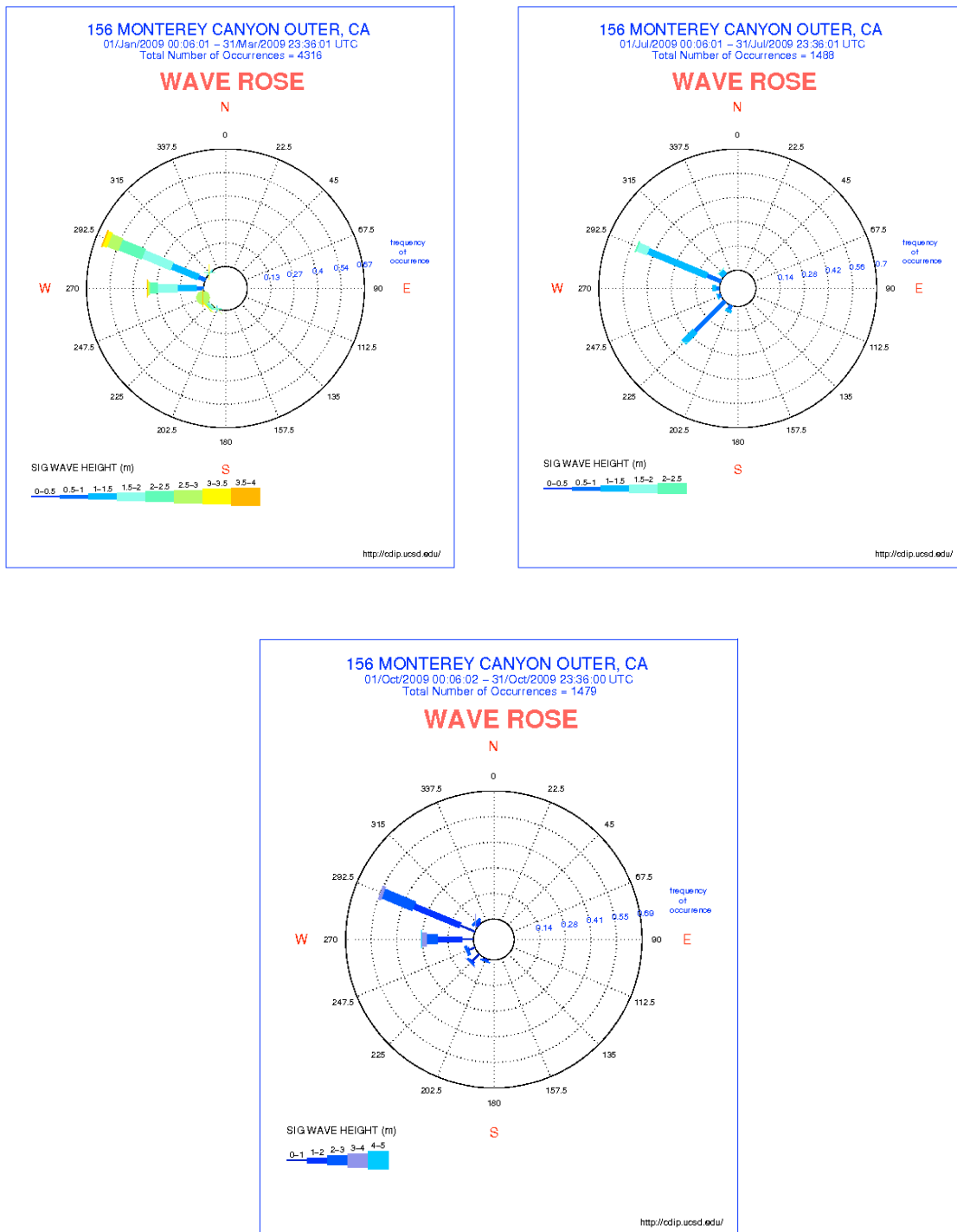


Figure 18: Swell direction and frequency plot for (A) Winter 2009 transects, (B) Summer 2009 transects and (C) October 2009 transects. Based on data from CDIP Buoy #156.

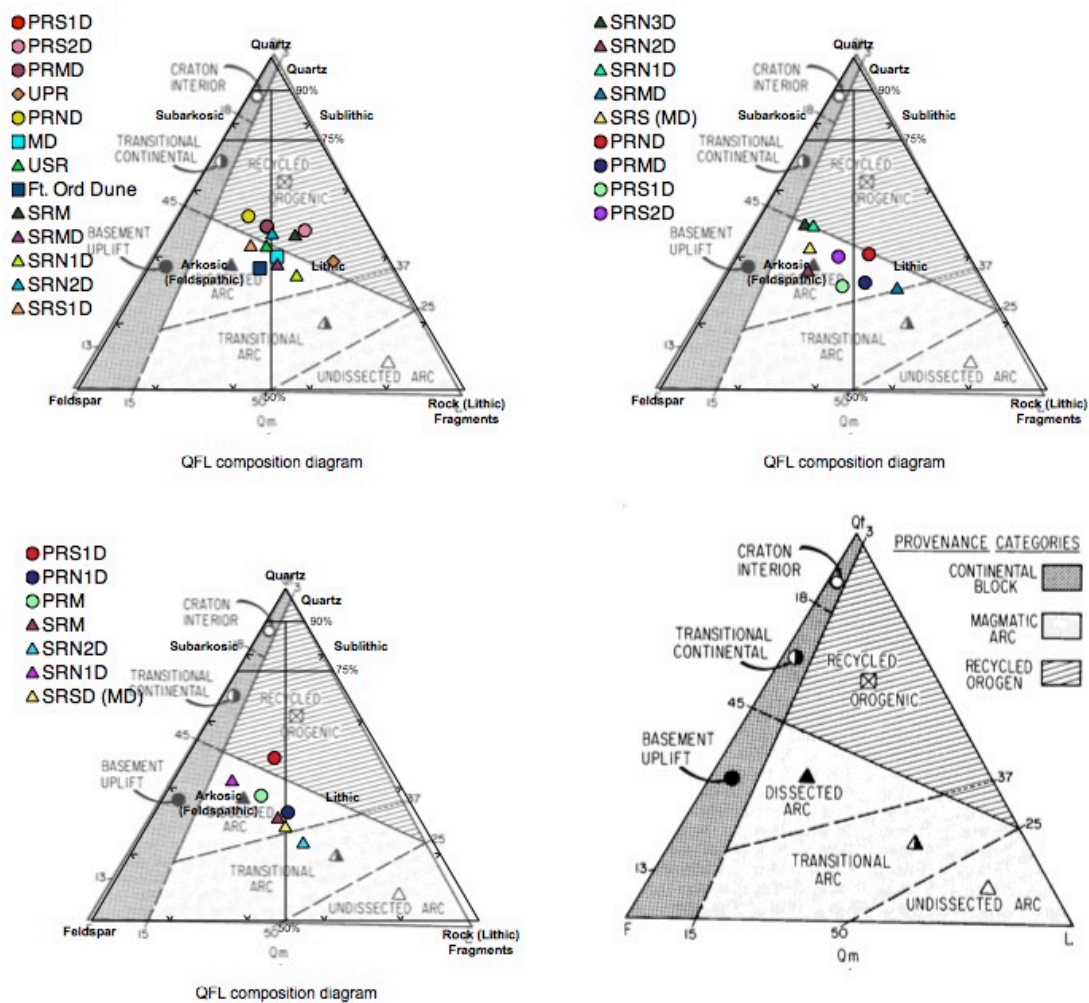


Figure 19: QFL composition plots for Winter (top left), Summer (top right), and Fall (bottom left) swash zone sediment. Plots are superimposed over Continental Block, Magmatic Arc and Recycled Orogen provenance categories shown in bottom right diagram and based on the research of Dickenson & Suczek (1979). PRS1D=swash zone sample from 1 km south of Pajaro River Mouth. SRS = 1 km south of Salinas River Mouth. Plots based on ternary diagram from Dickenson & Suczek (1979).

Figure 20(A): Winter 2009 Lithics

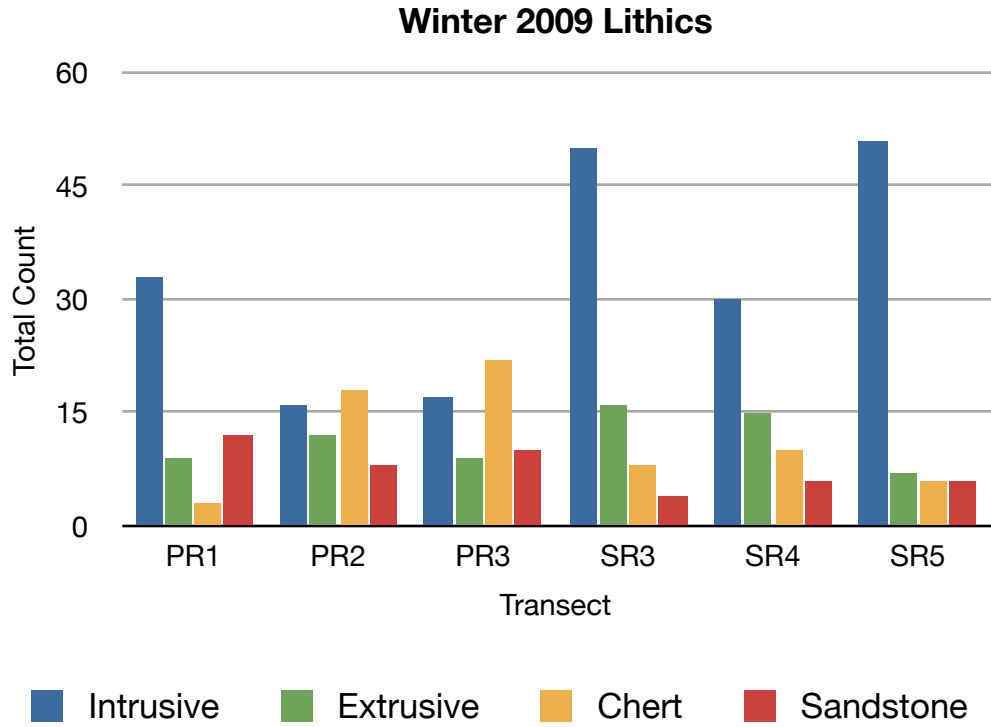


Figure 20(B): Summer 2009 Lithics

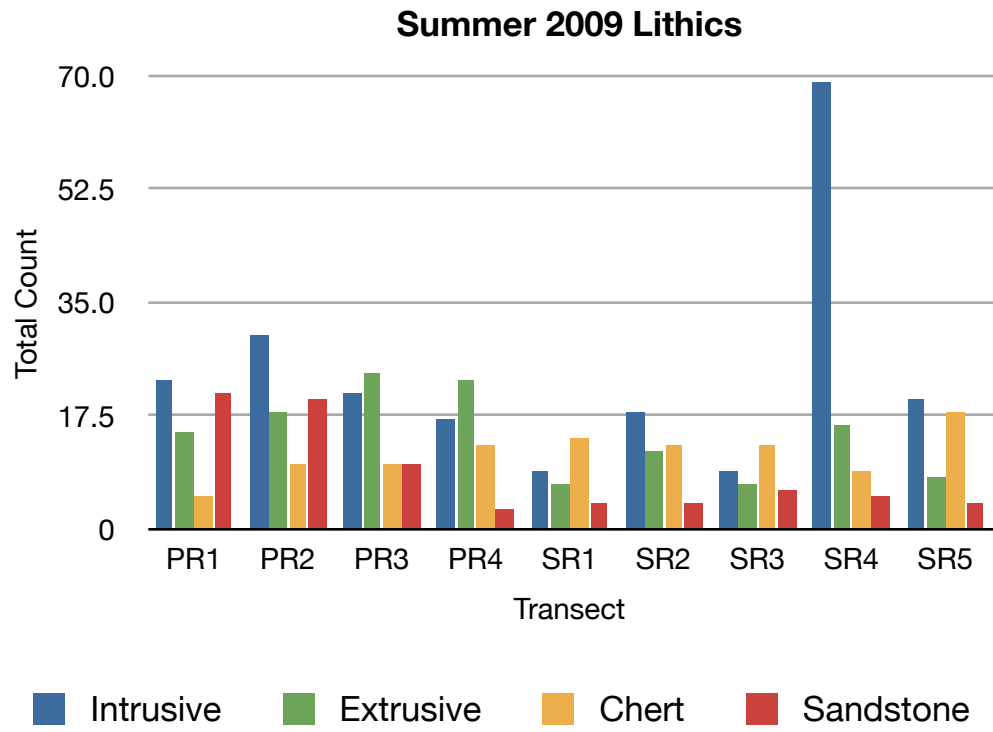
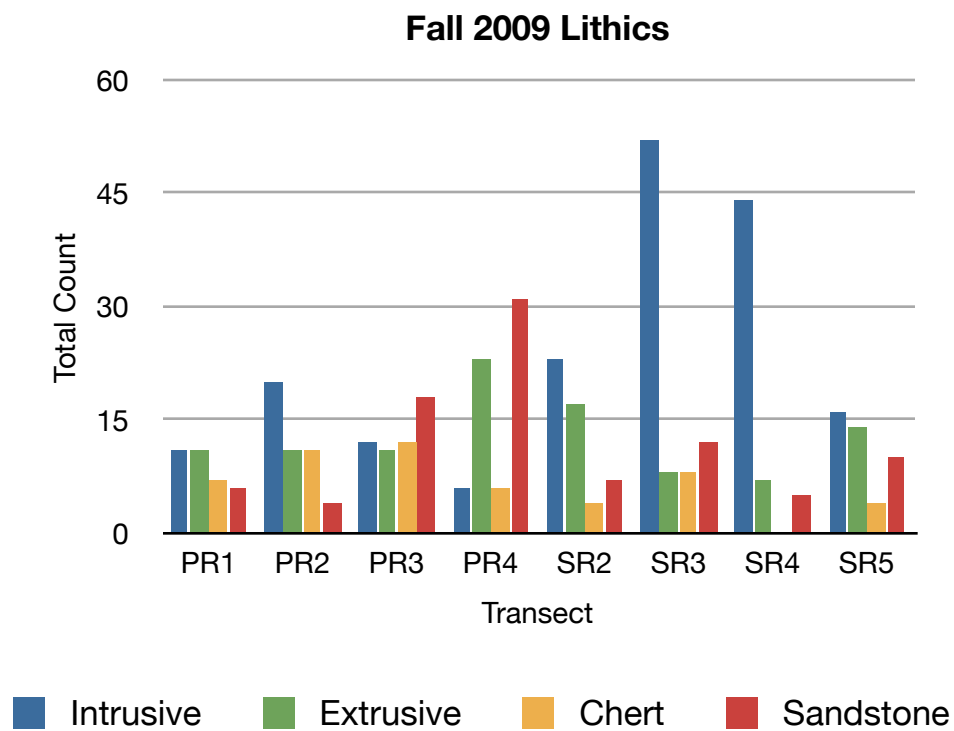


Figure 20(C): Fall 2009 Lithics



(C)

Figure 20: Lithic counts for (A) winter, (B) summer and (C) fall seasons. Lithics are classified as Intrusive, Extrusive, Chert or Sandstone rock fragments.

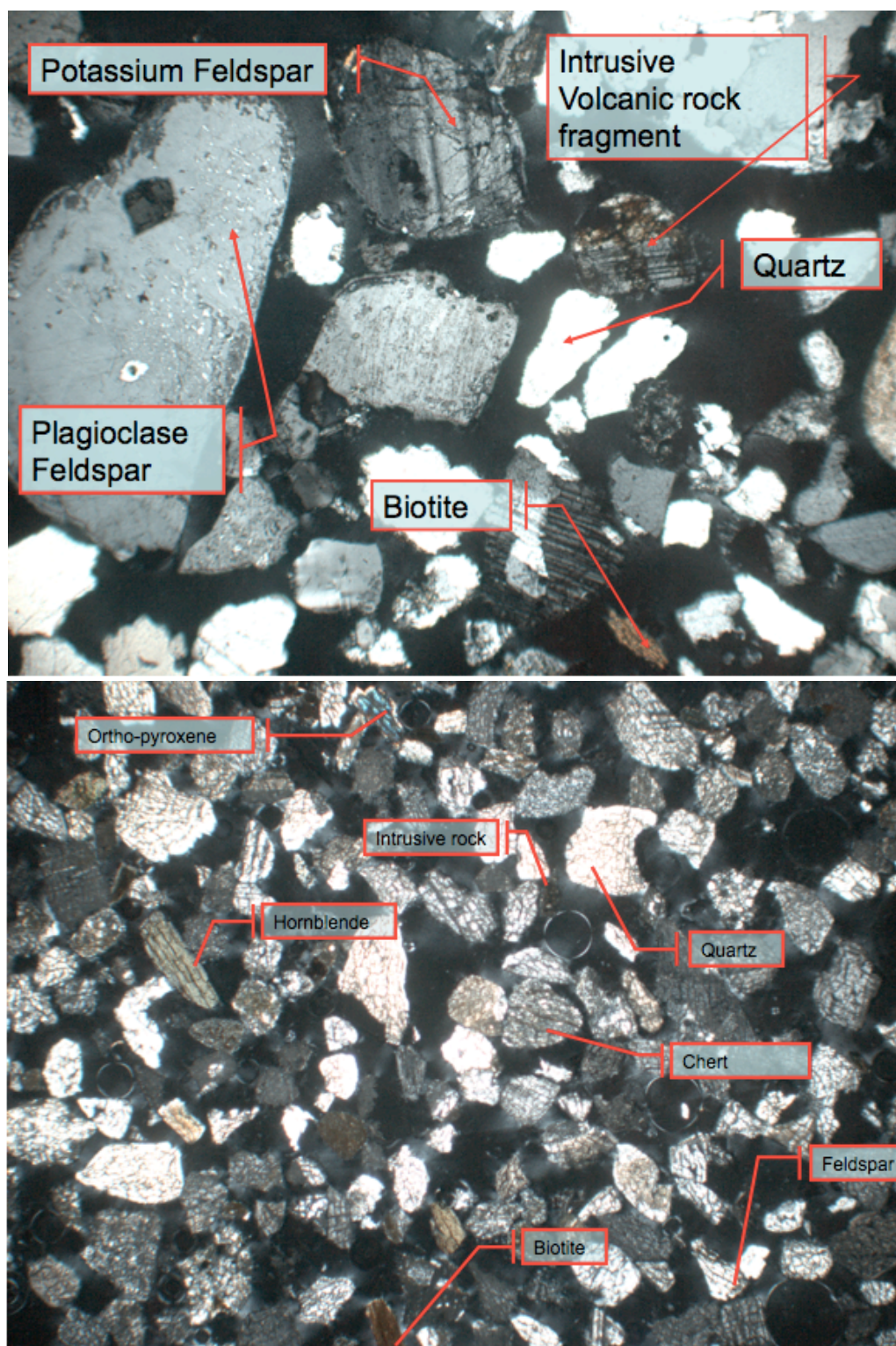


Figure 21: Cross-polarized photos of winter 2009 transect sediment from the swash zones of the Pajaro (Bottom) and Salinas (Top) River Mouths (PR2 & SR4). Key minerals are pointed out.

Figure 22(A): Winter heavy mineral abundance

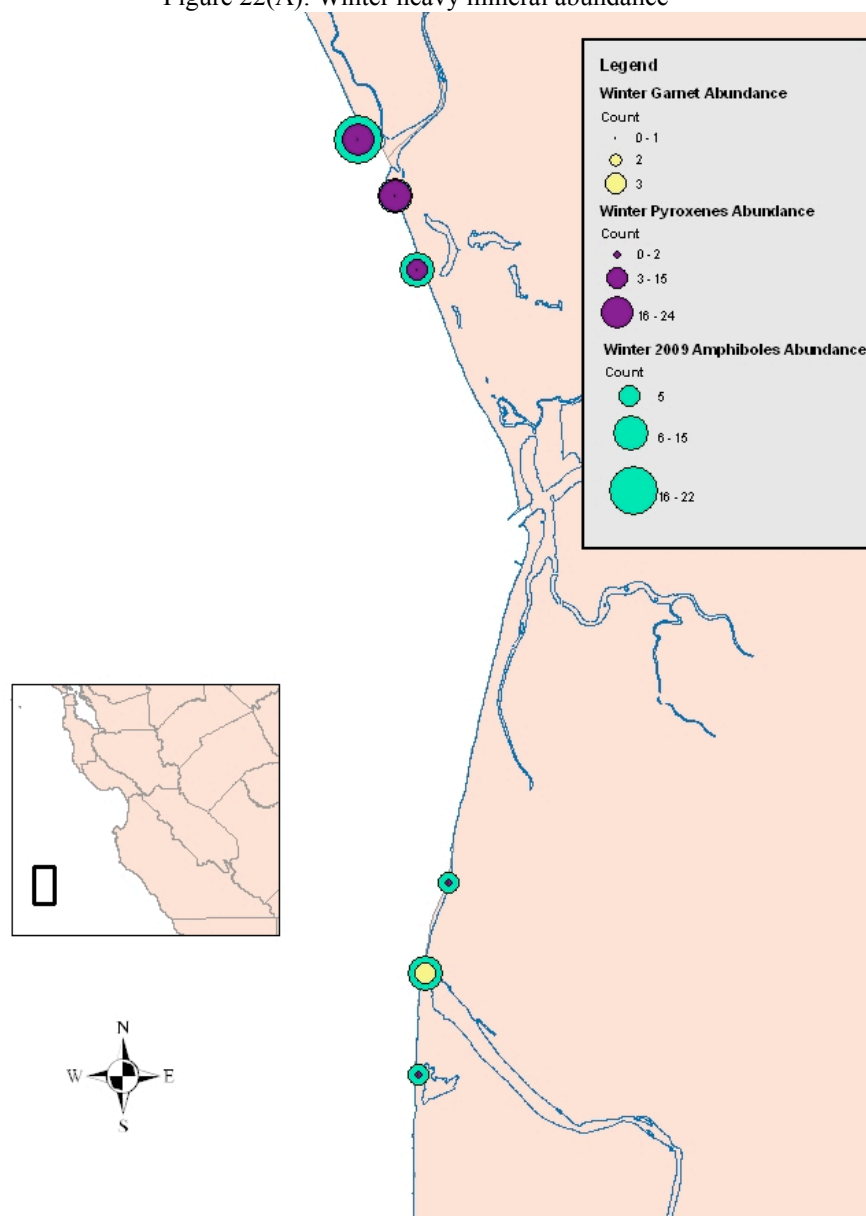


Figure 22(B): Summer heavy mineral abundance

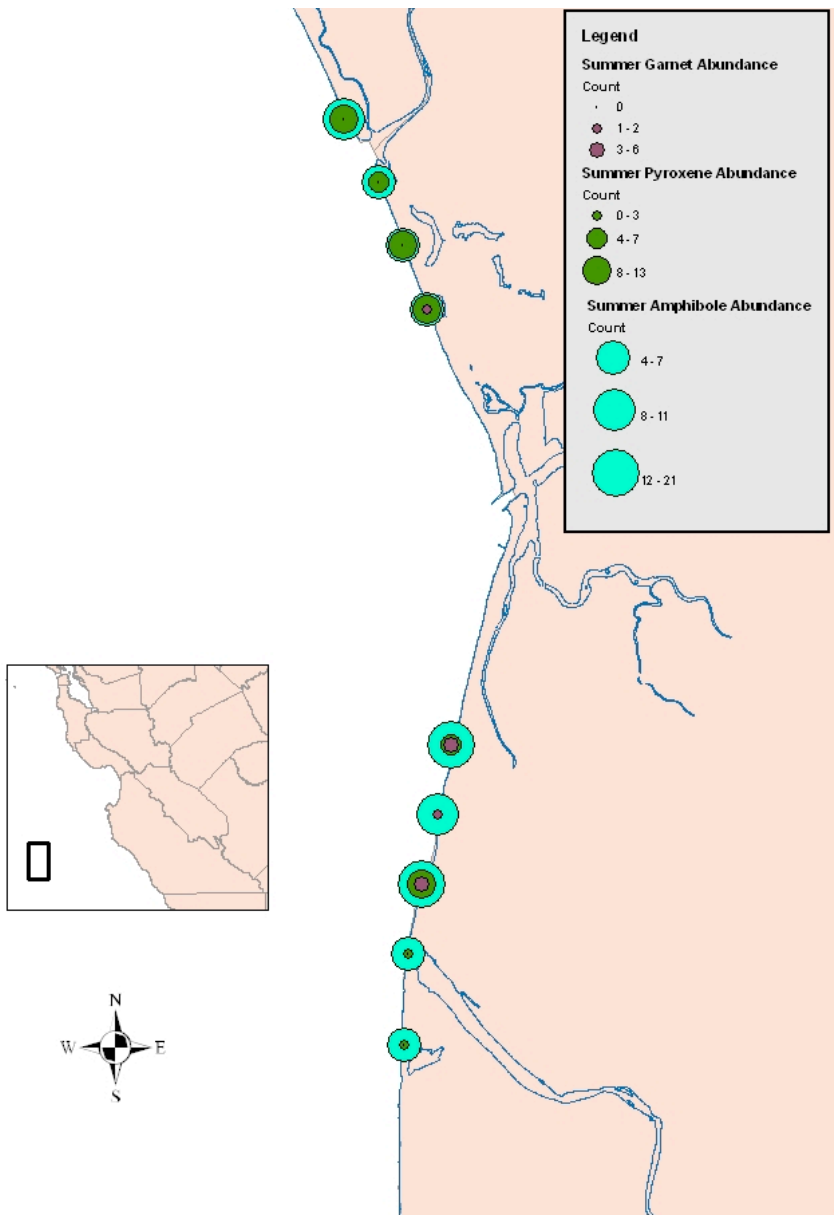


Figure 22(C): Fall heavy mineral abundance

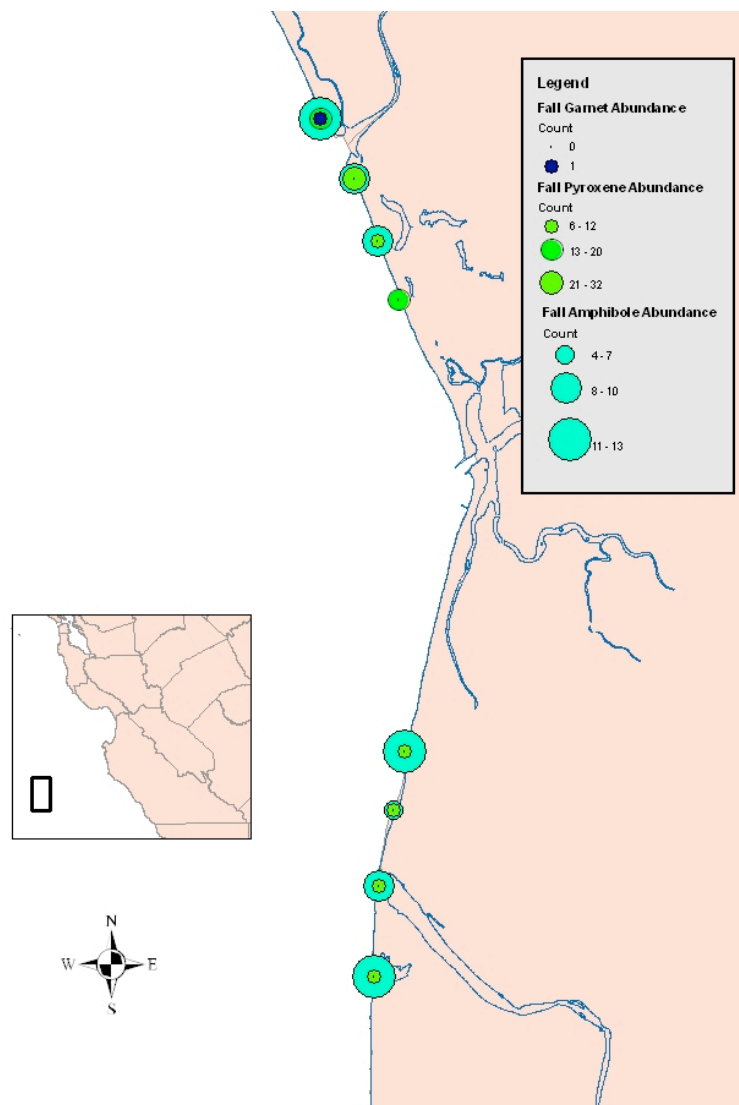
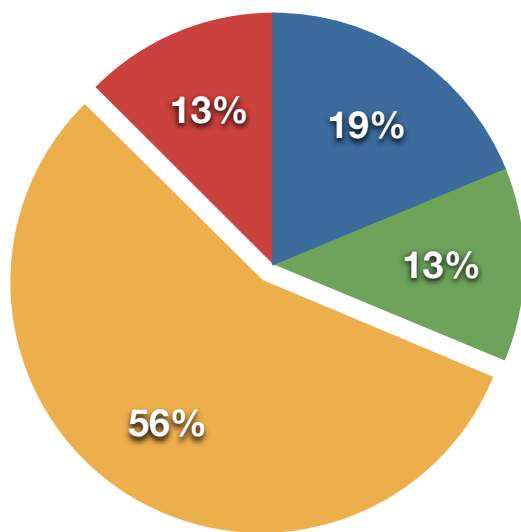
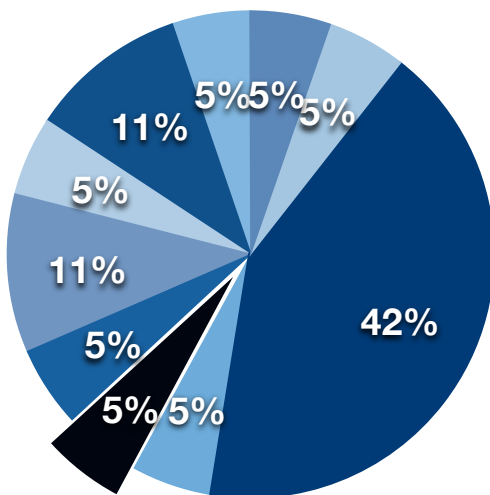


Figure 22: Heavy mineral abundance along the central Monterey Bay coastline for (A) winter, (B) summer and (C) fall seasons. Larger circles reflect larger counts of heavy minerals, with size and color listed on legend.



● Andesite ● Granodiorite ● Basalt ● Arkose



● Dacite ● Diorite ● Granodiorite ● Granite
 ● Basalt ● Arenite ● Arkose ● Breccia
 ● Conglomerate ● Pegmatite

Figure 23: Percent composition charts for both Pajaro (top) and Salinas (bottom) pebbles



Figure 24: Picture of Pajaro coastline during January 29th surveys.



Figure 25: Pictures of Salinas (Left) and Pajaro (Right) Coastlines during July 11th Transects



Figure 26: Pictures of Pajaro (top) and Salinas (bottom) coastlines during October 21st surveys.